The Atlantic Thermohaline Circulation in extreme climates

Settore Scientifico-disciplinare di afferenza: FIS/06

Tesi di dottorato di **RITA LECCI**, matricola 955466

Coordinatore del Dottorato

Prof. C. BARBANTE

Tutore del dottorando

Dr. S. MASINA

Co-tutori del dottorando

Dr. A. CHERCHI

Dr. M. BARREIRO

Ai miei genitori

Abstract

The present study investigates the sensitivity of the Atlantic Thermohaline Circulation (ATHC) to extreme external radiative forcing with the aim to contribute to the understanding of the mechanisms at work. A set of long experiments performed with a state of the art atmosphere-ocean coupled general circulation model under strong atmospheric CO_2 forcing has been used to study the mechanisms controlling the ATHC changes, their effects in the North Atlantic climate and in the energetics of the climate system. The ATHC weakens in response to a warming of atmosphere and ocean affecting the northward heat transport and leading to its decrease into the basin. The most extreme case shows distinctive features with an equatorward shift of ATHC convective sites and a salinity front formation at mid-latitudes. The analysis of the mechanisms at work shows a positive relationship between the high latitudes ocean vertical diffusivity and the circulation intensity. The Southern Ocean wind stress seems to influence the ATHC only when the meridional density gradients between high and low latitudes in the basin are kept fixed with a weaker Southern Ocean wind stress leading to a weaker ATHC. The meridional density gradients between high and low latitudes have been found inversely related to the ATHC intensity in the CO_2 simulations with the exception of the most extreme case. The high-density Mediterranean Outflow waters influence the ATHC as well: the ocean circulation decreases and shifts to mid-latitudes in response to a salinity input at the Gibraltar Strait latitude. The weakening of the ATHC under increasing CO_2 atmospheric concentration has been found associated with a large decrease of the kinetic energy input, mainly by the pressure-gradient work in the convective site areas in the North Atlantic. On the other hand, the atmospheric kinetic energy increases because of the intensification and poleward shift of the mid-latitudes jet-streams, the troposphere tends to be more stable and the Hadley circulation weakens.

Contents

Chapter 1

Introduction

The Atlantic thermohaline circulation (THC) is an important part of the Earth's climate system being responsible for most of the oceanic northward heat transport in the North Atlantic. It is an oceanic circulation that involves warm, saline surface water flowing northward and cold, dense water flowing southward at depth in the Atlantic basin (Wunsch, 2002). Tropical surface water, in particular, flows into high latitudes where it is cooled and sinks to depth. The water hence flows southward at about 3000m depth through the Atlantic Ocean, mainly as a deep western boundary current, until it reaches the Southern Ocean where it mixes with the rest of the World Ocean (Stouffer et al, 2006).

The ATHC is driven by global density gradients, hence it is largely influenced by surface heat and freshwater fluxes. Geological evidences suggest that the past abrupt climate changes are a result of rapid reorganizations of the ATHC (Clark et al, 2002). Modeling studies indicate that the ATHC is potentially sensitive to changes in surface buoyancy fluxes induced by global warming (Dixon et al, 1999; Cubash et al, 2001; Gregory et al, 2005) and that in the future there could be the risk of significant changes in the ocean circulation (Manabe and Stouffer, 1994; Wood et al, 1999; Zickfeld et al, 2007). Global warming conditions in the past were associated primarily with high atmospheric CO_2 concentration and proxy data indicate that maximum

carbon dioxide values were reached in the Paleocene with 5.000 p.p.m.V. (Zachos et al, 2008).

The response of the ATHC to heat and freshwater inputs has been widely studied using numerical simulations. Ocean general circulation models (OGCMs) both forced by atmospheric fluxes and coupled to atmospheric general circulation models or to simplified atmospheric component, as well as earth system models of intermediate complexity (EMICs) in IPCC scenario experiments or idealized water-hosing simulations or sensitivity CO_2 experiments (Stouffer et al, 2006) have been used showing that results are highly model dependent.

The so-called "hosing experiments", where a large uniform freshwater input is applied to the North Atlantic, have been used to simulate the magnitude of the freshwater discharge predicted for a large CO_2-induced climate change (i.e. 0.1 Sv in $4CO_2$ (Wood et al, 1999; Stouffer et al, 2006)). Larger freshwater input (i.e.1.0 Sv (Stouffer et al, 2006)) is extremely unlikely under realistic CO_2 scenarios, but it is within the range envisaged for events driven by meltwater release during the last glacial era and the deglaciation (Clarke et al, 2003). Such large forcing may weaken or even shutdown the ATHC, depending on the freshwater input applied and the model used to perform the analysis.

Differently from the hosing experiments, the set of simulations used in this thesis permits to investigate changes in the ATHC due to density field variations associated with heat fluxes changes. The imposition of an increased radiative forcing, as the enhanced atmospheric CO_2 concentration, leads in fact to changes in the ocean properties through changes in the density because of warmer temperature and of the freshwater input in the North Atlantic latitudes,as a consequence of the sea-ice melting. The advantage of the present study is hence the possibility to evaluate the overall impact of strong CO_2 forcing over the climate system considering the atmosphere-ocean interaction using a global coupled general circulation model. Further, the $16CO_2$ experiment represents a new particularly extreme case study in

the literature.

Simulations with increased atmospheric CO_2 show changes in the surface heat fluxes at high latitudes, accompanied by a slow down or collapse of the ATHC depending on the model used (Manabe and Stouffer, 1994; Thorpe et al, 2001; Schmittner et al, 2005). However, to date it is not clear whether the heat or the freshwater fluxes at high latitudes dominate the Atlantic THC response to the radiative forcing (Manabe and Stouffer, 1999; Dixon et al, 1999; Gregory et al, 2005; Weaver et al, 2007) and further analysis should be done in order to answer to this question.

The aim of the present study is to analyze the sensitivity of the ATHC to extreme external radiative forcing to contribute to the understanding of the mechanisms at work. In particular, the main objectives of this study are:

1. the analysis of the response of the North Atlantic and the ATHC to a large, but within the range of observed values in past climates, CO_2 atmospheric forcing;

2. the understanding of the mechanisms controlling the ATHC changes;

3. the analysis of the effects of the changes in the North Atlantic circulation to the energetics of the climate system.

The study compares a set of experiments forced with high atmospheric CO_2 concentration (4, 8, 16 times the present day mean value) to a long control simulation (with CO_2 present day mean value) performed with a state of the art atmosphere-ocean coupled general circulation model (CGCM). A further experiment has been performed with the aim to analyze the influence of the high-density Mediterranean Outflow waters on the ATHC applying a salinity input at Gibraltar Strait latitude in the most extreme CO_2 experiment.

This set of experiments (except for the $8CO_2$ experiment) has been analyzed in previous studies focused on changes in the Pacific Ocean and on implication for the monsoon hydrology (Cherchi et al, 2008, 2011). Building on those studies, this thesis intends to investigate the role of the surface heat and freshwater fluxes in the ATHC changes when the greenhouse gas

increases. The CGCM experiments allow to identify the resultant feedbacks between atmospheric and oceanic processes.

The thesis is organized as follows:

- Chapter 2 describes the model used to perform the simulations and the setup of the sensitivity experiments.

- Chapter 3 analyzes the impact of the radiative forcing over the Atlantic Ocean mean state.

- Chapter 4 investigates some possible mechanisms influencing the Atlantic THC intensity.

- Chapter 5 explores the climate system energetics related to the above changes.

- Chapter 6 summarizes and discuss the main results of the study.

Chapter 2

Model description and setup of the experiments

2.1 SINTEX-G Model

The SINTEX-G global coupled model (Gualdi et al, 2008) has been used to build experiments with modified CO_2 conditions, following previous studies by Cherchi et al. (2008). SINTEX-G represents an improved version of the SINTEX model (Gualdi et al, 2003b) with the inclusion of a module for the interactive sea-ice. The model consists of four parts: Atmosphere, Ocean, Sea-Ice and Coupler. The land-ice is not included.

The atmospheric component is Echam4.6 (Roeckner et al, 1996). It represents the fourth generation of the ECHAM model developed at the Max-Planck Institute fur Meteorologie in Hamburg. The resolution used for this analysis is a spectral T30 horizontal resolution with 3.75° x 3.75° grid-points and 19 vertical sigma levels with top level at 10hPa, 7 layers above 200 hPa and 5 layers below 850 hPa. The numerical scheme is a semi-implicit leap-frog time stepping and the prognostic variables are: vorticity, divergence, temperature, logarithm of surface pressure, water vapor and mixing ratio of total cloud water. Major parameterizations concern:

a. clouds: a prognostic scheme for optical cloud properties (Sundquist,

1978) with cloud water determined by Mie theory (Rockel et al, 1991; Roeckner, 1995);

b. tracer advection: transport of water vapor, cloud water and (optionally) tracers by a semi-lagrangian scheme (Williamson and Rasch, 1994);

c. convection: shallow, mid-level and deep cumulus convection with mass flux scheme by Tiedke (Tiedtke, 1989) and adjustment closure for deep convection as described by Nordeng (1996);

d. boundary layer and vertical diffusion: surface fluxes of momentum, heat, water vapor and cloud water calculated with Monin-Obukhov theory (Luis, 1979), with eddy diffusivity coefficients depending on roughness length and Richardson number. Above the surface layer, the coefficients depend on wind shear, thermal stability and mixing length;

e. radiation scheme: narrow-band model (Morcrette, 1984; Morcrette and Fouquart, 1985). Despite the high concentration of carbon dioxide considered, the scheme has been found to be robust and free from saturation even in the extreme CO_2 case (Cherchi et al, 2011).

f. orographic gravity wave drag.

The oceanic component is OPA8.2, the global ocean general circulation model developed at LODYC in Paris (Madec et al, 1998) used in ORCA2 configuration. It is a primitive equation model with a spatial resolution of 2° x 2° and a refinement up to 0.5 degrees in the proximity of the Equator. The grid is quasi-isotrope and tri-polar (2 poles in the northern hemisphere, one over Canada and the other over Siberia). Vertical resolution includes 31 vertical levels in z-coordinates with 14 levels lying in the top 150 meters and a free surface. The prognostic variables are the three dimensional velocity field and the thermohaline variables.The Mediterranean Sea salinity and temperature are relaxed to Levitus (1998) climatology values every year since the high salinity Mediterranean waters can lead to computational errors if left without constraints. The distribution of the variables is over a three-dimensional Arakawa-C-type grid with a leap-frog scheme except for a lateral diffusion (forward) and vertical diffusion (backward). Major para-

meterizations are:

a. eddy parameterization: isopycnal mixing on tracers (no horizontal background) with a constant coefficient of 2000 m^2/s. Eddy induced velocity with a coefficient varying in function of the growth rate of baroclinic instability (ranges 15 m^2/s to 2000 m^2/s). The coefficient is set to 0 in the vicinity of the Equator;

b. bottom boundary layer treatment and sill overflow treatment diffusive bottom boundary layer (Beckmann and Dorscher, 1997);

c. mixed-layer treatment: TKE scheme (Blanke and Delecluse, 1993);

d. sunlight penetration with 2 master lengths (Blanke and Delecluse, 1993) ;

e. no tidal mixing;

f. no river mouth mixing;

g. mixing isolated seas with the ocean: no mixing (Red Sea and Mediterranean Sea are explicitly connected to the remaining ocean). For closed "seas" (Black Sea, Great lakes, Caspian Seas) the mean sea level remain constant, excess (deficit) of water been either redistributed over the world ocean (Caspian Sea) or in St Laurent river mouth (Great lakes) or Dardanel strait area (Black Sea);

h. treatment of North Pole "singularity": semi analytical tri-polar grid, no singular point in the ocean domain (Madec and Imbard, 1996; Murray, 1996).

The OPA OGCM includes the Louvain-laneuve sea-Ice systeM (LIM) module for the interactive sea-ice (Fichefet and Morales, 1997; Timmermann et al, 2005). The LIM model has been developed at the "Institut d'Astronomie et de Geophysique Georges Lemaitre" (Universite Catholique de Louvain). It is a large-scale thermodynamic-dynamic sea-ice model with 3-layers (one for the snow and two for the ice). The ice momentum equation is solved on the ocean horizontal grid. The horizontal resolution is the same as the ocean model and the equations for ice motion and transport are written in curvilinear, orthogonal coordinates. The heat-diffusion equation

is based on a fully implicit scheme while the momentum equation is a semi-emplicit scheme (combination of a modified Euler time step scheme and a point successive relaxation procedure). Advection equations is based on a forward time marching scheme which conserves the second-order moments of the spatial distribution of the advected quantities. The prognostic variables are snow and ice thickness, ice concentration, ice velocity, internal temperature of snow and ice and heat content of brine reservoir. The model does not include a coupling with a land-ice component.

The atmospheric and oceanic components are coupled with Oasis2.4 (Valcke et al, 2000). OASIS main tasks are the synchronization of the models being coupled and the treatment and interpolation of the fields exchanged between the models at the land-sea interface.

The models are integrated in parallel. The communication between models occurs, through the coupler, at each coupling time step (96 minutes) which correspond to 1 time step for the ocean model and 8 time steps for the atmospheric model. The ice model communicates with the ocean at each ocean time step.

The fields sent from the ocean model to the atmospheric model are the Sea Surface Temperature (SST) and the information about the Sea Ice Cover (SIC). The fields sent from the atmosphere to the ocean are solar and non solar heat fluxes, water flux, snow fall, zonal and meridional wind stress. The air-sea fluxes and the SST are exchanged every 3h. No flux corrections are applied to the coupled model.

In the hydrological cycle, the computation of the water fluxes does not consider the river runoff. This constraint may negatively impact the results as it influences the ocean salinity and it avoids the contribution of the precipitation excesses, if any, from the continents.

2.2   Setup of the experiments

The present study focuses on the comparison between a control experiment (CTRL) and a set of sensitivity experiments with increased atmospheric carbon dioxide concentration. In the CTRL the carbon dioxide concentration is 353 ppmV, corresponding to the present's day mean value. It has been multiplied by a factor of 4, 8 and 16 to build 4 x CO_2, 8 x CO_2 and 16 x CO_2 experiments, respectively.

This kind of experiments follows from a previous analysis focused on the impact of extreme CO_2 levels in the tropical climate (Cherchi et al, 2008, 2011). In all the experiments, the oceanic initial conditions are the same, and they correspond to the mean climatology from Levitus temperature and salinity datasets (Levitus et al, 1998). The CO_2 forcing has been applied at the beginning of each simulation and maintained for the whole length of the experiments. All the simulations are 600 years long.

In the CO_2 experiments, the forcing applied drives the system toward an equilibrium with different adjustment times depending on the forcing intensity. The net heat flux globally averaged at the ocean surface (fig. 2.1a), computed as the sum of the shortwave and longwave radiation and the latent and sensible heat fluxes, show very slow variations toward the end of each experiment indicating an almost stable climate. In the $16CO_2$ experiment, for example, the global mean of net surface heat flux shows striking changes within the first 100 years (56% of reduction with respect to the initial value) and very slow variations during the last 100 years (4% of reduction).

Similarly, the balance at the top of the atmosphere (TOA), computed as the sum of the TOA net shortwave radiation and longwave radiation (fig. 2.1b), shows climate stability both in the CTRL and in the last 100 years of the CO_2 simulations. The perturbative experiments show an increased TOA net heat flux due to the greater absorption of longwave radiation by the CO_2 through the atmosphere. The net heat flux not closed balance in the CTRL case is due to a common bias in climate models, as suggested by several coupled model studies (Luo et al, 2004)

In the following chapters, mean climate fields refer to the average over the last 100 years of integration of each experiment, unless differently specified.

To simplify and quantify the description of the differences between CO_2 and CTRL experiments a number of Global or Atlantic mean parameters have been defined and summarized in table 3.1

To study the effect of the Mediterranean Outflow (MOW) waters, mainly in terms of salinity input, on the Atlantic THC intensity a further experiment (hereafter 16xCO_2M) has been performed. The 16CO_2M experiment has the same initial condition of 16 CO_2 experiment and it differs for a salinity input applied at the Gibraltar Strait latitude (close to 40°N). In fact, in 16xCO_2M the relaxation to Levitus climatology is applied only to the temperature field, while the salinity changes responding to the CO_2 forcing without any constraint. The temperature relaxation has been held in order to avoid model numerical instability due to high temperature and salinity values reached by the Mediterranean waters under CO_2 extreme forcing. Even this last experiment is 600 years long and the comparison between the 16xCO_2M and 16xCO_2 is done comparing the last 100 years of simulation.
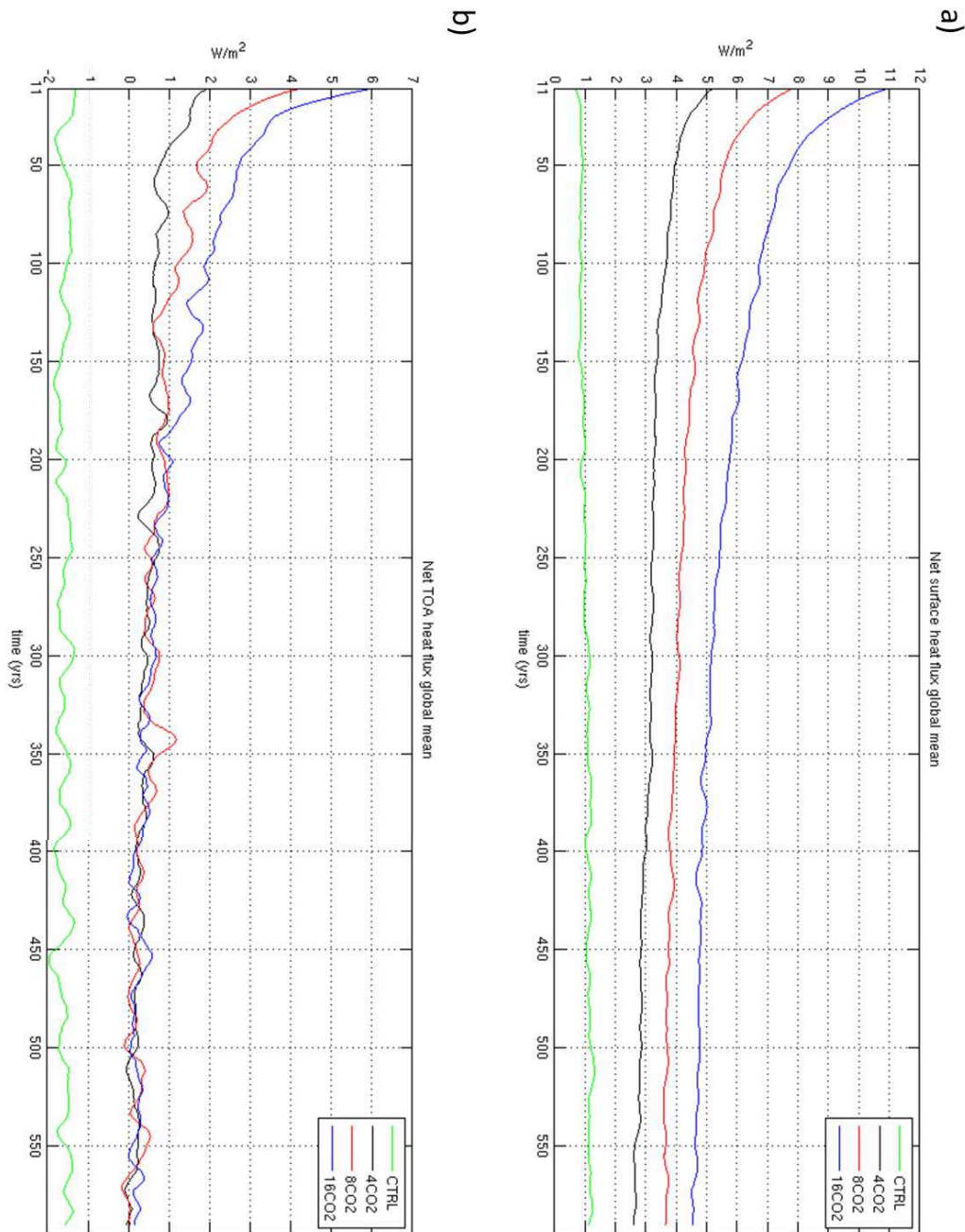
Figure 2.1: Time series of (a) net surface heat flux (W/m^2), computed as SWR (Short Wave Radiation) + LWR (Long Wave Radiation) + SHF (Sensible Heat Flux) + LHF (Latent Heat Flux) over the ocean, and of (b) net heat flux at the top of troposphere (TOA) (W/m^2), computed as the sum of the TOA net SWR and LWR, for CTRL (green line), 4xCO_2 (black line), 8xCO_2 (red line) and 16xCO_2 (blue line) experiments. Surface and TOA fluxes are globally averaged A filter of ten years has been applied to the time series

Chapter 3

Simulated mean state: sensitivity to CO_2 forcing

3.1 Introduction

The Atlantic thermohaline circulation (THC) is an important part of the Earth's climate system being responsible for most of the oceanic northward heat transport in the North Atlantic, peaking at about 1.2 PW at 24°N (Ganachaud and Wunsch , 2000). It is an oceanic circulation that involves warm, saline surface water flowing northward and cold, dense water flowing southward at depth in the Atlantic basin (Wunsch, 2002). Tropical surface water flows into high latitudes where it is cooled and then it sinks to depth mainly in the Labrador Sea and in the Nordic Seas. At about 3000m depth the water flows southward through the Atlantic Ocean, mainly as a deep western boundary current, until it reaches the Southern Ocean where it mixes with the rest of the World Ocean waters (Stouffer et al, 2006).

No such deep overturning occurs neither in the North Pacific, where the surface waters are too fresh to sink (Weaver et al, 1999), nor in the Southern Ocean, where the lack of a meridional land barrier precludes the existence of strong east-west pressure gradients needed to balance a southward geostrophic surface flow (Clark et al, 2002).

Geological past evidences suggest that reorganizations of the Atlantic THC were involved in climatic temperature changes of several degrees in a few decades (Clark et al, 2002; Rahmstorf, 2002) and there is the risk, in the future, that significant changes in ocean circulation could result from a global warming (Manabe and Stouffer, 1994; Wood et al, 1999; Schaeffer et al, 2002; Zickfeld et al, 2007).

Paleo data strongly suggest that latitude shifts of convection (between the Nordic Seas and the region south of Iceland) have occurred (Alley and Clark, 1999) and that at certain times NADW formation was interrupted (Keigwin et al, 1994). The most pronounced abrupt climate changes have been identified as the Dansgaard-Oeschger (D/O) warm events, with a warming exceeding 10°C within a decade or so (Severinghaus et al, 2003), during which the Nordic Seas convection sites shifted to mid-latitudes and the Atlantic THC weakened.

Others major climatic events, the so-called Heinrich events that occurred mostly in the latter half of the last glacial (Rahmstorf, 2002), have been associated with a large discharge of icebergs into the northern Atlantic (Heinrich, 1988) and a shutdown of NADW formation (Keigwin et al, 1994). The freshwater forcing discharged into the Atlantic has been estimated of the order of 0.1 Sv (Hemming, 2004).

At the end of the last glacial period, as the climate warmed and ice sheets melted, the ocean circulation went through a number of oscillations that may be explained by meltwater input (i.e., the Younger Dryas and the 8.2 kyr cold event) (Kuhlbrodt et al, 2007).

Many aspects of the abrupt events found in proxy data have been reproduced in model simulations. Large freshwater input, such as that associated with Heinrich events, has been reproduced in many models and an Atlantic THC non-linear response with multiple equilibrium states has been found in response to changed surface fluxes (Stommel, 1961). The ATHC shows a bistable regime in its parameter space where the deep-water formation can be "on" (as in the present climate) or "off", depending only on initial condi-

tions. For increasing freshwater inflow to Atlantic, this bistable regime passes a saddle-node bifurcation to a monostable regime where the deep waters do not form (off state) (Rahmstorf, 2002). For lesser freshwater inflow, another monostable regime exists where the NADW form (on state) (Hofmann and Rahmstorf, 2009).

This non linear behavior is explained by the positive salt-advection feedback first described by Stommel (1961). Higher salinity in the deep-water formation area enhances the circulation and the circulation in turn transports higher salinity waters into the deep-water formation regions (Rahmstorf, 2002).

Furthermore, Rahmstorf (2002) suggested that the salt-transport feedback is not the only feedback making the system non-linear. The convective mixing process at high latitudes is itself a highly non-linear, self-sustaining process, which at least in models can lead to multiple stable convection patterns. Recent studies suggest that the direction of the net freshwater transport at the southern boundary of the Atlantic by the ATHC, as a measure of Stommel's salt-advection feedback, may be a useful physical indicator of the existence of bistability (Hawkins et al, 2011). If the freshwater transport is positive than the ATHC exports salt; in this case a small decrease in the strength of the ATHC would export less salt encouraging a recovery of the ATHC as a higher salinity tends to promote deep mixing and a stronger ATHC. However if the freshwater transport is negative then there is a positive feedback, reinforcing any decline in the strength of the ATHC (Hawkins et al, 2011). The estimates of recent time evolution of the freshwater transport at 34°S in the Atlantic basin show typical negative values indicative of a bistable regime.

Instrumentals records show a global surface temperature mean increase of 0.74 °C during the 20th century and climate model projections indicate that during the 21st century it will rise likely of about 1.5°C to 1.9 °C for the lowest emissions scenario and of 3.4°C to 6.1°C for the highest (IPCC, 2007). As a consequence of the recent warming, a rapid non linear response

of the THC,with a concomitant climatic impact in western Europe, would occur (Ganopolski et al, 1998).

This chapter aims to investigate the changes in the Atlantic Ocean mean state as a consequence of the changes occurring to density and salinity fields because of an increase in temperature associated with a CO_2 forcing. In particular, this part of the study aims to answer to the following questions:

1. Which is the impact of the radiative forcing over the Atlantic Ocean mean state?

2. How do the Atlantic THC respond to the strong CO_2 perturbation?

This chapter is organized as follows: section 3.2 analyzes the influence of the CO_2 perturbation over the processes occurring at the atmosphere-ocean surface, section 3.3 investigates the mean state of the Atlantic Ocean circulation, section 3.4 shows the tropospheric response to the radiative forcing applied and section 3.5 gives some concluding remarks. As specified in chapter 2, the analysis is focused on the annual mean state averaged over the last 100 years of integration for each experiment. A table is inserted to summarize the intensity of specific metrics, even in terms of differences between CO_2 experiments and CTRL, characteristics of oceanic and atmospheric properties (table 3.1).

3.2   Change at ocean-atmosphere interface

The annual mean Atlantic sea surface temperature (fig. 3.1) increases in response to an atmospheric CO_2 increase (table 3.1). In the simulations, the maximum Atlantic Ocean surface temperature increase is located in a belt confined between 30°S and 50°S, which is the result of a poleward shift of the subtropical gyre induced by a southward shift of the wind stress maximum at the Southern Ocean (table 3.1), as proposed by Cai et al. (2003) for global warming conditions.

The North Atlantic is as well subject to a warming and the temperature gradient between the low and the high latitudes, computed as the SST

	CTRL	$4 \times \text{CO2}$	$8 \times \text{CO2}$	$16 \times \text{CO2}$
Global atm T (°C)	-	+7	+11	+17
Atlantic SST (°C)	-	+4	+7	+12
Atlantic SST gradient (°C)	27	26	25	24
Labrador SST (°C)	-	+2	+4	+6
Atlantic SSS (psu)	-	+1	+2	+4
Labrador SSS (psu)	-	-0.5	-1	-2
Freshwater input due to sea-ice melting (Sv)	-	0.01	0.02	0.06
Arctic ice stabilization time period (yrs)	-	86	69	17
Atlantic THC max (Sv)	32	27	24	15
Atlantic THC max 25°N (Sv)	31	25	21	13
Atlantic HT max (PW)	1.16	1.12	1.03	0.72
Atlantic HT 30°S (PW)	0.36	0.53	0.53	0.32
26 Kg/m^3 Atlantic isopycnal depth (m)	120	130	160	180
NA vertical diffusivity (m^2/s)	1.44	1.43	1.33	1.20
SO wind stress (10^{-2}N/m^2)	7.7	8	7.6	5.9
SO wind stress max (N/m^2)	0.15	0.16	0.15	0.13
SO wind stress max lat	46°S	51°S	53°S	55°S

Table 3.1: From top to bottom the values refer to annual mean differences (CO_2 experiments minus CTRL) of global 2m height air temperature and of SST averaged in the Atlantic Ocean, annual mean meridional SST gradient in the North Atlantic (difference between 0° and 80°N), differences (CO_2 experiments minus CTRL) of SST averaged in the Labrador Sea and of SSS averaged in the Atlantic basin and in the Labrador Sea, freshwater input due to sea-ice melting, time period necessary to reach the Arctic ice stabilization, annual mean Atlantic THC maximum, Atlantic THC maximum at 25°N, Atlantic heat transport maximum, Atlantic heat transport at 30°S, depth of the 26 Kg/m^3 Atlantic isopycnal computed at the Equator, North Atlantic (20°N-80°N) vertical diffusivity computed between 100-2000m for MJJA, Southern Ocean (30°S-80°S) wind stress, Southern Ocean wind stress maximum and latitude of the Southern Ocean wind stress maximum, North Atlantic (30°N-90°N) wind stress, North Atlantic wind stress maximum and latitude of the North Atlantic wind stress maximum
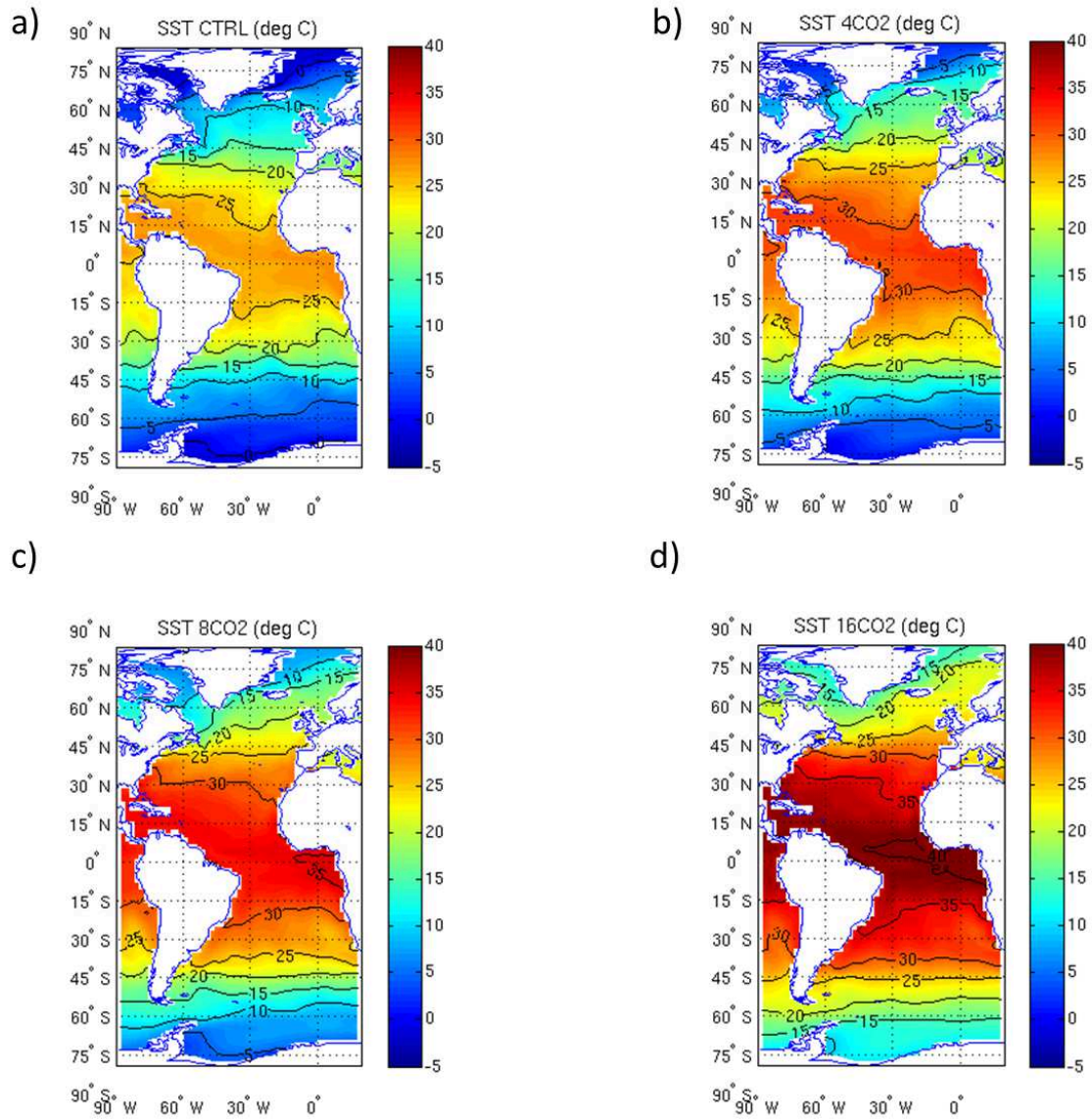
Figure 3.1: Annual mean SST (°C) for (a) CTRL, (b) 4xCO_2, (c) 8xCO_2 and (d) 16xCO_2 experiments.

difference between the Equator and 80 °N, decreases among the simulations (table 3.1). The Labrador Sea is one of the regions showing the weakest temperature increase: in $4CO_2$, $8CO_2$ and $16CO_2$ experiments the surface water temperature is 2°C, 3°C and 4 °C, respectively, lower than the North Atlantic warming (fig. 3.1b,c,d).

The simulated climatology of the Atlantic net surface heat fluxes field (computed as sum of net surface shortwave radiation, net surface longwave radiation, surface sensible and latent heat fluxes) shows as well a non-linear behavior in the Labrador Sea for all the simulations (fig. 3.2). In the CTRL experiment (fig. 3.2a) along the western boundary currents the ocean loses heat to the atmosphere being warmer then the air above. In the most extreme CO_2 experiment (fig. 3.2d) the net heat flux reverses sign in the Labrador Sea and the ocean gains heat from the atmosphere. The Atlantic basin also shows an alternation of zonally oriented regions where the ocean gains or loses heat which are also visible in the SST pattern (fig. 3.1d).

Fig. 3.3 shows each component of the net surface heat flux averaged in the Atlantic Ocean longitudes for the CTRL and CO_2 simulations. The net surface shortwave radiation (SW) shows a symmetric inter-hemispherical pattern with highest values in tropical and subtropical latitudes, where the insolation is maximum, and weakest at the poles (fig. 3.3a). Its intensity decreases as the CO_2 increases at the tropical latitudes since more solar radiation is reflected back to the space by the increased water vapor concentration. The net surface longwave (LW) radiation depends from the difference between the upward emission from the Earth's surface and the downward emission from clouds and greenhouse gases (GHGs) in the atmosphere and it shows decreased intensity among the experiments due to the GHG's effect (fig. 3.3b). The net surface latent heat (LH) flux is associated with evaporation of water at the surface and subsequent condensation of water vapor in the troposphere. In the CO_2 simulations, the LH flux increases in the Tropics because of a greater evaporation (fig. 3.3d). The net surface sensible heat flux is influenced by wind velocity and air-ocean temperature differences. In
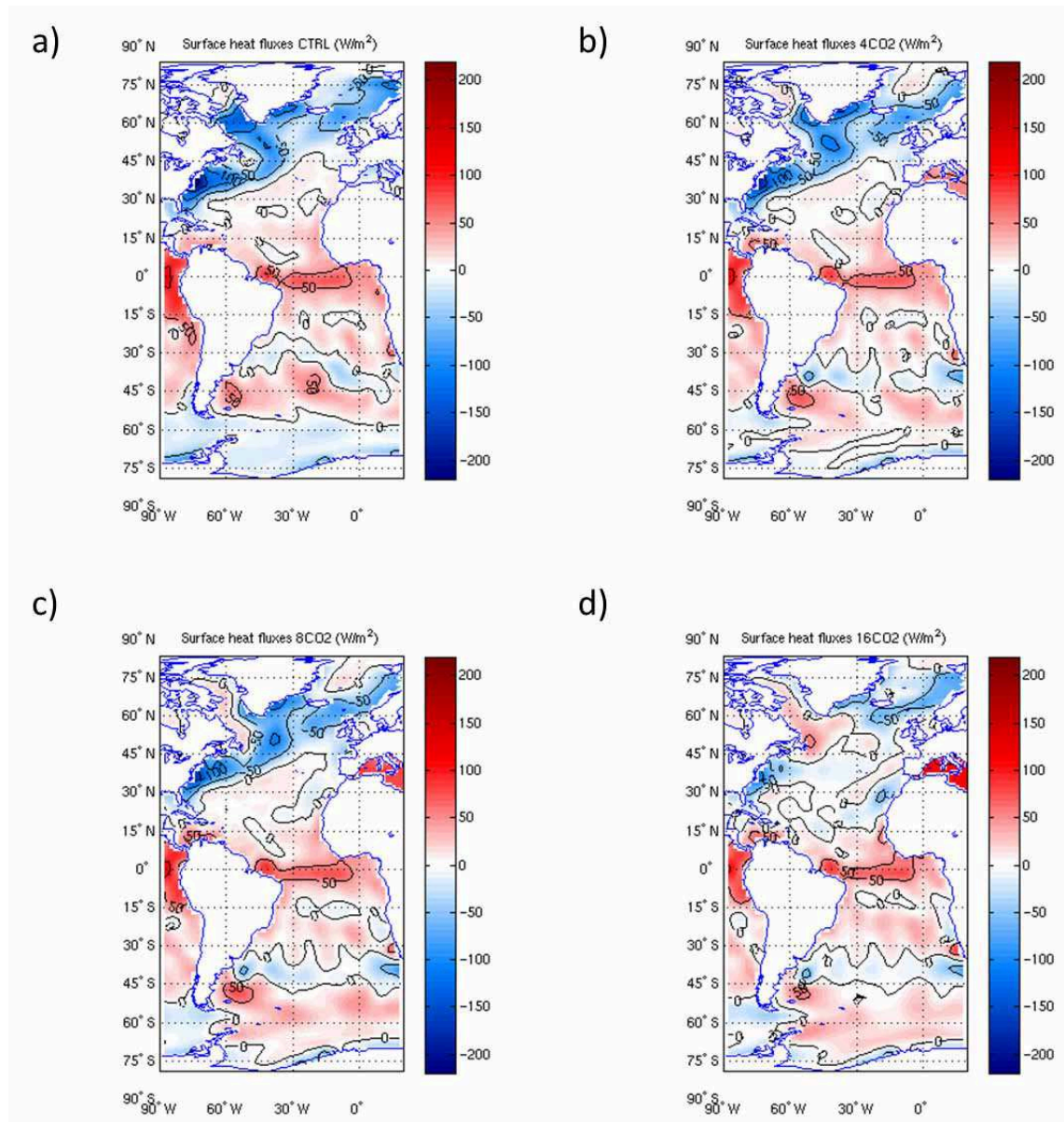
Figure 3.2: Annual mean net surface heat fluxes (W/m^2) for (a) CTRL (b) 4xCO_2, (c) 8xCO_2 and (d) 16xCO_2 experiments

fact, as the CO_2 concentration increases, the Labrador Sea surface waters become colder than the air above leading to reduced heat loss in the northern latitudes. In the $16CO_2$ experiment it reverses sign (fig. 3.3c) becoming positive in the Atlantic high latitudes (between 45°N and 80°N).

Fig. 3.4 shows the map of geopotential height (gph) of 1000 mb pressure level which is equivalent to a sea-level pressure map where high (low) gph values indicate HP (LP) areas. The suptropics near 30° latitude are dominated in both hemispheres by semipermanent HP cells bordered by a LP zone near the equator (ITCZ) and poleward by a LP belt. In the CO_2 simulations, the HP zone at 30°N shifts westward decreasing in intensity, while the LP belt at 60°N widens and intensifies (fig. 3.4b,c,d). On the other hand, in the Southern Hemisphere the HP zone shifts poleward and weakens. The new distribution of HP and LP areas leads in the North Atlantic to a strengthening of pressure gradient at high latitudes and a weakening at mid-latitudes (not shown).

Fig. 3.5 shows the Atlantic annual mean winds field computed at 850 mb for all the simulations. In the CTRL experiment the arrows show the subtropical anti-cyclonic circulation (around 30°N) characterized by a high pressure zone (fig. 3.4a), westerly winds on the northern side of the anti-cyclone and the trade winds on the southern side (fig. 3.5a). The cyclonic circulation is visible around 60°N in the Labrador Sea with an anticlockwise circulation around a low pressure area (fig. 3.4a). The main features present in the CTRL experiment persist in all CO_2 simulations, although the center of the subtropical anti-cyclone shifts slightly westward (fig. 3.5b,c,d). In $16CO_2$ experiment (fig. 3.5d) the westerlies close to 40°N become more zonal and less intense (-4 m/s) with respect to the CTRL case. The subpolar cyclone seems to vanish in this latter experiment while the winds intensify over the Nordic Seas as the atmospheric CO_2 increases (+2 m/s, + 4 m/s and +6 m/s in $4CO_2$, in $8CO_2$ and $16CO_2$ experiments, respectively).

At the Southern Ocean latitudes (30°S-80°S) there is a clear poleward shift of the westerlies. This shift has been related to the effects of global
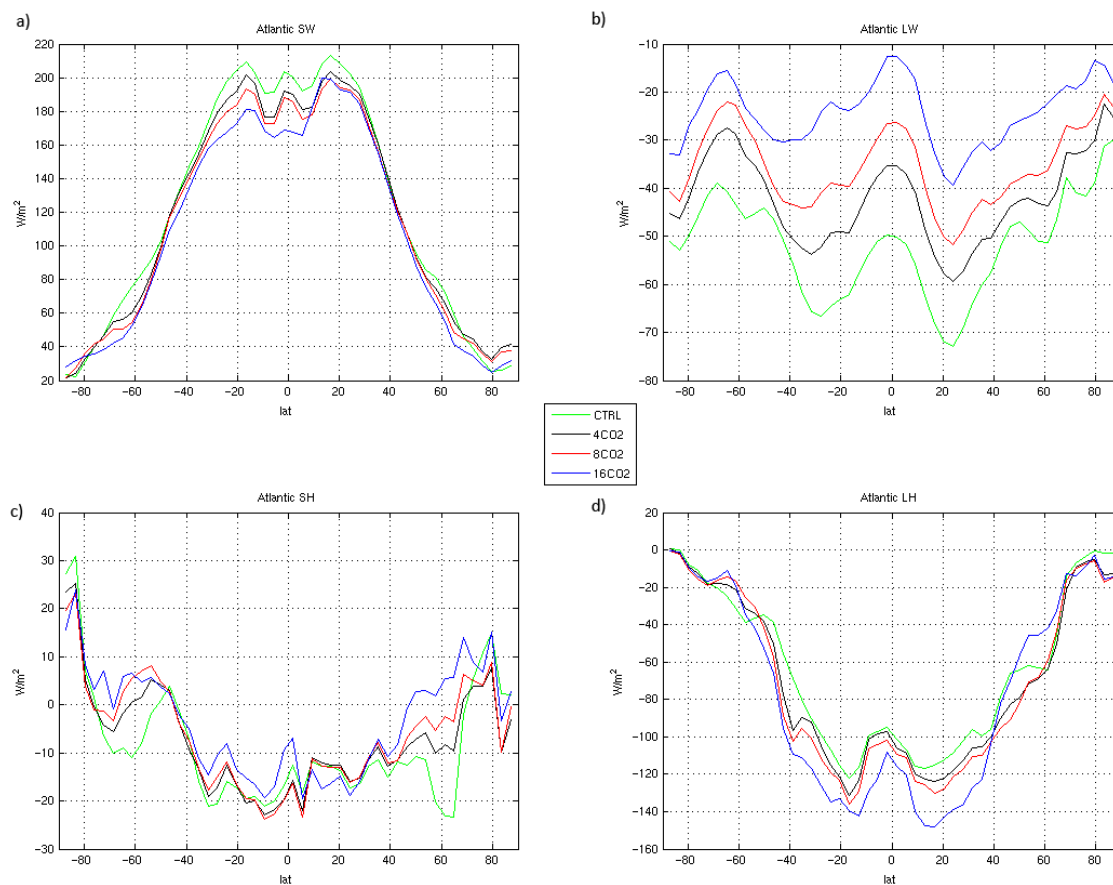
Figure 3.3: Annual mean net surface heat flux (W/m^2) components averaged in the Atlantic Ocean longitudes: (a) SW (shortwave radiation), (b) LW (longwave radiation), (c) SH (sensible heat) and (d) LH (latent heat) for CTRL (green line), 4xCO_2 (black line), 8xCO_2 (red line) and 16xCO_2 (blue line) experiments
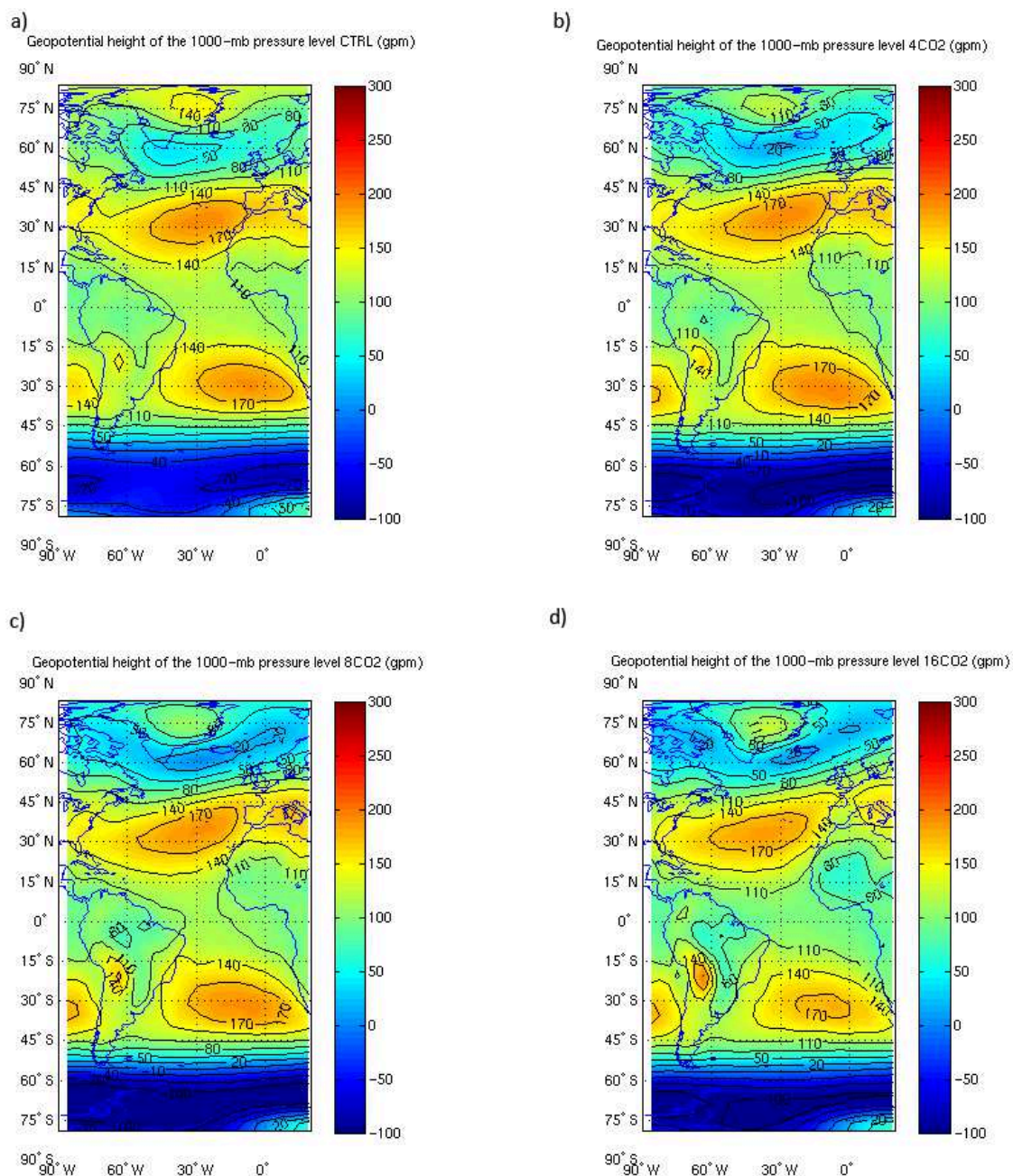
Figure 3.4: Annual mean geopotential height (gpm) of 1000-mb pressure level computed for (a) CTRL (b) $4xCO_2$, (c) $8xCO_2$ and (d) $16xCO_2$ experiments

warming in previous studies (Cai et al, 2003). Toggweiler (2009) suggested the occurrence of a poleward shift and strengthening of the westerlies over the past 50 years and 17.000 years ago, at the end of the last ice age, as a response to the warming experienced by the planet. In our experiments there is a poleward shift of the westerlies over the Southern Ocean with increased perturbation (fig. 3.5) but the response is nonlinear: westerlies strengthen in $4CO_2$, remain largely unchanged in $8CO_2$ and decrease in $16CO_2$ experiments (table 3.1) (discussed also in section 4.4).

Surface winds influence the ocean surface currents. In CTRL, $4CO_2$ and $8CO_2$ experiments (Fig. 3.6a,b,c) the maximum velocities in the North Atlantic are located along the Gulf Stream pathway, but a further increase in CO_2 concentration leads to a complete disappearance of that current (Fig. 3.6d). The Gulf Stream is mainly wind-driven and it decreases in intensity in the $16CO_2$ case in response to weakened surface winds. However, many model studies have shown a weakening of strength of the Gulf Stream as response to a North Atlantic freshening induced by global warming (Cai et al , 1996; O'Hare et al, 2005) mainly due to changes in the thermohaline circulation (Greatbatch et al, 1991; Cai, 1994).

The large decrease of the westerlies's northward component at mid-latitudes causes the warm and salty surface tropical waters to stop at about 40°N allowing the Labrador Current to spread more southward (with respect to the CTRL), as it is not anymore obstructed by the Gulf Stream northward flow. Hence a convergence zone forms in mid-latitudes where tropical warm surface waters meet cold surface waters originated in the Labrador Sea (Fig. 3.6d).

The changes in surface winds and ocean currents reflect also in the surface salinity pattern(fig. 3.7). The CTRL experiment has a salinity pattern 1psu generally saltier than the Levitus XX century climatology since the hydrological cycle computed by the model lacks the contribution of the river runoff (as it is climatological, as described in chapter 2) an important source of freshwater input into the ocean. As for the SST field, the Labrador Sea shows a peculiar behavior compared to the North Atlantic in all CO_2
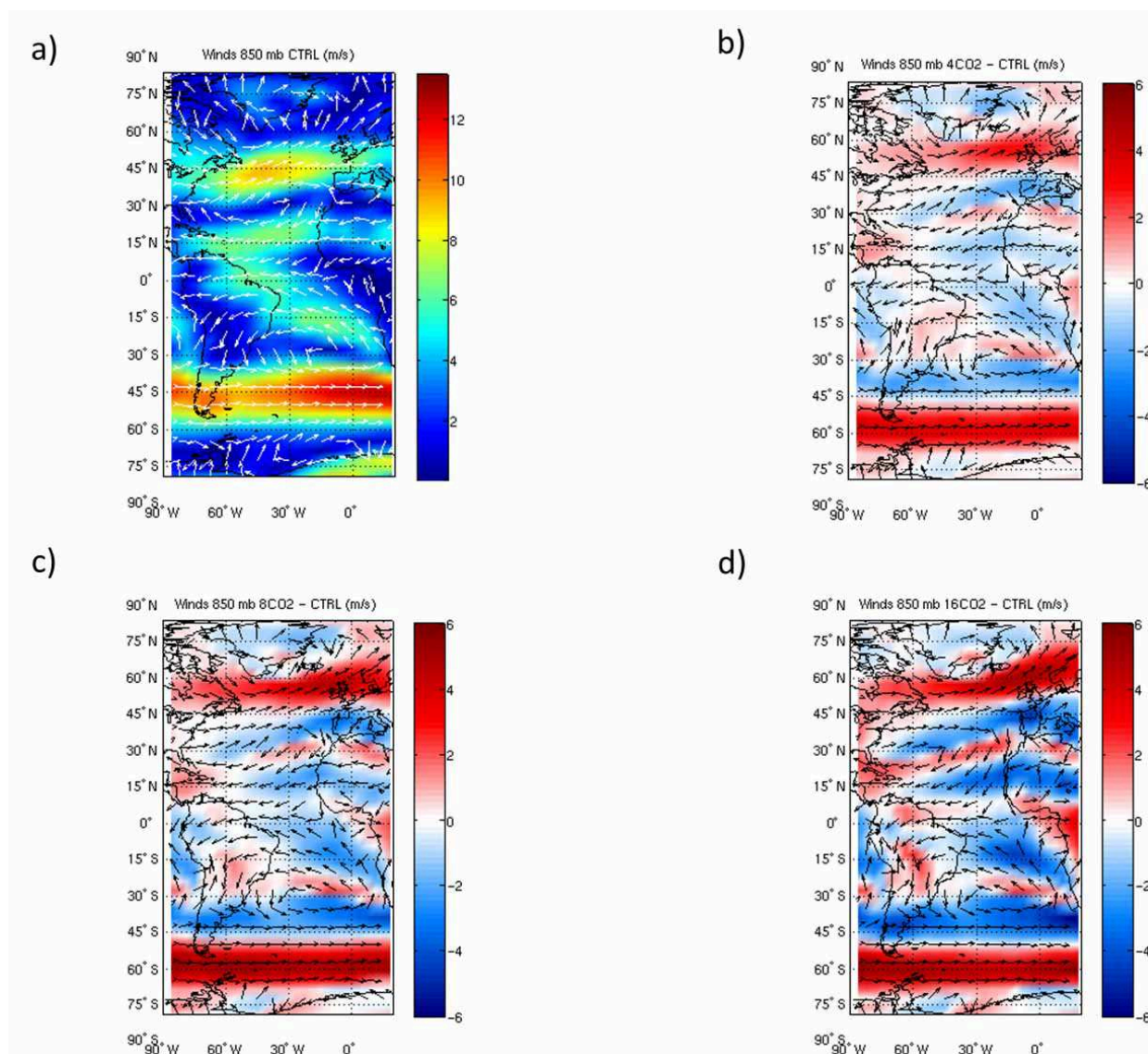
Figure 3.5: Annual mean 850 mb winds computed for (a) CTRL experiment (arrows give direction and shaded the intensity (m/s)) and differences between (b) $4xCO_2$, (c) $8xCO_2$ and (d) $16xCO_2$ and the CTRL simulation (arrows give wind direction in $4xCO_2$, $8xCO_2$, $16xCO_2$ experiments and shaded the intensity differences $4xCO_2$-CTRL, $8xCO_2$-CTRL, $16xCO_2$-CTRL (m/s)).
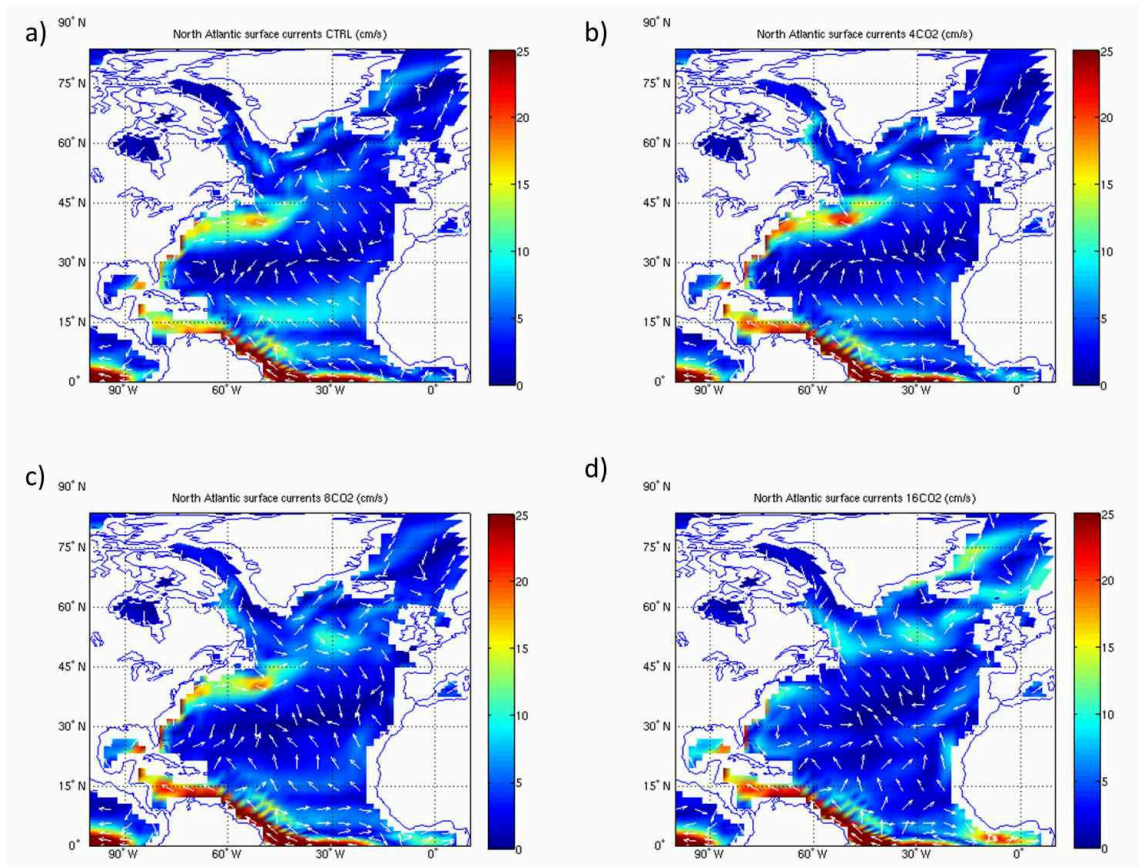
Figure 3.6: Annual mean surface currents (arrows give direction and shaded the intensity (cm/s)) computed for (a) CTRL (b) 4xCO_2, (c) 8xCO_2 and (d) 16xCO_2 experiments.

simulations: there is a significant SSS decrease with respect to the CTRL (table 3.1) (fig. 3.7b,c,d) . Except for the area north of 45°N, the SSS increases everywhere inside the Atlantic basin (fig. 3.7b,c,d) due to an excess of the evaporation over the precipitation, as shown in fig. 3.8. The case of $16CO_2$ experiment is different (fig. 3.7d) since it shows the formation of a salinity front close to 45°N with fresher waters to the north and saltier to the south. Surface waters less saline than in the CTRL could be due, as for the SSTs, to the changed surface currents (fig. 3.6d). Manabe and Stouffer (1994) in their $4CO_2$ simulation found a marked SSS increase over the tropical Atlantic and a pronounced reduction of surface salinity at high latitudes as a result of increased supply of fresh water.

The surface freshwater fluxes, computed as the difference between evaporation minus precipitation (E-P), influence the ocean sea surface salinity (fig. 3.8). The pattern shows an increased (decreased) freshwater flux at the Tropics (high latitudes) and a poleward shift of the regions with positive fluxes (fig. 3.8b,c,d). Positive (negative) freshwater flux tends to increase (decrease) the surface water salinity.

The areas where the surface salinity reaches its maximum (minimum) correspond to areas with maximum (minimum) evaporation (figs. 3.9, 3.10). The maximum evaporation values in the CTRL case are located in the subtropical band and along the Atlantic Ocean western boundary where the surface waters are warmer than the air above (fig. 3.9a). The $4CO_2$ and $8CO_2$ experiments do not show any striking difference with respect to the CTRL case except for the Labrador Sea where the evaporation decrease with increasing radiative forcing (-0.5 mm/d in $4CO_2$ experiment and -1 mm/d in $8CO_2$ experiment) (fig. 3.9b,c). In $16CO_2$ experiment the decrease in evaporation becomes larger (-2 mm/d) (fig. 3.9d). Southward of 30°N instead the evaporation largely intensifies (about 2mm/d more with respect to the CTRL value, fig. 3.9d) influencing the SSS (fig. 3.7d).

Fig. 3.10 shows for the CTRL case the maximum precipitation values associated with the strong convection in the ITCZ while lower values reflect
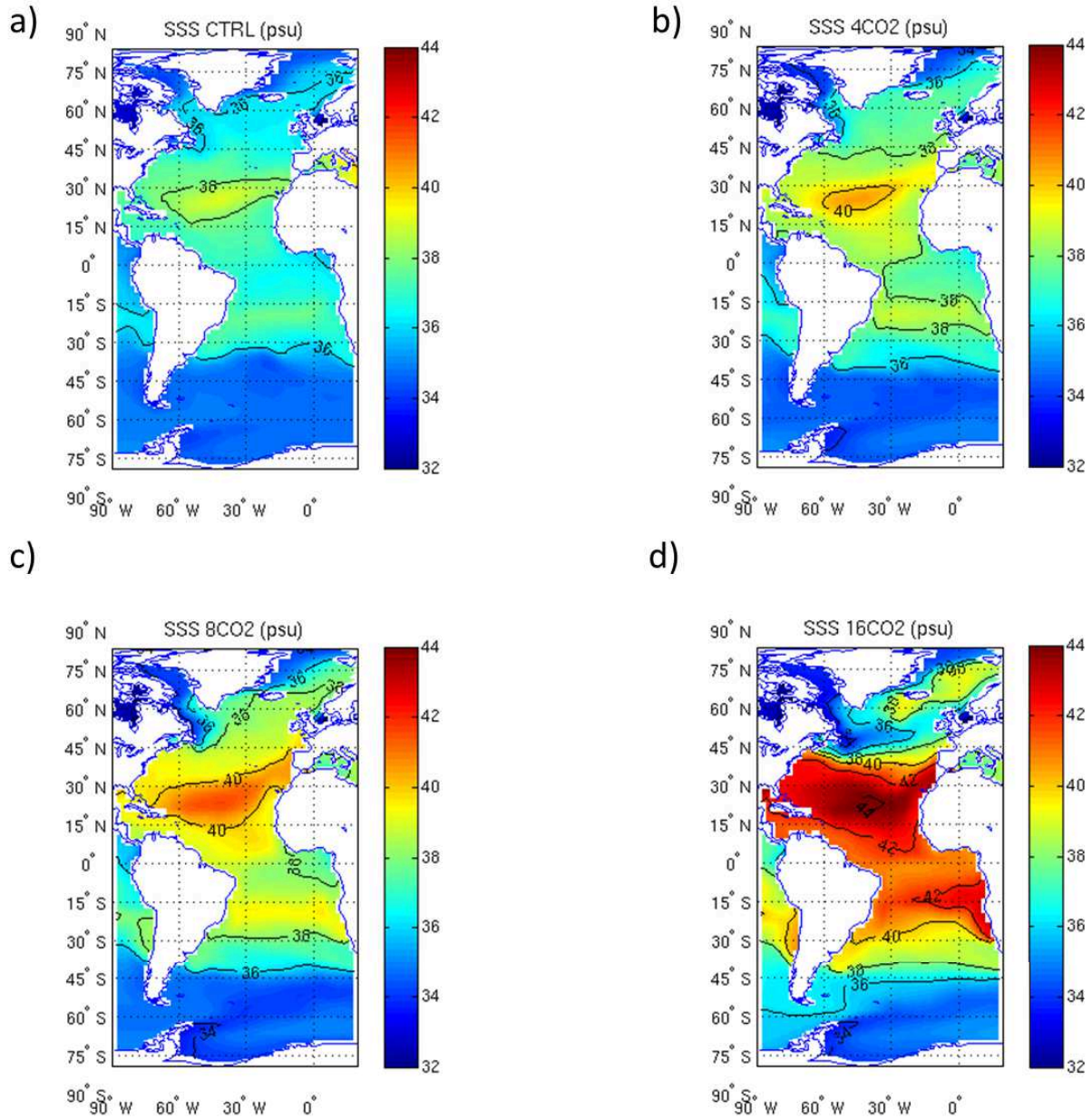
Figure 3.7: Annual mean SSS (psu) computed for (a) CTRL, (b) 4xCO_2, (c) 8xCO_2 and (d) 16xCO_2 experiments.
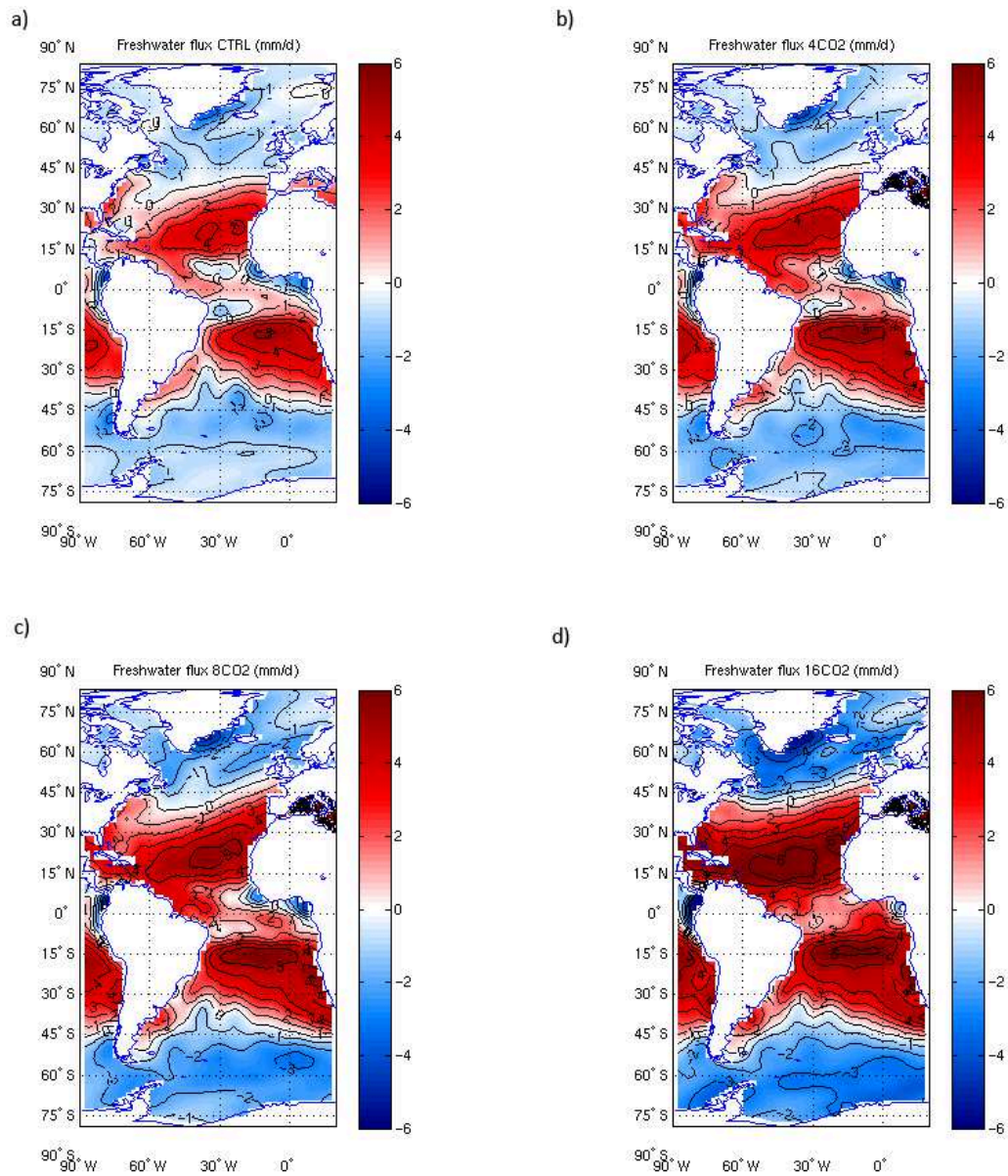
Figure 3.8: Annual mean freshwater flux (computed as evaporation minus precipitation) (mm/d) computed for (a) CTRL (b) 4xCO_2, (c) 8xCO_2 and (d) 16xCO_2 experiments
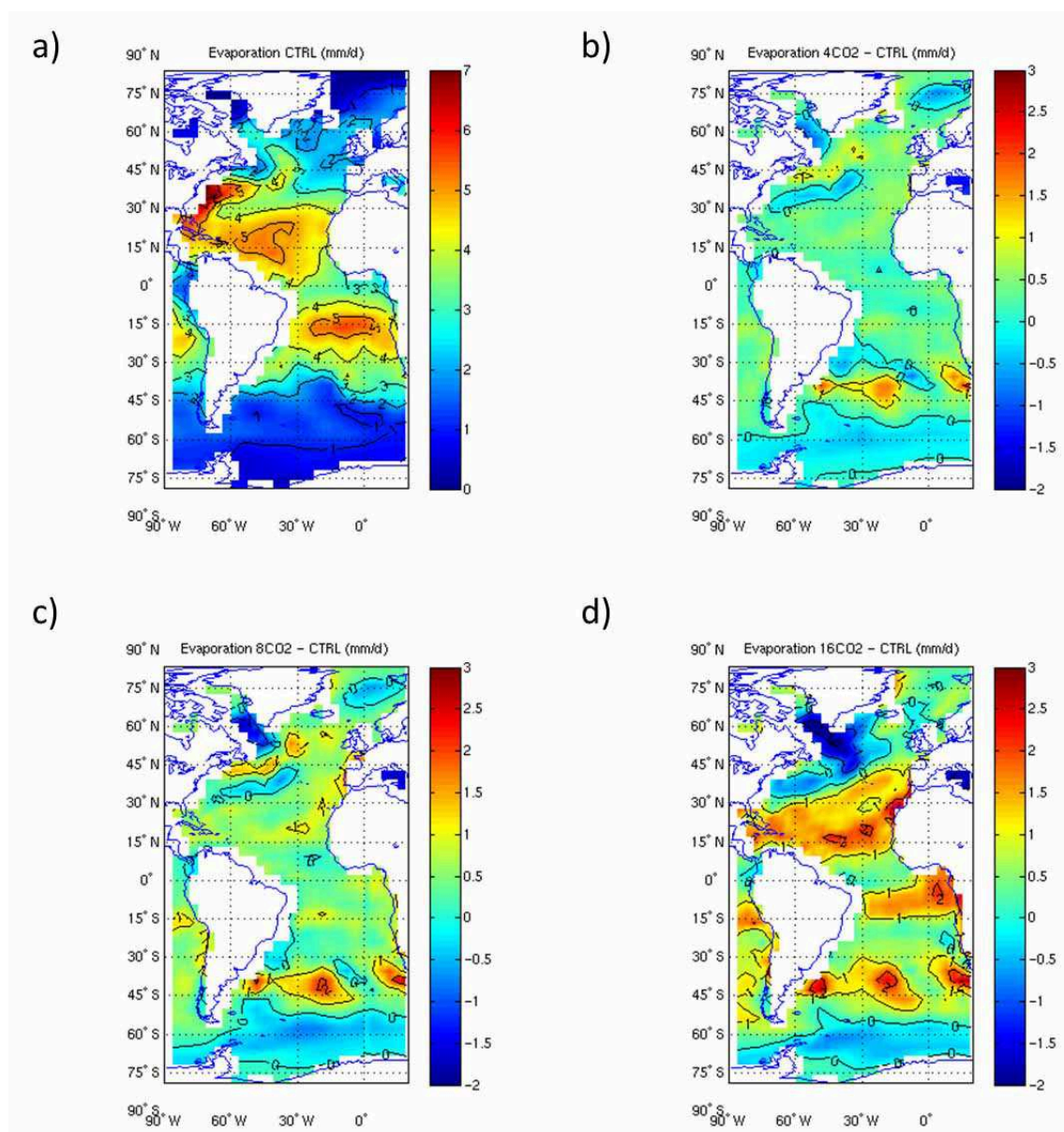
Figure 3.9: Annual mean evaporation (mm/d) computed for (a) CTRL experiment and differences (mm/d) between (b) 4xCO_2, (c) 8xCO_2 and (d) 16xCO_2 and the CTRL simulation.

the distribution of high pressure areas (fig. 3.4a). Over the polar regions the atmospheric moisture content is very low and the amount of precipitation is small. As response to the forcing, the precipitation over the ocean increases at high latitudes and decreases at sub-tropical band. The increased precipitation over the land in response to the enhanced CO_2 concentration does not influence the ocean density through an increased freshwater input since the hydrologycal cycle lacks the river runoff contribution. In the tropical Pacific a more stable tropospheric column combined with a more stable ocean-atmosphere interface (with SST colder than the air above) and a cloud feedback drastically decreases the convective component of the precipitation (Cherchi et al, 2008).

The low latitude increase in evaporation and the high latitudes precipitation enhancement are in good agreement with several global warming studies suggesting a changed hydrological cycle in a warmer world (Kattemberg et al , 1996; Thorpe et al, 2001; IPCC, 2007).

The freshwater input due to Arctic sea-ice melting influences as well the salinity pattern at high latitudes. In the present simulations the enhanced radiative forcing leads the North Pole sea-ice cap to melt, as mentioned above, although with different melting rate. The $4CO_2$ experiment shows a stabilization of Arctic sea ice volume after 86 years of simulation with a volume reduction of 99% with respect to the CTRL. In the $8CO_2$ and $16CO_2$ experiments the North Pole is completely free of ice after 69 and 17 years, respectively (fig. 3.11). The sea ice melting in northern latitudes releases freshwater at the rates of 0.01 Sv , 0.02 Sv and 0.06 Sv in $4CO_2$, $8CO_2$ and $16CO_2$ experiments , respectively (table 3.1). It is important to note that in $4CO_2$ and $8CO_2$ experiments the freshwater input due to sea-ice melting is much smaller than the freshwater forcing used in the classical 0.1 Sv hosing experiments (Stouffer et al, 2006), while in the $16CO_2$ experiment is almost comparable being the 60% of 0.1 Sv. As described in chapter 2, the coupled model used does not include a land-ice component. In the event that the land-ice melting had been considered, the freshwater input obtained
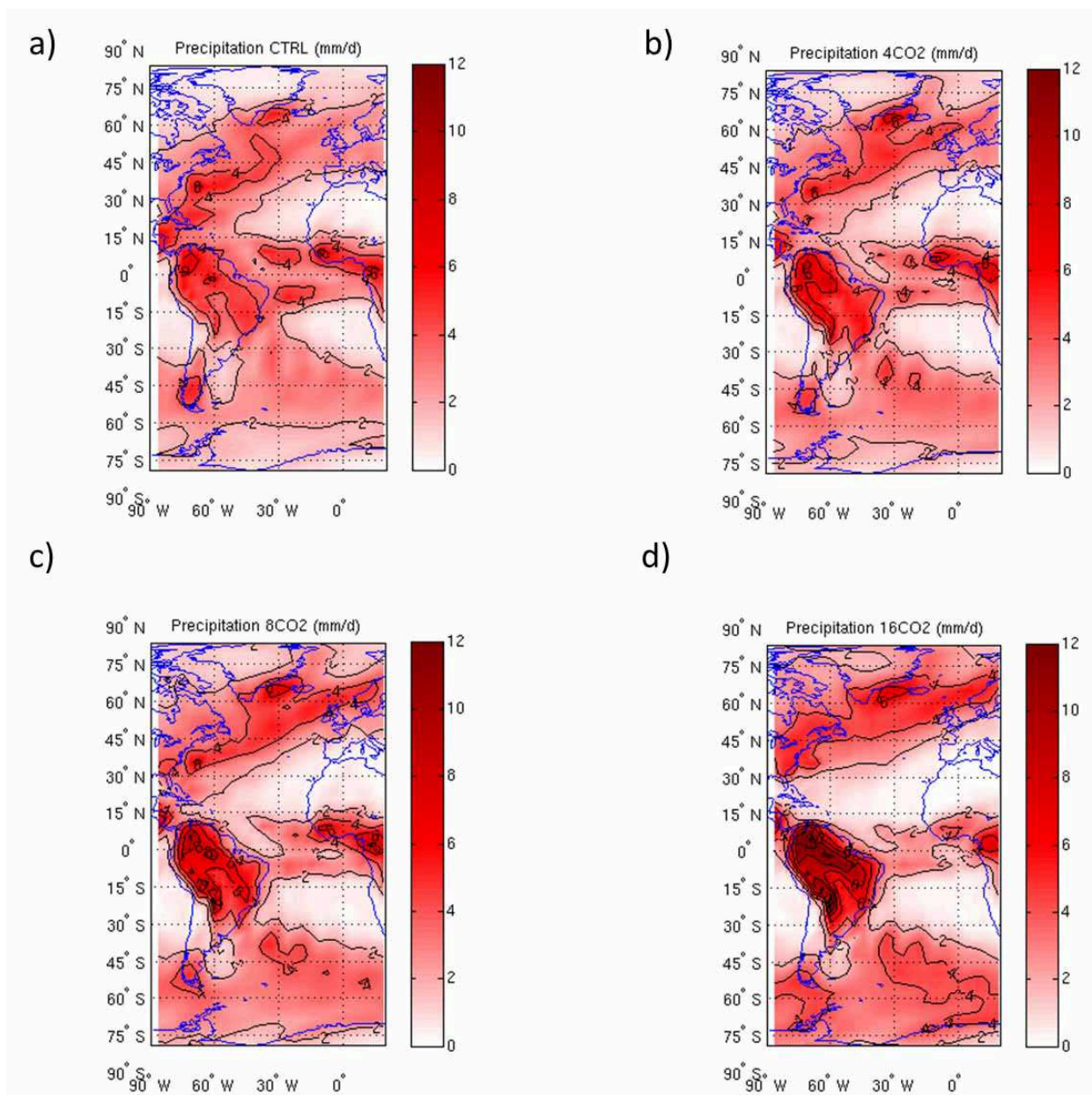
Figure 3.10: Annual mean precipitation (mm/d) computed for (a) CTRL, (b) 4xCO_2, (c) 8xCO_2 and (d) 16xCO_2 experiments.
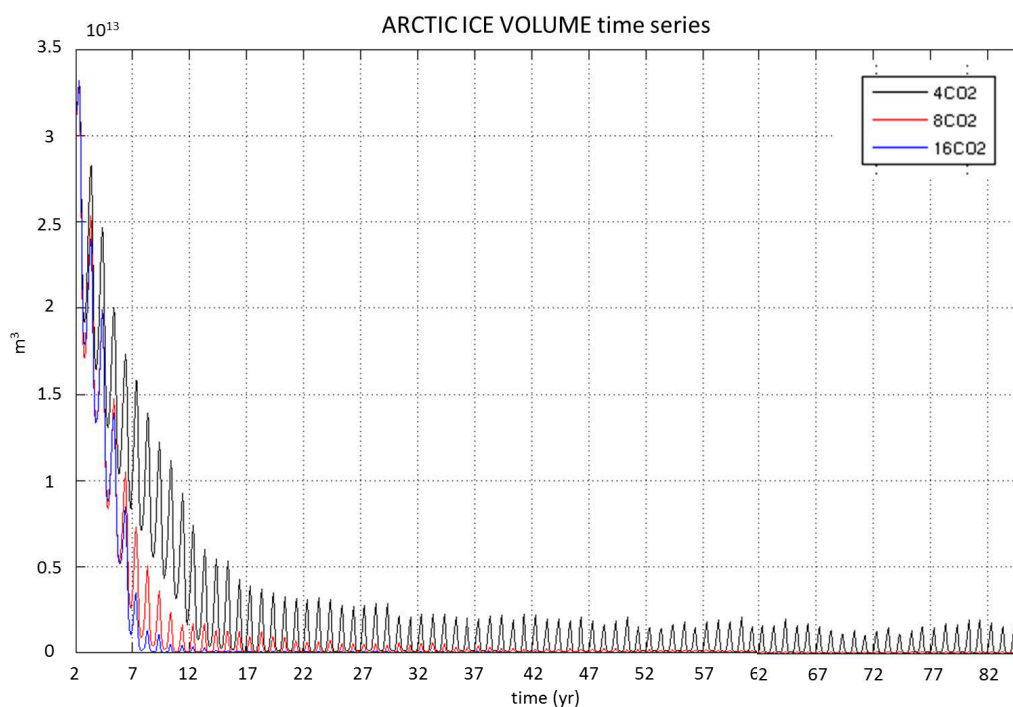
Figure 3.11: Time series of Arctic sea-ice volume computed for the first 86 years of $4xCO_2$ (black line), $8xCO_2$ (red line) and $16xCO_2$ (blue line) experiments

in the CO_2 simulations at high latitudes in the Altantic Ocean would have been greater. Estimating the Greenland ice-sheets melting in response to the increased CO_2 concentration applied in our simulations, considering the Greenland melting rate close to the one observed in the present days under global warming conditions (Zachos et al, 2008), in our CO_2 simulations we would obtain an additional freshwater input of 0.02 Sv, 0.05 Sv and 0.1 Sv in $4CO_2$, $8CO_2$ and $16CO_2$ experiments, respectively, if calculated over the time period needed to the North Pole sea-ice cap to stabilize.

3.3   Ocean vertical structure mean state

Salinity and temperature fields also show changes in their vertical profile with increasing forcing. Fig. 3.12 shows the Atlantic temperature and salinity zonal mean pattern for all experiments (Fig. 3.12). The water column tends to become warmer and more saline as the CO_2 atmospheric concentration increases. The maximum of both warming and salinification is located within the upper 4000m in $4CO_2$ experiment, 3000m in $8CO_2$ experiment and 2000 in $16CO_2$ experiment. The greatest warming is at depth in the tropical areas since the surface does not warm up as much as the subsurface due to the evaporation by winds blowing over the ocean surface. This subsurface warming is a feature that develops in all the experiments but with different intensities ($+5°$C in $4CO_2$, $+10°$C in $8CO_2$, $+20°$C in $16CO_2$ experiments). The salinity vertical profile (fig. 3.12b,d,f,h) follows the temperature profile with saltier (fresher) waters in correspondence of warmer (colder) waters and the salinity maximum is located in correspondence of the temperature maximum ($+1$ psu in $4CO_2$, $+3$ psu in $8CO_2$, $+7$ psu in $16CO_2$ experiments). As Manabe and Stouffer (1994) pointed out, the enhanced subsurface warming and salinification may be due to a reduction in the upward advection of cold and fresh water in low latitudes as response to a weakened Atlantic deep circulation. The increased water cooling and freshening at depth (below 4000m, 3000m and 2000m in $4CO_2$, $8CO_2$ and $16CO_2$ experiments respectively) suggest changes in deep ocean circulation and deep waters formation at high latitudes (fig. 3.13).

The Atlantic thermohaline circulation is measured by the meridional overturning streamfunction (fig. 3.13) . Its mean pattern shows an ATHC intensity of about 30 Sv in the CTRL experiment, with the maximum value of 31 Sv at 1400m depth (fig. 3.13a). The ATHC obtained in the CTRL case shows an overturning cell overly strong if compared with the existing estimates of the present climate ATHC strength (about 21 Sv). This difference can be attributed to the anomalous large SSS in the convective areas of the North Atlantic due to the lack of river runoff contribution in the model hydrologycal
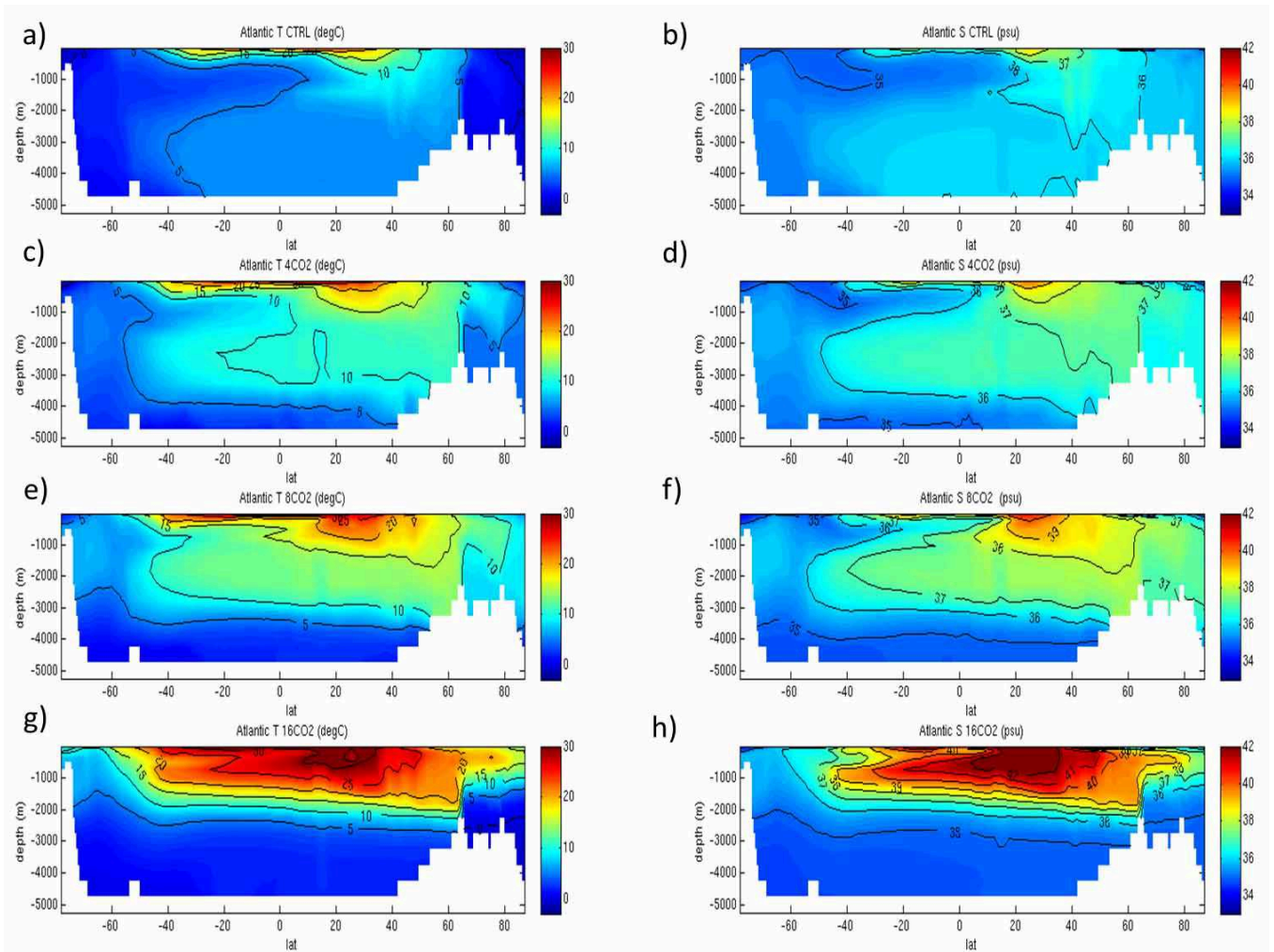
Figure 3.12: Annual mean temperature (°C) and salinity (psu) vertical profile averaged in the Atlantic Ocean longitudes for (a,b) CTRL, (c,d) 4xCO_2, (e,f) 8xCO_2, (g,h)16xCO_2 experiments.

cycle which leads the waters to become more dense and to sink more vigorously. The northward flow in the upper 1400m transports warm and salty seawater to the high latitudes where it is cooled sinking to the deep ocean. The cold salty water then flows southward at 1500-3500m depth. The 30 Sv flow across 30°S indicates an intense inter-hemispheric water mass exchange. The anticlockwise cell beneath the ATHC cell is associated with Antarctic Bottom Water formation, while cells in the upper tropical Atlantic are wind-driven Ekman circulations. In response to increased atmospheric CO_2, the entire ATHC cell weakens and becomes shallower with respect to the CTRL (fig. 3.13b,c,d). The streamfunction max value lies between 40°N and 60°N in $4CO_2$ and $8CO_2$ experiments as in the CTRL (fig. 3.13a,b,c) (table 3.1). In $16CO_2$ experiment the maximum is located between 20°N and 40°N and the circulation at mid-latitudes weakens up to 12 Sv with respect to the CTRL case (fig. 3.13d).

The weakening of the ATHC in the CO_2 simulations is associated with a shift and a a weakening of the convective sites. Fig. 3.14 shows the mixed layer depths indicative of the water column depth over which the overturning happens. It has been computed for the winter time (JFM) when the mixed layer depth should reach its maximum value. The CTRL case shows the active convective sites in the Nordic Seas (close to 75°N) and in the Labrador Sea (close to 60°N). As the radiative forcing increases, the mixed layer becomes shallower and the convective sites weaken both in the Nordic Seas and the Labrador Sea (fig 3.14b,c,d). In particular, the 16xCO_2 experiment shows a collapse of the old convective sites and the formation of a new one, even though very shallow, south-east of Greenland (fig 3.14d).

The ATHC weakening under increasing CO_2 forcing is in agreement with several coupled model results (Dixon et al, 1999; Wood et al, 1999; Mikolajewicz and Voss, 2000; Thorpe et al, 2001; Schmittner et al, 2005; Gregory et al, 2005; Weaver et al, 2007). However, the ATHC response to a CO_2 forcing is highly model dependent: while some simulations show a weakening, others do not show significant reduction in the circulation strength (Latif et
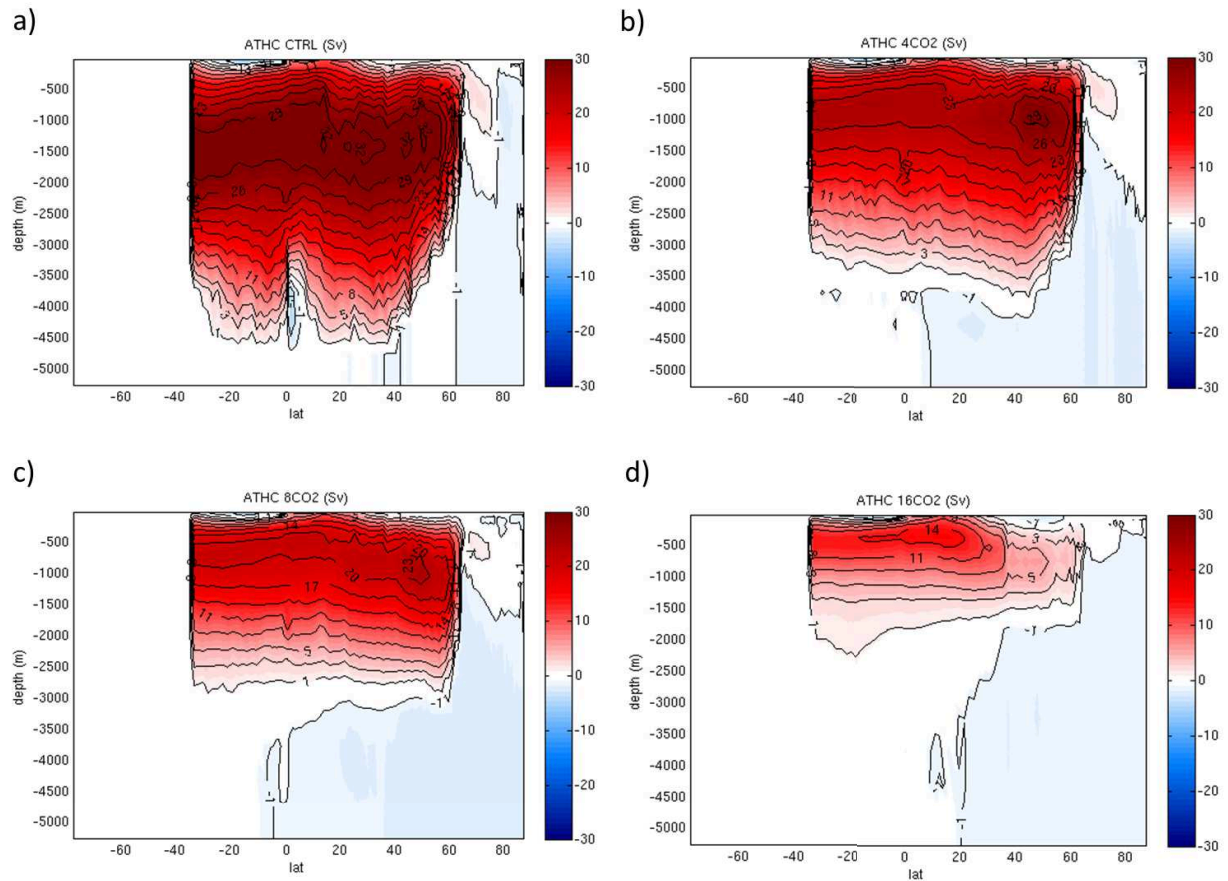
Figure 3.13: Annual mean meridional overturning streamfunction (Sv) computed in the Atlantic Ocean longitudes for (a) CTRL, (b) 4xCO_2, (c) 8xCO_2 and (d) 16xCO_2 experiments.
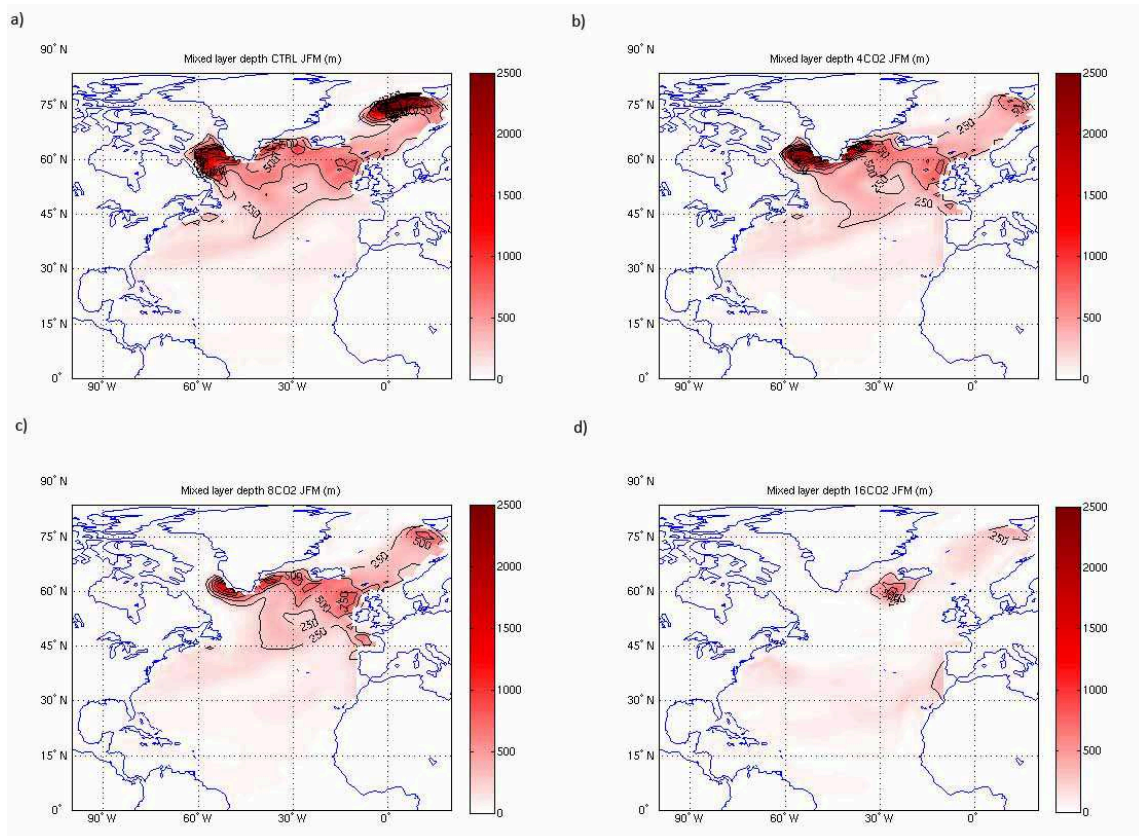
Figure 3.14: Annual mean mixed layer depth (JFM) (m) for (a) CTRL, (b) 4xCO_2, (c) 8xCO_2 and (d) 16xCO_2 experiments.

al, 2000) or simulate its complete shutdown under a $4CO_2$ forcing (Manabe and Stouffer, 1999). To date it is not clear whether heat or the freshwater fluxes at high latitudes dominate the Atlantic THC response to the radiative forcing (Manabe and Stouffer, 1999; Dixon et al, 1999; Gregory et al, 2005; Weaver et al, 2007). In the present study, because of experimental design and model configuration, we may consider that changes in heat flux dominate. In fact the freshwater input, due to sea-ice melting and precipitation, is weak, but anyway able to influence the salinity pattern making the waters lighter. Only in the most extreme case is the freshwater input due to sea-ice melting (0.06 Sv) may be considered comparable to the values used in the traditional hosing experiments (Stouffer et al, 2006). As the river discharge into the ocean is not taken into account in our CO_2 simulations a further likely small contribution of freshwater input is lacking.

Despite the extreme radiative forcing applied, the ATHC seems to be in a monostable equilibrium since the overturning cell undergoes to a progressive reduction and spatial reorganization but it never shows a complete shutdown. Many mechanisms may be responsible for this behavior. A reason may resides into an high latitudes freshwater input due to sea-ice melting not great enough to leads the ATHC over the "Stommel bifurcation point", the threshold beyond which no NADW formation can be sustained (Rahmstorf, 2000; Rahmstorf et al , 2005). The freshwater input due to sea-ice melting are smaller than the ones used in previous traditional water-hosing experiments. In our CO_2 simulations the consideration of the Greenland ice-sheet melting in the model could influence greatly the freshwater input at high latitudes leading the ATHC close to a collapse, in particular in the most extreme case. In the $16CO_2$ in fact the sum of the freshwater input due to sea-ice melting and the one due to Greenland ice-sheet melting (i.e. considering a Greenland ice-sheet melting rate close to the one observed in present-day global warming conditions, as discussed in the previous section) can reach likely the 0.16 Sv input. However, the analysis of the freshwater transport at 34°S in the Atlantic Ocean, as a measure of the salt-advection feedback

through the basin (Hawkins et al, 2011), shows always positive values for all our experiments (0.51 Sv, 0.50 Sv, 0,47 Sv and 0.57 Sv in CTRL,$4CO_2$, $8CO_2$ and $16CO_2$ experiments, respectively) suggesting a monostable regime of the ATHC. A continuous salt advection is in fact guaranteed through the southern boundary of the Atlantic basin feeding the formation of NADW at high latitudes. Nevertheless, more simulations with different CO_2 forcing are necessary to confirm the THC mono- or bi-stable behavior through an hysteresis curve, for example. This finding is in agreement with the one found by Hawkins et al.(2011) which shows using a coupled model study under present- climate conditions a positive freshwater transport (0.5 Sv) at 34°S for values of the hosing lower than 0.35 Sv in the North Atlantic (a stable ATHC). However, when the freshwater input exceeds that threshold the ocean shows a bistable regime.

The Atlantic heat transport depends on changes in the circulation and temperature pattern and it will changes in our experiments (fig. 3.15). The input of heat in the basin increases with respect to CTRL in $4CO_2$ and $8CO_2$ experiments. On the contrary it is similar to CTRL in the $16CO_2$ case (table 3.1,fig. 3.2). Since there is a large reduction in the heat transported by the ocean in the $16CO_2$ experiment, a balanced heat budget requires a reduction in the uptake of heat across the surface. The Atlantic cold tongue is not well represented in these simulations, a common bias of many GCM, and the ocean can not reduce its heat uptake by deepening the thermocline (Barreiro et al, 2008). Instead, the ocean decreases its surface heat absorption more or less uniformly between 15°S and the Equator (fig. 3.2). Due to a diminished vertical diffusivity through the water column (discussed in section 4.3) the magnitude of the maximum heat transport in the basin is 1.16 PW, 1.12 PW, 1.03 PW and 0.72 PW for CTRL, $4CO_2$, $8CO_2$ and $16CO_2$ cases, respectively, and it is located between 10°N and 25°N, the latitudes where the water column achieves its maximum warming (fig. 3.12a,c,e,g).
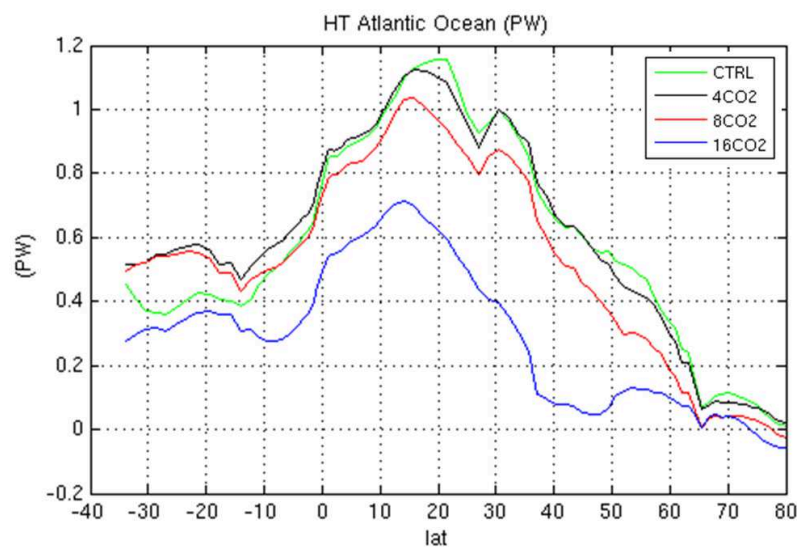
Figure 3.15: Annual mean heat transport (PW) computed in the Atlantic Ocean longitudes for CTRL (green line), 4xCO_2 (black line), 8xCO_2 (red line) and 16xCO_2 (blue line) experiments.

3.4   Tropospheric mean state

The temperature distribution in the atmosphere is fundamental to define the thermodynamic state and the wind structure in the atmosphere. Fig. 3.16 shows the temperature mean vertical structure for the CTRL and CO_2 simulations. The CTRL shows the highest temperatures in the inter-tropical regions depending on the largest amounts of solar radiation. The lowest temperatures occur over the polar regions with a strong pole-to-equator temperature gradient at the tropospheric bottom. The influence of the continents and oceans diminishes with height and at mid-tropospheric levels (500 mb = 50000 Pa) the isotherms are more uniform along a latitude circle. The fig. 3.16 shows, at the Equator, a rapid decrease of the temperature with height in the troposphere with a temperature difference between the ground and the tropopause (at 100 mb) of about 100°C (fig. 3.17) in the CTRL case. The tropopause varies in altitude from about 300 mb at the poles (not shown) to 100 mb at the equator where its height increases among the CO_2
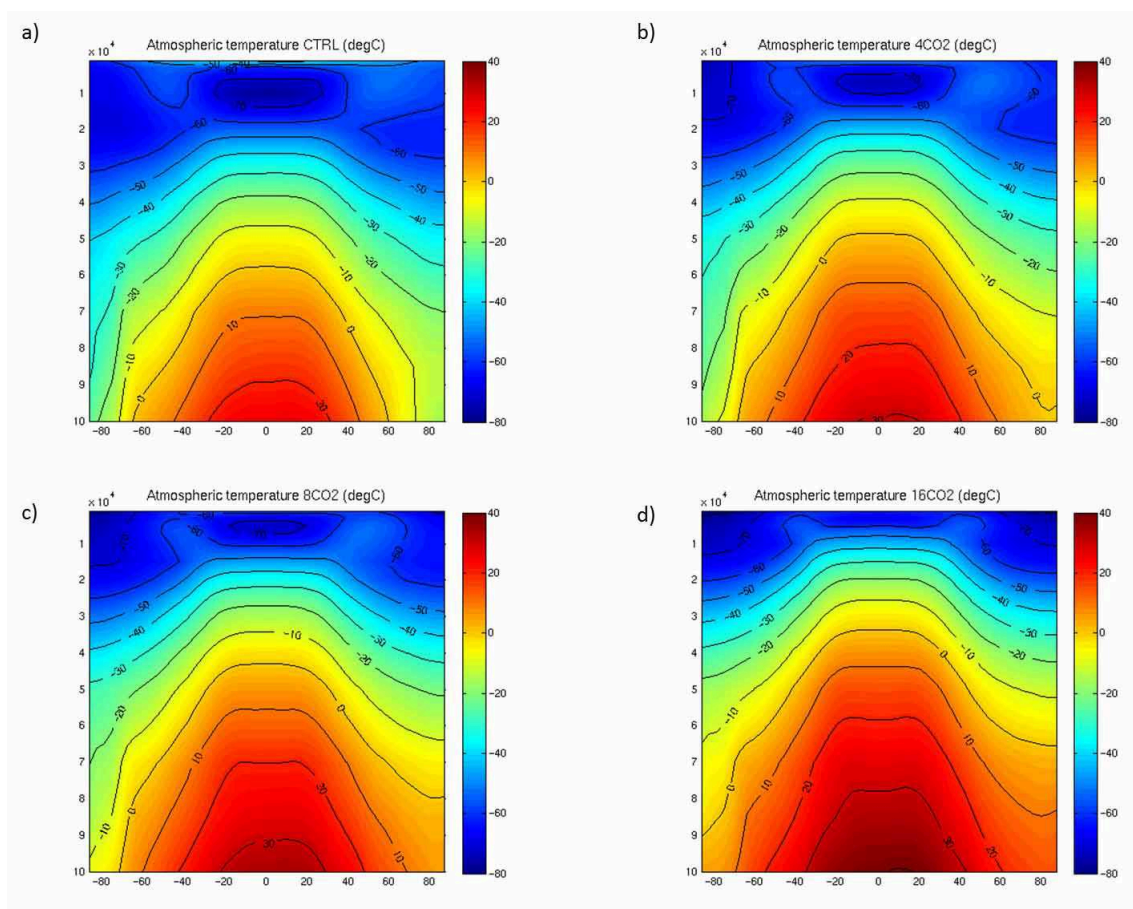
Figure 3.16: Zonal-mean cross sections of the global annual mean atmospheric temperature (○C) computed for (a) CTRL, (b) 4xCO_2 , (c) 8xCO_2 and (d) 16xCO_2 experiments

simulations (fig. 3.17).

In response to the enhanced greenhouse effect induced by increased atmospheric CO_2, the troposphere shows a global warming (fig. 3.16b,c,d) and a diminished meridional temperature gradient at the surface between high and low latitudes depending on the retreat of sea-ice. The polar ice-cap in fact acts reflecting back to the space the solar radiation at high latitudes keeping the atmospheric temperature relatively low. When the sea-ice melts, the albedo decreases, more sunlight is absorbed and the temperature tends

Figure 3.17: Vertical profile of the global mean atmospheric temperature (∘C) computed at the Equator for CTRL (green line), $4xCO_2$ (black line), $8xCO_2$ (red line) and $16xCO_2$ (blue line)experiments.

to increase. In the CO_2 experiments the high latitudes warm more than the tropics while in the upper troposphere the situation reve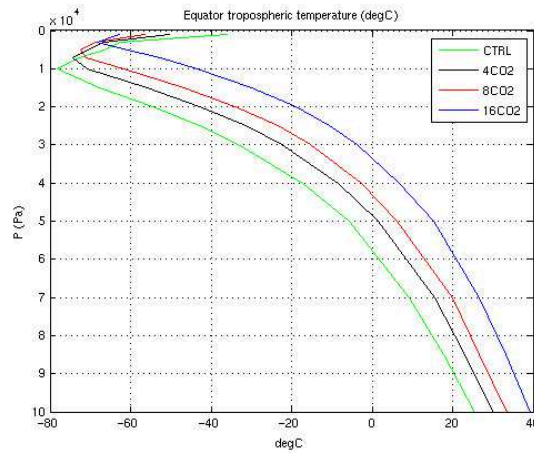rses (fig. 3.16b,c,d). As result of the global warming, the tropopause height rises (fig. 3.17), in accordance with both observations and climate model simulations (Kushner et al, 2001; Santer et al, 2003) .

In addition to a rise in the tropopause height, the CO_2 simulations show an intensification and a poleward shift of the mid-latitude jet streams (fig. 3.18b,c,d) as a consequence of thermal wind balance in the presence of stratospheric cooling and tropospheric warming, as suggested by several climate model simulations under IPCC scenarios (Kushner et al, 2001; Raisanen , 2003; Williams, 2006; Lorenz et at, 2007).

Fig. 3.19 shows the vertical velocity in the troposphere for CTRL and CO_2 simulations. The annual mean strongest rising motions are centered near 10°N associated with the mean position of the ITCZ. The equatorial belt is flanked in each hemisphere by sinking motions between about 20° and 40° latitude, followed by rising motions between 50° and 70° latitude, and weak sinking motions poleward 70° latitude. As the forcing increases,
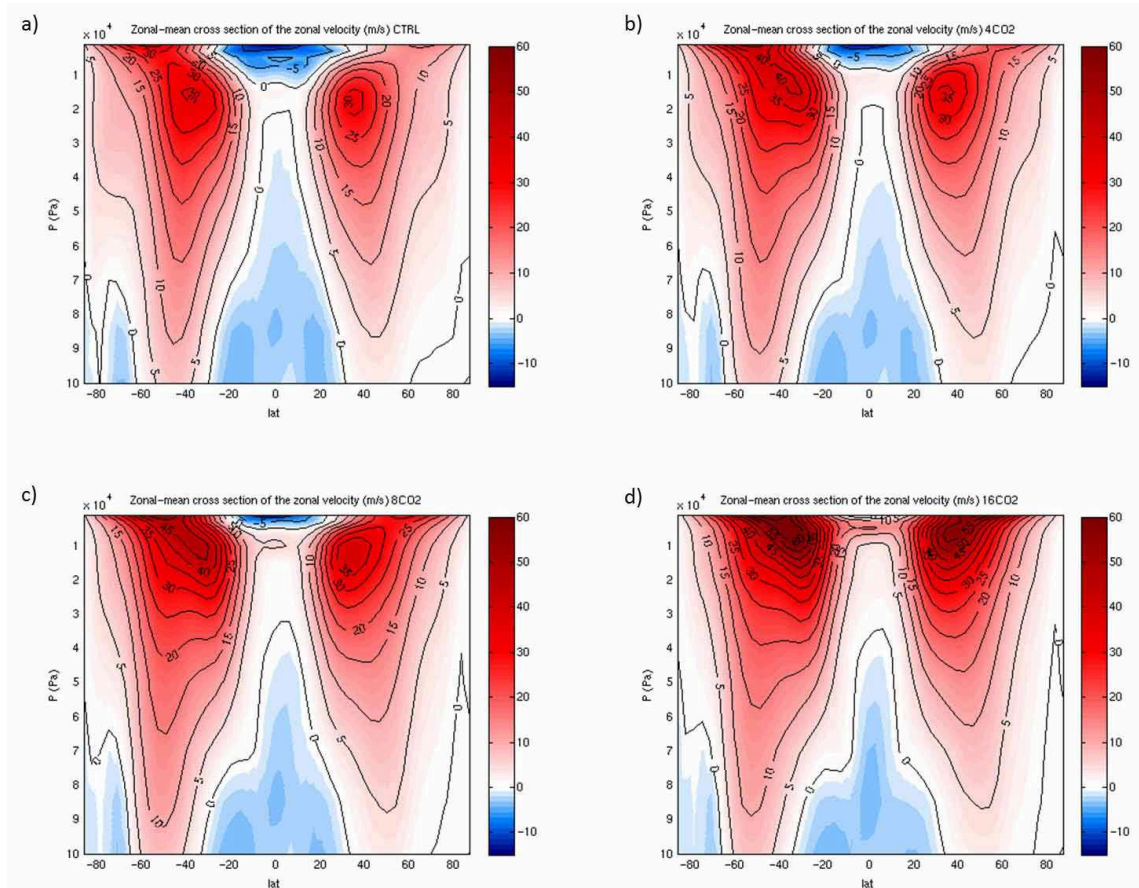
Figure 3.18: Zonal-mean cross sections of the zonal wind component (m/s) for global annual-mean conditions for (a) CTRL, (b) 4xCO_2, (c) 8CO_2 and (d) 16CO_2 experiments .

so do the vertical velocities at all latitudes (fig. 3.19b,c,d). The vertical velocity plays a key role in the vertical transport of the water vapor, with the maximum upward transport over the equatorial region, associated with the ascending branches of the Hadley cells, and the centers of maximum downward flux occurring in the subtropics where subsidence prevails.

The highest water vapor concentration is found in the equatorial regions (fig. 3.20) while it decreases strongly with latitude down to very low values over the polar regions. The global pattern of humidity reflects the temperature pattern (fig. 3.16) since the capacity of the atmosphere to retain water vapor depends strongly on the temperature. The water vapor decreases rapidly with the height. In the CTRL case, more than 50% of the water vapor is concentrated below the 850 mb surface, while more than 90% is confined to the layer below 500 mb (fig. 3.20a). The CO_2 simulations show an increased tropospheric water vapor concentration which extends upward and poleward, in agreement with the changes described in the vertical and meridional circulations.

Previous studies done using the same set of experiments revealed a precipitation rate increase not proportional to the water vapor increase, in agreement with the so-called "suppressant effect of CO_2" described by Allen and Ingram (2002), showing distinct contribution of thermodynamic and purely dynamic processes to the precipitation changes in the monsoon areas (Cherchi et al, 2011).

3.5   Conclusions

This chapter analyses the sensitivity of the North Atlantic Ocean and of the Atlantic THC to different CO_2 increase in the atmosphere. Increased atmospheric CO_2 concentration leads to warmer global climate with a warmer and more saline Atlantic Ocean. The Labrador Sea shows a distinctive behavior since it is subject to a freshening caused by changes in surface heat and freshwater fluxes.
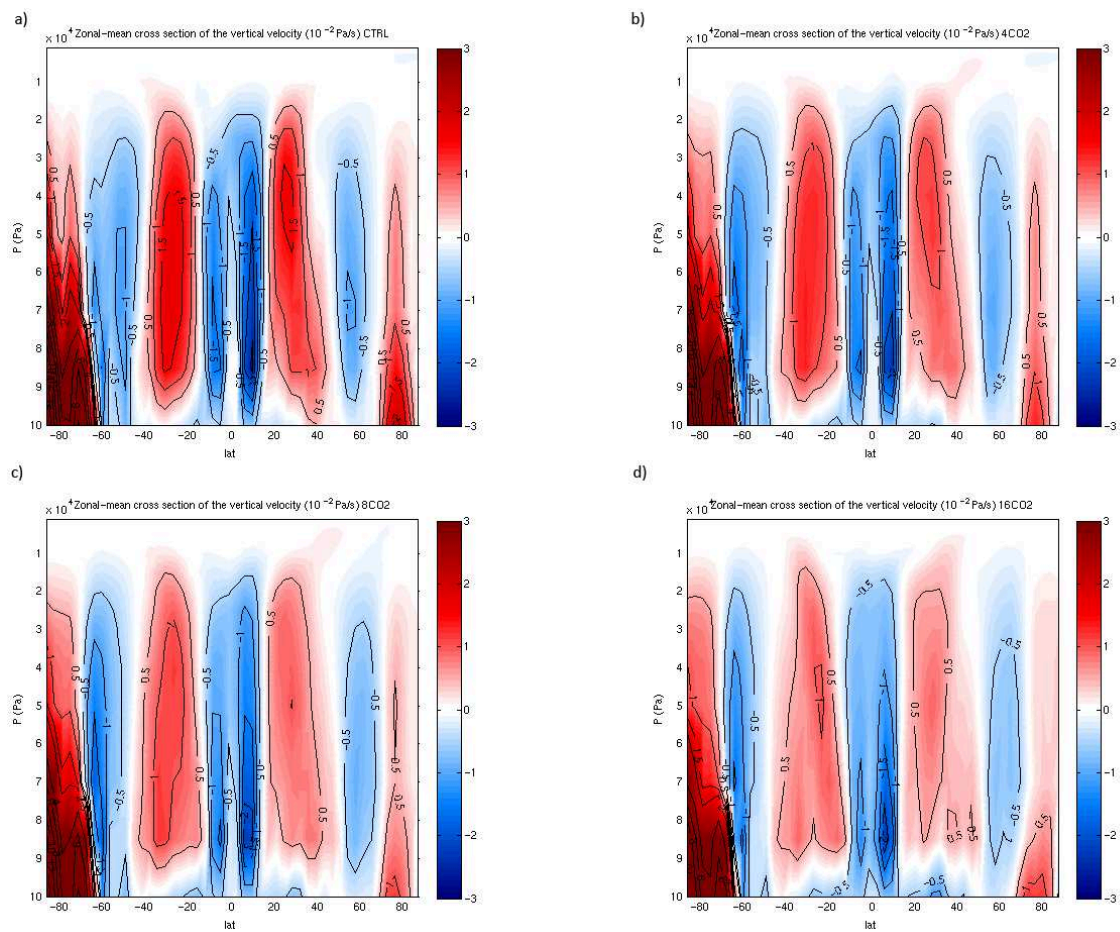
Figure 3.19: Zonal-mean cross sections of the atmospheric vertical velocity for global annual mean (10^{-2} Pa/s) computed for (a) CTRL, (b) 4xCO_2, (c) 8xCO_2 and (d) 16xCO_2 experiments
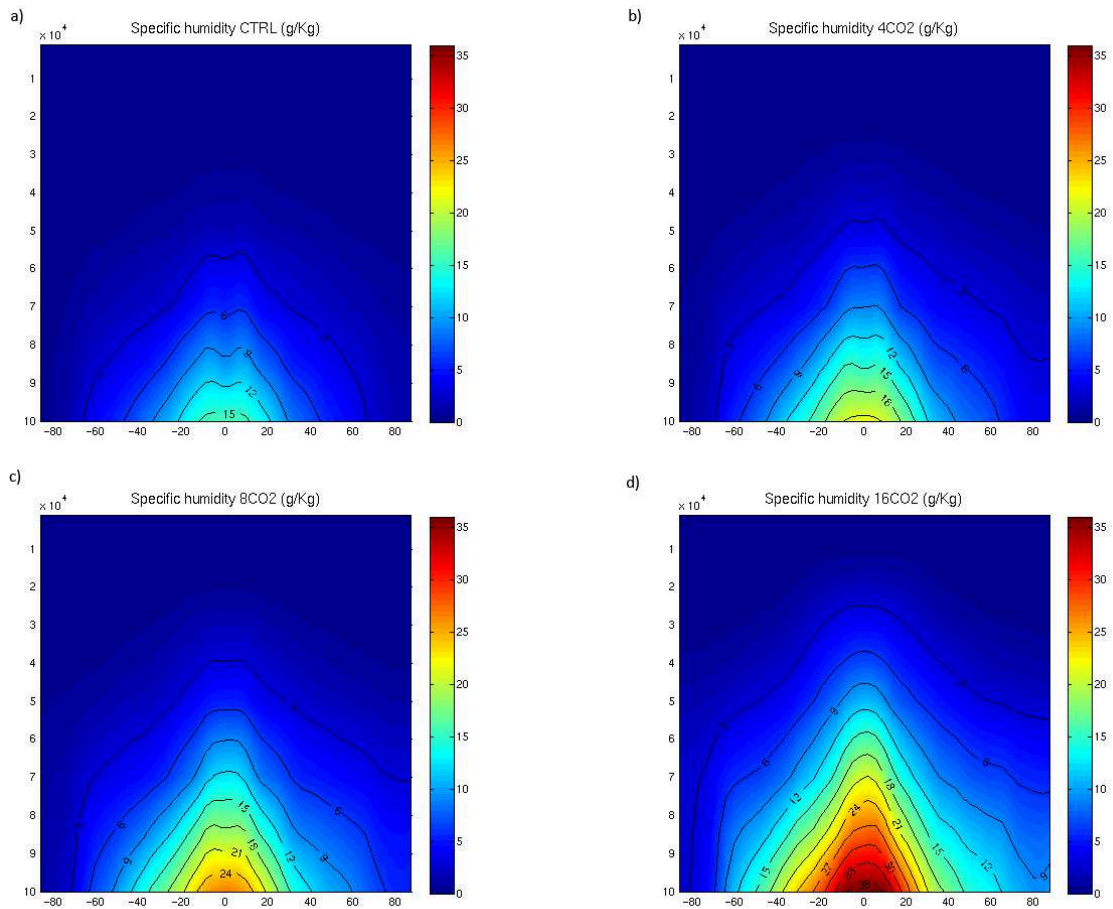
Figure 3.20: Atmospheric global annual mean specific humidity (g/Kg) computed for (a) CTRL, (b) 4xCO_2, (c) 8xCO_2 and (d) 16xCO_2 experiments

The sea-ice Arctic cap completely melts under global warming conditions in the two more extreme experiments, while it stabilizes at 1% of its initial volume in $4CO_2$ experiment. This melting induces a freshwater input in the North Atlantic of 0.01 Sv, 0.02 Sv and 0.06 Sv in $4CO_2$, $8CO_2$ and $16CO_2$ simulations, respectively, which is far enough from the freshwater forcing of the hosing-experiments, except for the $16CO_2$ where the value is almost comparable. As a land-ice component is missing, the model does not simulate the freshwater input of the land-ice melting which could be an important source of freshwater at high latitudes. Similarly, the river runoff contribution lacks in the hydrologycal cycle computation, possibly reducing the total input of freshwater into the ocean.

In response to the CO_2 forcing, the Atlantic THC weakens and becomes shallow, in agreement with previous studies (Dixon et al, 1999; Wood et al, 1999; Mikolajewicz and Voss, 2000; Thorpe et al, 2001; Schmittner et al, 2005; Gregory et al, 2005; Weaver et al, 2007). It never shows a collapse not even in the most extreme case since the freshwater input at high latitudes is probably far from the "Stommel bifurcation point", the threshold beyond which no NADW formation can be sustained (Rahmstorf, 2000; Rahmstorf et al , 2005). The ATHC shows in fact a monostable regime influenced by the continuous salt-advection through the southern boundary of the Atlantic basin. To analyze the ATHC hysteresis behavior a larger number of experiments with increasing CO_2 levels would be necessary.

In the most extreme case, the ATHC shows also a spatial reorganization, with the collapse of the convective sites in the Labrador Sea, because of a stratification of the water column and inhibition of NADW formation, but the creation of new convective sites southeast of Greenland. In the $16CO_2$ experiment the maximum overturning shifts at mid-latitudes. The heat transport is affected as well by the weakening of the ATHC and the stabilization of the water column with a decreased northward heat transport.

The decreasing heat advection into the high latitudes in response to the increasing CO_2 concentration is influenced by the weakening of the Gulf

Stream as well. The most extreme case shows an extinction of that current directly connected with the decreased wind stress over the ocean surface in the North Atlantic. Our finding is not in agreement with several studies suggesting the weakening of the Gulf Stream under global warming conditions mainly related to the weakening of the ATHC (Cai et al , 1996; O'Hare et al, 2005). According to the mentioned studies, the Gulf Stream can be created without explicit wind forcing being generated by bottom pressure torque effect (Gill and Bryan, 1971; Greatbatch et al, 1991). Although our analysis shows a Gulf Stream intensity directly connected with the wind forcing over the North Atlantic sector, we can not exclude a possible dependence of that current from the ATHC. Further studies should be done in order to evaluate the barotropic and the baroclinic components of the ATHC.

In the atmosphere the greenhouse gas properties of the water vapor, combined with that of the CO_2, influence the tropospheric temperature, subjected to a warming at all levels and latitudes, and the Earth's surface radiative balance. A changed tropospheric temperature pattern causes a tropopause height increase and a wind pattern variation, as suggested by several studies (Kushner et al, 2001; Raisanen , 2003; Williams, 2006; Lorenz et at, 2007). In the upper troposphere, the jet-streams intensify and shift poleward while at the atmosphere-ocean surface the westerlies become weaker and more zonal at mid-latitudes.

Chapter 4

The Atlantic Thermohaline circulation under extreme climate conditions

4.1 Introduction

The understanding of the physical mechanisms driving the Atlantic THC is an important theme in the scientific community and the main results are still controversial. Historically, the first candidate as driving mechanism for the thermohaline circulation has been identified in the meridional density gradient between low and high latitudes. Stommel (1961), using a box model, was the first to define the Atlantic THC as essentially a gravity-driven current system facilitated by meridional density gradient in the North Atlantic. The density contrast between the Northern and Southern Hemispheres has been taken into account later(Rooth, 1982; Scott et al, 1999; Klinger et al, 1999). With the aid of an ocean GCM, Rahmstorf (1996) identified a linear relationship between thermohaline overturning circulation and the inter-hemispheric meridional density difference. Similar results were obtained by Thorpe et al. (2001) using a coupled ocean-atmosphere general circulation model in a range of climate change simulations: a good linear

relation was found between the Atlantic THC strength and the meridional gradient of steric height (equivalent to column-integrated density) between 30°S and 60°N.

Later on, the relation between meridional density gradients and Atlantic THC strength has been widely investigated by many studies (Nilsson and Walin, 2001; Nilsson et al, 2003; Kuhlbrodt et al, 2007; De Boer et al, 2010; Wang et al, 2010) but with controversial results. Among them, Wang et al. (2010), using the SODA reanalysis from 1974 to 2005, found that the ATHC's strength is strongly related to the meridional density gradient between the sub-polar and sub-tropical North Atlantic Ocean, with a positive correlation coefficient of 0.52 (above the 99% significance level). On the contrary, De Boer et al. (2010), using a set of experiments with the MOM4 OGCM coupled to an energy-moisture balance model, found a negative correlation between the ATHC and the meridional density gradient in the Atlantic regardless of whether the density difference was computed at the surface or averaged over the upper ocean and from the Equator or 30°S.

The ocean vertical stratification influences the vertical diffusivity since more turbulent kinetic energy is required to displace water across a strong vertical density gradient (Gargett and Holloway, 1984). The vertical diffusivity in turn is strictly connected with the vertical mixing in the ocean interior (Welander, 1986; Nilsson and Walin, 2001; Nilsson et al, 2003). A strongly stratified ocean shows a smaller vertical mixing when the total rate of small scale mixing energy supply (from winds and tides) is kept constant (Kuhlbrodt et al, 2007). The majority of the current climate models uses constant diffusivities in the ocean interior, while others employ parameterizations for vertical diffusion (Gnanadesikan et al, 2006; Jungclaus et al, 2006b). The analysis of Nilsson et al. (2001,2003), conducted with a one-hemisphere ocean circulation model, shows a decreasing vertical diffusivity with an increasing water column stratification and a THC slow down in response to an increased equator-to-Pole density difference. Similar results were found in a box model by Marzeion and Drange (2006). The importance

of the influence of where the ocean stratification occurs on the Atlantic THC stability is an open matter of discussion. While previous studies focused on the main role of low latitude mixing (Munk and Wunsch, 1998), Marzeion et al. (2007) showed that high latitude mixing may be critical in controlling the vertical propagation of buoyancy anomalies imposed at the surface, and thereby influence stratification and circulation in the Nordic Seas.

Another distinct mechanism discussed as a driver for the thermohaline circulation is the wind-driven upwelling at the Southern Ocean. The Atlantic THC changes due to modifications in energy supply by the surface wind stress over the Southern Ocean were analyzed by many studies (Toggweiler and Samuels, 1995; Gnanadesikan, 1999; Saenko and Weaver, 2004; Gnanadesikan, 2007; Hirabara et al, 2007). In their numerical experiments, Toggweiler and Samuels (1995) found that the increased westerly wind stresses over the Southern Ocean enhance the remote northern sinking meridional overturning in the North Atlantic (i.e. Drake Passage effect). At the latitudes of Drake Passage (about 56°S-63°S) the westerlies induce a northward Ekman transport compensated by the southward flow primarily below the sill depth as a geostrophically balanced flow. However, Saenko and Weaver (2004) showed that there is not a direct relation between the input of mechanical energy by the wind and the ocean heat transport and that the same mechanical energy supply may results in different ocean heat transports. Furthermore, they found that the mechanical energy provided by the westerly winds in the Southern Ocean is important to drive the circulation cell associated with the formation of bottom water around Antarctica, rather than in driving the deep water flow and heat transport in the North Atlantic. Hirabara et al. (2007) then demonstrated that the Drake Passage effect should be understood through the global buoyancy flux changes. An enhancement of wind stress at the Southern Ocean surface leads to an increasing buoyancy gain hence to buoyancy anomalies which propagate into the North Atlantic. These anomalies intensify the zonal density gradient at high latitudes and enhance the North Atlantic overturning cell (Hirabara et

al, 2007).

The Southern Ocean wind stress, the ocean density and vertical diffusivity may by influenced by global warming conditions. Several studies analyze the response of the Atlantic THC to an increased radiative forcing (Manabe and Stouffer, 1994; Wood et al, 1999; Thorpe et al, 2001; Schmittner et al, 2005; Weaver et al, 2007; Marzeion et al, 2010) and, under 21st century scenarios based on IPCC criteria. Most of coupled models show a weakening of the North Atlantic deep water formation as mainly due to surface heat and freshwater fluxes (Cubash et al, 2001; Gregory et al, 2005). Some model simulations suggest, in fact, that the increased GHGs concentration causes a reduction of heat loss and an enhanced freshwater input at high latitudes making the surface waters less dense in the northern sinking regions (Gregory et al, 2005; Weaver et al, 2007). The warming anomaly, due to enhanced CO_2 atmospheric concentration, penetrates the ocean and increases the stratification at pycnocline depth. The stratification hence leads to a decreased diffusivities affecting the Atlantic THC strength (Marzeion et al, 2010). Furthermore, Cai et al. (2003) showed a poleward shift of the westerly winds and an increase of the buoyancy gain over the Southern Ocean as response to a global warming. The buoyancy flux changes at the Southern Ocean affect hence the enhancement of the Atlantic THC overturning in the context of the Drake Passage effect.

Among the mechanisms influencing the ATHC intensity, the effect of the Mediterranean Outflow (MOW) waters has been considered by many studies (Rahmstorf, 1998; Candela, 2001; Artale et al, 2003, 2006; Wu et al, 2007). In the Mediterranean Sea high-density waters form into the basin since there is an excess of evaporation over precipitation plus river runoff (Da Silva et al, 1994; Mariotti et al, 2002; Wu et al, 2007). Light waters from the Atlantic Ocean enter the basin through the Gibraltar Strait in the surface layers while dense and saline waters flow into the Atlantic Ocean at deeper layers. The MOW produces a tongue of very salty water (1psu saltier than the Atlantic inflow in the Mediterranean (Gerdes et al, 1999)) in the entire

North Atlantic at intermediate depths, identified throughout the whole North
Atlantic at depth of about 1100m (Candela, 2001). This input is able to
precondition the surface water column of the convective cells in the northern
North Atlantic (Artale et al, 2006).

Rahmstorf (1998), with the aid of a global ocean circulation model coupled
to a simple atmospheric energy balance model, investigated the impact of a
more saline MOW, due to a reduced freshwater input of 0.0027 Sv by the
Nile, in the Mediterranean basin, on the ATHC intensity. He showed that
the change in MOW was far too small to have have any noticeable effect.
However, the comparison between experiments with and without the MOW
input at the Gibraltar Strait showed the ATHC influenced by the Mediter-
ranean salty waters. In particular, the Atlantic THC increased its strength
with the maximum streamfunction variation located below the surface at
the Gibraltar Strait latitude (Rahmstorf, 1998). The overall maximum of
the (zonally integrated) overturning was therefore not affected, in contrast
to what happens when freshwater is added at the North Atlantic surface.
However, there is a substantial uncertainty covering the path of MOW in
the North Atlantic (Bower et al, 2002; Sparrow et al, 2002) and its im-
pact on deep water formation occurring in the North Atlantic (Reid, 1979;
McCartney et al, 2001).

The increasing freshwater input at high latitudes as result of the global
warming has been simulated by many studies with the aid of the water-hosing
experiments performed with models of intermediate complexity (EMICs), in-
cluding ocean general circulation models (OGCMs) coupled to highly simpli-
fied atmosphere (Stouffer et al, 2006; Barreiro et al, 2008). The sensitivity
of the THC to an external freshwater input has been analyzed applying to
the North Atlantic a uniformly water flux forcing between 50°N-70°N. The
freshwater perturbation of 0.1 Sv has been taken to represent the expected
freshwater input in a largeCO_2-induced climate change, for instance at 4
times the present-day's CO_2 atmospheric concentration (Wood et al, 1999;
Dixon et al, 1999). The 1.0 Sv freshwater forcing instead, used in some sim-

ulations, is comparable to the meltwater release during the last glacial era and the deglaciation (Clarke et al, 2003). The response of the THC to the freshwater perturbation was found to vary among the models in dependence of the magnitude and the duration of the perturbation (Stouffer et al, 2006). A strong weakening, by about 30%, or a total collapse of the North Atlantic overturning cell resulted when the freshwater input applied was equal to 0.1 Sv or 1.0 Sv, respectively (Stouffer et al, 2006), being anyway the THC response highly model dependent.

In our experiments, the freshwater input associated to sea-ice melting is small and large changes in the density properties are driven by increased temperature and associated changes in the heat fluxes. The only simulation showing a freshwater flux due to Arctic ice melting not negligible is the most extreme one, as already discussed in section 3.2.

The aim of this part of the study is to investigate the details of the processes at work in the simulated ATHC changes. In particular we have focused on three important mechanisms: the meridional density gradient between high and low Atlantic latitudes, the ocean vertical diffusivity and the Southern Ocean wind stress. The influence of the MOW on the ATHC is investigated as well in order to answer to the following scientific questions:

1. Which mechanisms control the oceanic circulation under extreme climates?

2. Which is the effect of the Mediterranean Outflow waters over the Atlantic THC intensity?

This chapter is organized as follows: section 4.2 analyzes the influence of the meridional density gradients over the Atlantic THC, section 4.3 investigates the relation between the Atlantic THC strength and the ocean vertical diffusivity, section 4.4 studies the impact of the Southern Ocean wind stress over the Atlantic THC intensity, section 4.5 analyzes the effect of the high-density MOW on the ATHC intensity and section 4.6 gives some concluding remarks.

4.2 Influence of density gradients

The North Atlantic annual mean surface sigma density field, calculated for each experiment, is shown in fig. 4.1. In $4CO_2$ and $8CO_2$ experiments, as well as in CTRL, denser waters are confined at high latitudes while lighter to the tropics. The comparison of sensitivity experiments with the CTRL shows that there is a uniform decrease of the sigma density inside the basin with the increase in atmospheric carbon dioxide (fig. 4.1a,b,c). In the $16CO_2$ experiment the sigma density pattern assumes a distinctive shape with the presence of a front close to 40°N with lighter waters (with sigma density less than $25\mathrm{Kg/m^3}$) northward of this latitude and denser waters southward (fig. 4.1d). At middle latitudes, between 40°N and 60°N, precipitation larger than evaporation (fig. 3.8d) helps in decreasing the surface water sigma density in addition to the contribution of freshwater from sea-ice melting.

The evaporation pattern (fig. 3.9) influences mainly the mid-latitudes leading to more dense waters between 15°N-40°N where the evaporation increases under global warming conditions. The sigma density changes are related as well to changes in the surface heat fluxes (fig. 3.2): the areas where lighter waters are located correspond to the regions of ocean heat uptake. As indicated by many studies, the Labrador Sea is a susceptible region to increasing CO_2 and the changes in heat and freshwater fluxes consequence of the global warming act to reduce the water column density and hence the formation of deep waters south of Greenland (Mikolajewicz and Voss, 2000; Weaver et al, 2007). Further, Wood et al. (1999) suggested that convection sites in the Labrador Sea and the Nordic Seas respond differently to global warming showing in their $4CO_2$ simulation a convection collapse in the Labrador Sea and a preservation of convection, or even reinforced, in the Nordic Seas. In the present study, the weakening of the Atlantic THC with increasing CO_2 (fig. 3.13) is mainly the result of the shut-down of the convective sites in the Labrador Sea (fig. 3.14) due to a decreased sigma surface density in the region of Labrador Sea Waters (LSW) formation. In $16CO_2$ simulation, the convective sites of Nordic Seas (fig. 3.14d) are still active, although
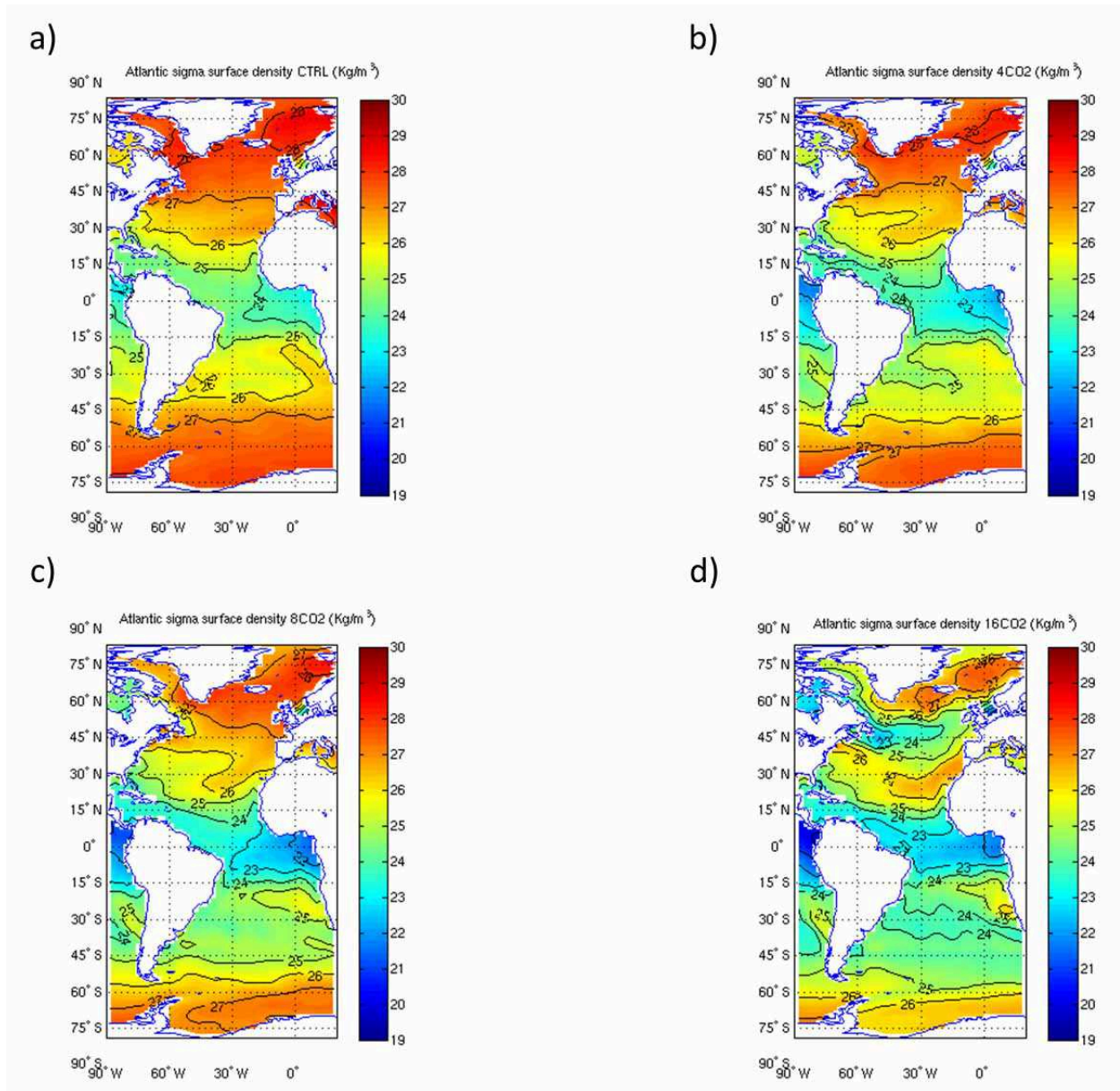
Figure 4.1: Annual mean surface sigma density (Kg/m^3) for (a) CTRL, (b) $4xCO_2$, (c) $8xCO_2$ and (d) $16xCO_2$ experiments.

with a diminished intensity. The warm and salty tropical waters, which do not reach the high-latitudes, stop close to the density front at 40°N and sink there. Only a weakened branch of the ATHC, not influenced by the upper level sigma density front at mid-latitudes, flows further north and sink in the Nordic Seas (fig. 3.13d).

Fig. 4.2 shows the Atlantic annual mean sigma density vertical profile for all the simulations computed for the first 500m. In CO_2 experiments, the water column becomes lighter than in the CTRL case, since it is subjected to a strong warming (fig. 3.12c,g,e), and the isopycnals hence deepen (table 3.1). At high latitudes, the sigma density decrease can be identified, between 60°N to 80°N, with the deepening of the 28 Kg/m^3 isopycnal in $4CO_2$ and $8CO_2$ experiments and its totally absence within the uppermost 400m in the $16CO_2$ simulation. The latter case suggests that no dense and deep waters form north of 60°N, as indicated by the meridional overturning streamfunction changes (fig. 3.13d) and the mixed layer depth pattern (fig. 3.14d). The surface freshening between 40°N and 60°N deepens to about 50-100m (fig. 4.2d). The surface sigma density front is also visible close to 40°N with lower sigma density values northward of this latitude (25Kg/m^3) and higher southward of it (26Kg/m^3).

The changes in the sigma density pattern lead to changes in the meridional density gradient between high and low latitudes. Fig. 4.3a shows the maximum value of the overturning streamfunction for all the simulations in the Atlantic basin, computed at 25°N, as a function of the meridional sigma density difference between 60°N and the equator. The Atlantic THC intensity has been computed at 25°N in order to take into account the streamfunction maximum value for all the simulations, since the ATHC maximum shifts equatorward in the $16CO_2$ experiment.

The choice of the latitudinal end-points of sigma density was made based on the model study made by Stommel (1961) which related the THC intensity to the meridional density difference in one hemisphere (i.e. North Atlantic). Fig. 4.3b differs from fig. 4.3a as the meridional sigma density gradients have
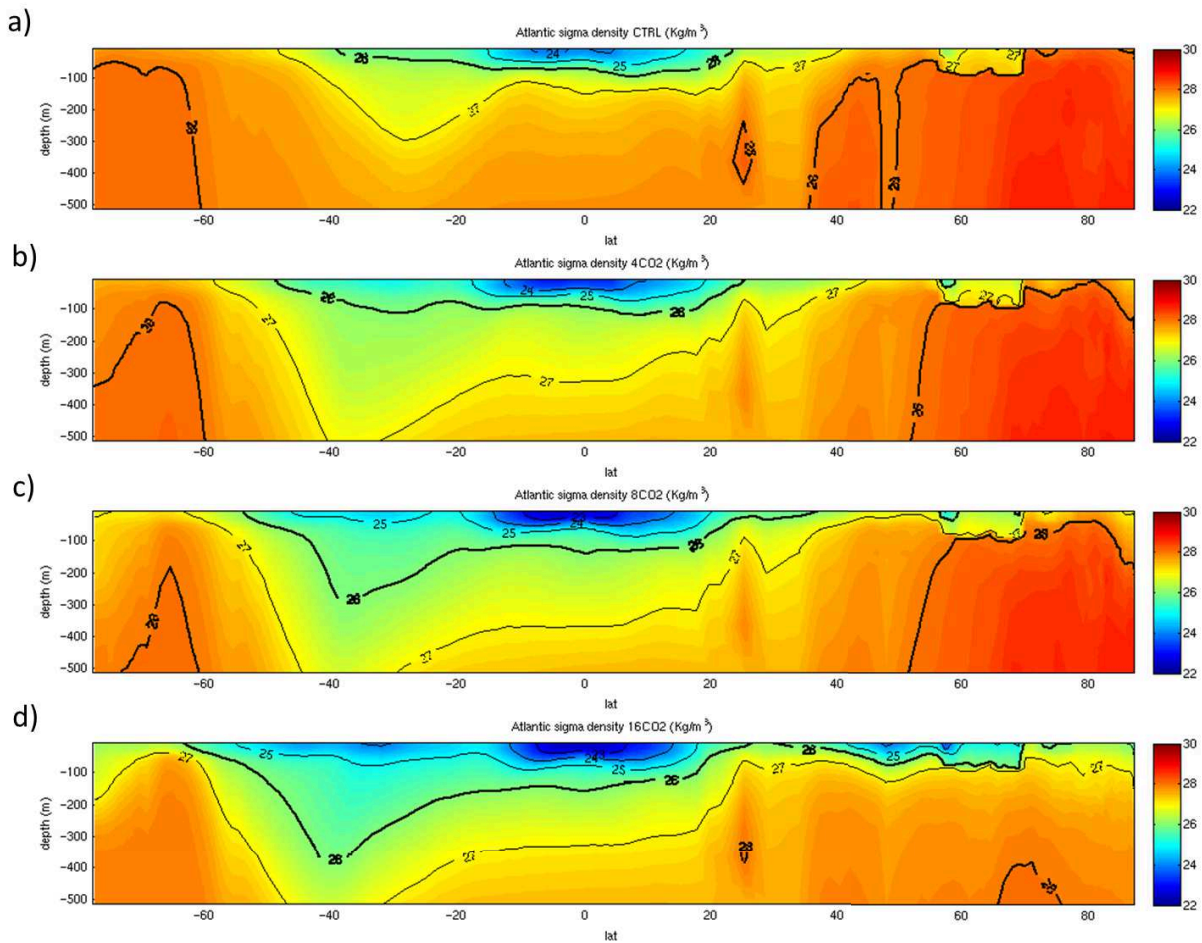
Figure 4.2: Vertical profile (0-500m) of annual mean sigma density (Kg/m^3) averaged in the Atlantic Ocean longitudes for (a) CTRL, (b) $4xCO_2$, (c) $8xCO_2$ and (d) $16xCO_2$ experiments.

been calculated between 60°N and the 30°S as done by many studies (Hughes and Weaver, 1994; Rahmstorf, 1996; Scott et al, 1999; Thorpe et al, 2001; De Boer et al, 2010).

The comparison between fig. 4.3a and fig. 4.3b evidences that the results are not sensitive to the choice of the southern end-point. In fig. 4.3 the sigma density has been vertically integrated over different water column depths (300m, 500m, 700m and 1000m) to test the sensitivity of the relationship between density gradients and the northward flow of the Atlantic circulation. As the radiative forcing increases, the Atlantic waters are subjected to a differential lightening with the tropical waters showing a bigger sigma density decrease than the northern ones. This leads to meridional density gradients that increase with respect to the CTRL values in the $4CO_2$ and $8CO_2$ simulations (fig. 4.3) independently of the depth of the considered water column and the southern end point. The $16CO_2$ simulation shows instead meridional density gradients almost equal to the CTRL ones, because the sigma density at high and low latitudes changes by similar amounts. Thus, we found an inverse relationship between the ATHC intensity and the meridional density gradients in $4CO_2$ and $8CO_2$ cases: as the CO_2 concentration is enhanced, the meridional density gradients increase and the ATHC weakens. This relation breaks in $16CO_2$ experiment since the meridional density gradients do not change significantly with respect to the CTRL case but the Atlantic THC shows a large weakening by more than half of its initial value. The similar meridional density gradients between the CTRL case and the $16CO_2$ experiment could be index of an hysteresis in the ATHC response to the radiative forcing, nevertheless to confirm this more simulations with different CO_2 forcing would be necessary.

Our findings differ from those of many other ocean general circulation model simulations that suggest a linear relationship between the Atlantic maximum overturning streamfunction and the meridional density gradients (Rahmstorf, 1996; Thorpe et al, 2001). Nevertheless this relationship can be reversed if the advective-diffusive balance in the thermocline is taken into
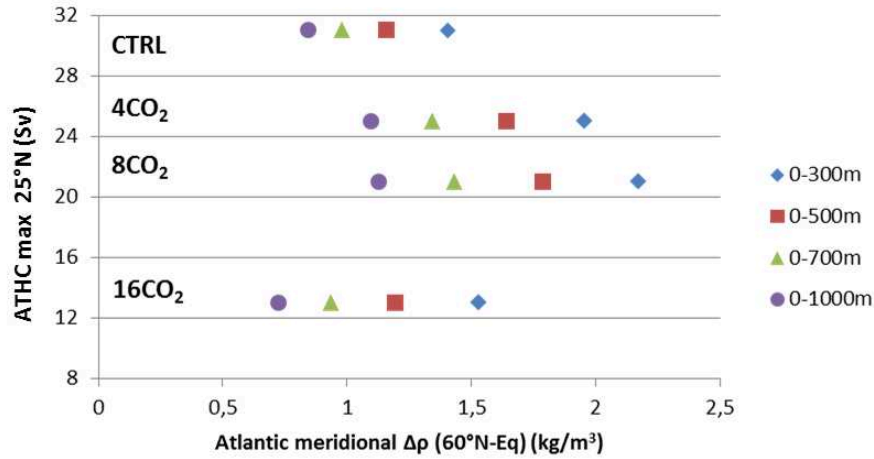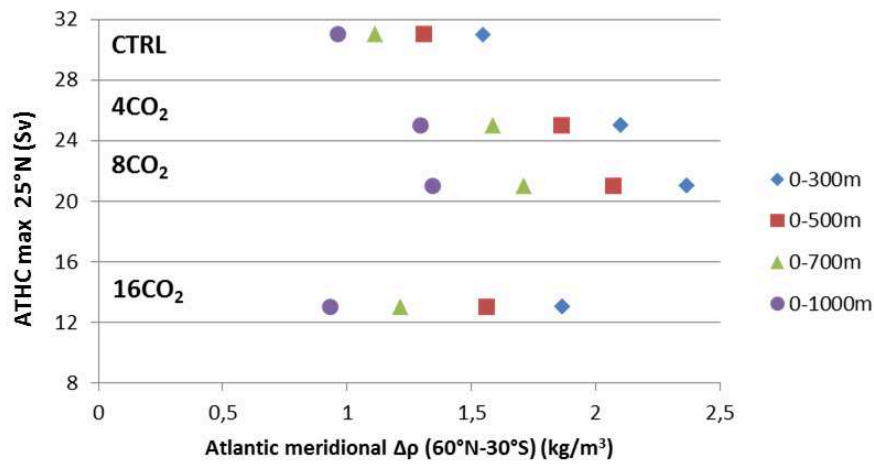
Figure 4.3: Max Atlantic THC intensity (Sv) at 25°N versus annual mean density gradient (Kg/m^3) computed between (a) 60°N and Equator and (b) 60°N and 30°S for CTRL, 4xCO_2, 8xCO_2 and 16xCO_2 experiments (from top to bottom). The density gradients have been integrated in different oceanic depths as evidenced in the legend.

account (Bryan, 1987). The results obtained in the present study are in good agreement with De Boer at al. (2010) although the authors found in the meridional pressure gradient a better indicator of the overturning instead of the meridional density gradient since it is proportional to zonal currents by geostrophy.

4.3 Vertical diffusivity and ATHC strength

The anti-correlation found between the ATHC intensity and the meridional density gradients in $4CO_2$ and $8CO_2$ simulations suggests to consider the diffusive processes in the ocean interior as a possible mechanism influencing the oceanic circulation strength (Bryan, 1987; Nilsson et al, 2003). Many studies showing a positive relation between density gradients and the ATHC strength use models with a constant vertical diffusivity in the ocean interior (Rahmstorf, 1996; Thorpe et al, 2001; Wang et al, 2010). Welander (1986), assuming an advective-diffusive balance in the thermocline, found, instead of a linear scaling law,

$$\psi \sim \Delta\rho^{1/3}k^{2/3} \tag{4.1}$$

where ψ is the strength of the ATHC, $\Delta\rho$ the equator-to-Pole density difference and k the ocean vertical diffusivity. In agreement with this law, if the vertical diffusivity is kept constant, the oceanic circulation enhances as a response to an increasing meridional density gradient. However, the vertical diffusivity is strongly influenced by the vertical density stratification and Nilsson et al. (2001) have shown that, if the vertical diffusivity decreases due to an enhanced ocean vertical stratification, the Atlantic THC weakens.

Fig. 4.4 shows the relation between the maximum value of the Atlantic THC at 25°N and the vertical diffusivity coefficients for the sensitivity experiments. The vertical diffusivity values are calculated as an annual mean over the North Atlantic basin (60°N-80°N) and over the first 2000m of the water column for the winter months (DJF). The time period was chosen to consider
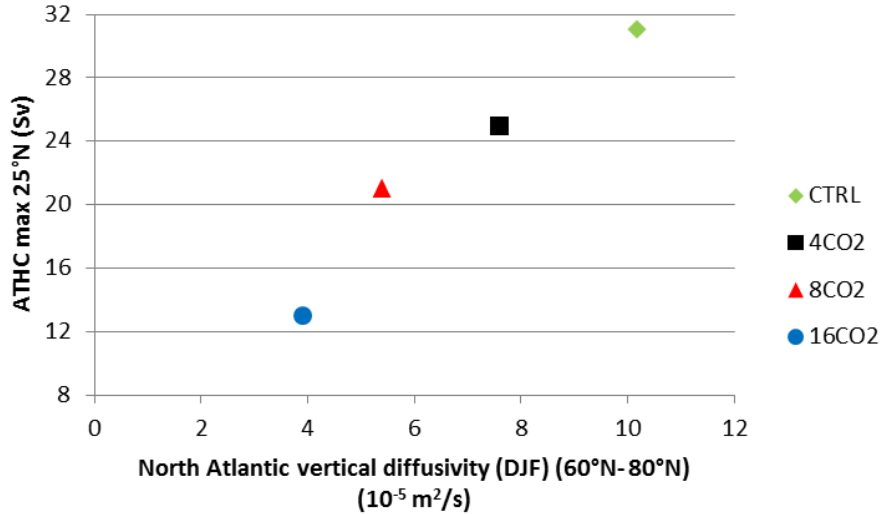
Figure 4.4: North Atlantic (averaged between 60°N-80°N) DJF mean vertical diffusivity (10^{-5} m^2/s) integrated between 100-2000m depth, versus ATHC max intensity computed at 25°N for CTRL (green diamond), $4xCO_2$ (black square), $8xCO_2$ (red triangle) and $16xCO_2$ (blue circle) experiments.

the occurrence of the maximum water column overturning while the depth level considered includes the location of the maximum Atlantic overturning circulation.

As the CO_2 radiative forcing increases the vertical diffusivity through the ocean interior decreases. The mechanism acting may be explained in the following way: global warming, induced by the positive radiative forcing applied, induces the Atlantic water column to become lighter over the upper 2000m as response to heat and freshwater fluxes anomalies. In the whole basin, temperature and salinity changes tend to compensate each other with an overall decrease in density. In particular, between 60°N to 80°N there is an increase in stratification of the water column (as suggested by the Atlantic vertical density profile (fig. 4.2)), which causes a decrease in vertical diffusivity.

In agreement with the above discussion the linear relationship found

between vertical diffusivity and the Atlantic THC strength (fig. 4.4) implies that as the vertical diffusion decreases with increased CO_2 forcing so does the circulation intensity into the ocean basin (table 3.1). The increased stratification at high latitudes, associated with a decreased vertical diffusivity, leads to less dense water forming (mainly in the Labrador Sea, as already discussed) and to a reduced Atlantic overturning. In our simulations the mixing at high latitudes is the critical parameter that controls the propagation of buoyancy anomalies from the ocean surface to depth and that influences the circulation in the Nordic Seas. This result agrees with Marzeion et al. (2007) as opposed to the finding by Munk and Wunsch (1998) showing a more crucial role to the mixing at low latitudes. Our findings are in agreement with Nilsson et al. (2001) who showed in their conceptual and single-hemisphere model an increasing overturning with a decreasing north-south density gradient, in opposition to the Stommel feedback (Stommel, 1961). However, the study of Nilsson et al. (2001) has the deficiency of referring to processes acting only in one hemisphere and not considering possible mechanisms involving the Southern Ocean and which could affect the strength of the Atlantic THC.

4.4 The Southern Ocean winds

As already discussed, the westerly winds blowing over the Southern Ocean respond to the increased temperature, with a poleward shift (fig. 3.5), in agreement with Cai et al. (2003). The wind intensity is influenced as well showing a non linear response with the applied perturbation. This behavior reflects in the Southern Ocean wind stress intensity and in the poleward shift of its maximum value (table 3.1). The westerly wind stress maximum increases in the $4CO_2$ experiment, does not change in the $8CO_2$ experiment and weakens in the $16CO_2$ experiment with respect to the CTRL value (table 3.1).

As suggested by several studies (Toggweiler and Samuels, 1995; Saenko and Weaver, 2004; Gnanadesikan, 2007; Hirabara et al, 2007), increased
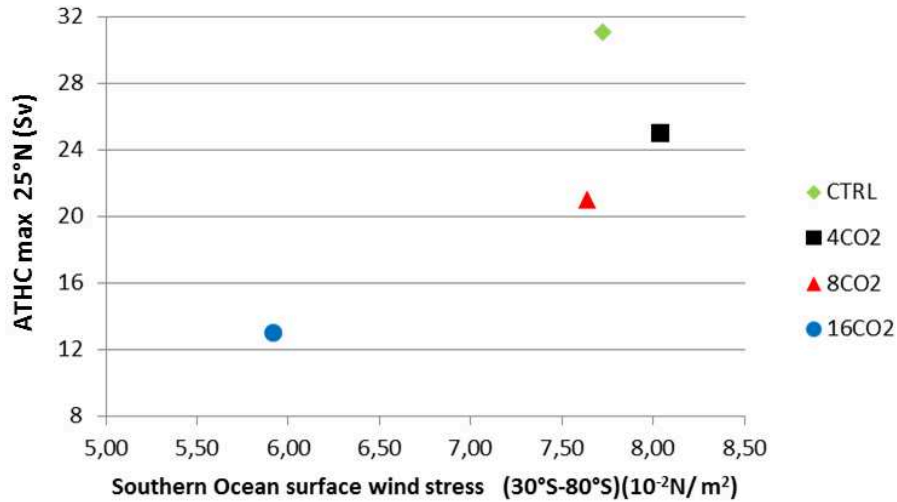
Figure 4.5: Southern Ocean zonal wind stress (averaged between 30°S and 80°S) annual mean (10^{-2} N/m^2) versus ATHC max intensity computed at 25°N at steady state for CTRL (green diamond), 4xCO_2 (black square), 8xCO_2 (red triangle) and 16xCO_2 (blue circle) experiments.

Southern Ocean wind stresses should lead to a stronger Atlantic overturning circulation and viceversa. Our findings show instead an Atlantic THC strength that does not show a linear response to the strength of the wind stress at the Southern Ocean (fig. 4.5).

In the figure, the relationship is shown in terms of annual mean wind stress averaged between 30°S and 80°S versus the maximum ATHC strength at 25°N. The $4CO_2$ experiment shows a weaker ATHC in response to an intensification of the wind stress over the Southern Ocean, while in the $8CO_2$ simulation a great decrease of the ATHC is associated with a little decline of SO winds intensity. The $16CO_2$ experiment instead shows a decreased Atlantic THC strength accompanied by a strong wind stress reduction over the Southern Ocean. The theory according to the Southern Ocean wind stress influences the ATHC intensity (Gnanadesikan, 1999) hence seems to hold among the sensitivity simulations only in the $16CO_2$ experiment. The reason may lie in the meridional density gradients changes since the influence

of Southern Ocean wind stress anomalies over the Atlantic THC intensity, as indicated by Gnanadesikan (1999), holds assuming constant the meridional density gradients. Our results however show that in $4CO_2$ and in $8CO_2$ simulations the meridional density gradient changes as response to global warming and only in the $16CO_2$ experiment the meridional density differences are held fixed being close to the CTRL ones. Furthermore, the disconnection of the strength of the Atlantic THC from the westerly wind stress in the Southern Ocean in $4CO_2$ and $8CO_2$ experiments could be also due to the ocean vertical diffusion. As suggested by Sevellec and Fedorov (2011), if the North Atlantic ocean vertical diffusivity is strong enough to sustain the maximum part of the overturning, the Atlantic THC becomes less sensitive to the wind stress over the Southern Ocean.

4.5 The effect of Mediterranean Outflow on the Atlantic Thermohaline Circulation

The set of experiments discussed above does not consider the effect of the Mediterranean Outflow Waters (MOW) on the Atlantic THC since a relaxation of temperature and salinity to Levitus XX century climatology (Levitus et al, 1998) was applied every year to the Mediterranean waters.

In order to evaluate the impact of higher MOW salinity over the ATHC intensity, a new experiment has been performed ($16CO_2$M) without salinity relaxation of the Mediterranean waters. The temperature relaxation has been maintained in order to avoid model numerical instability due to very high temperature and values reached by the Mediterranean waters under extreme CO_2 forcing.

The model hydrological cycle, which considers a XX century climatologic river runoff contribution, allows the Mediterranean waters in the $16CO_2$M experiment to become more saltier and denser than those in the $16CO_2$ simulation. The salinity difference among the two experiments is mainly due to an increased evaporation over the basin in the $16CO_2$M experiment (fig. 4.6)
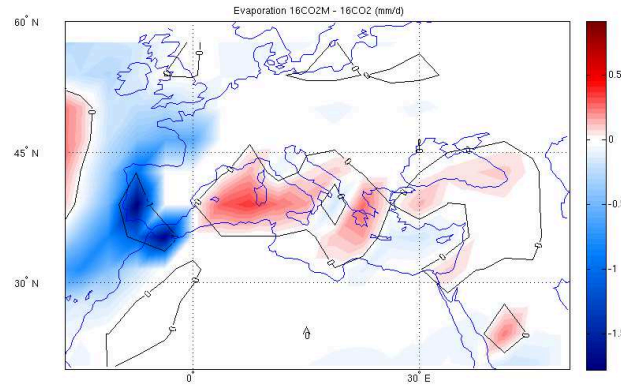
Figure 4.6: Annual mean evaporation difference (mm/d) between 16xCO_2M and 16xCO_2 simulations.

in turn enhanced by an increased surface winds intensity (not shown), being the temperature gradient between surface waters and the air above kept fixed through the temperature relaxation.

In the Atlantic Ocean hence an high input of salinity has been obtained by the Mediterranean Outflow waters through the Gibraltar Strait. Comparing 16CO_2M and 16CO_2 experiments, the annual mean salinity pattern, averaged over the upper 3000m in the Atlantic longitudes, increases by about 2 psu at 1800m depth close to the Gibraltar Strait latitude (about 40°N; see fig. 4.7b versus 4.7a). The high salinity anomaly then spreads southward along the Atlantic latitudes with decreasing intensities. At upper levels the salinity decreases, in particular at high latitudes (of about 0.5 psu) suggesting an influence on the density of NADW.

The vertical sigma density pattern in the Atlantic basin (fig. 4.8) is strongly influenced by the salinity input. At 40°N a strong density front forms in the water column (between 250m and 2500m) with higher density waters (maximum increase of 0.5 Kg/m^3) in the 16xCO_2M simulation. The positive anomaly then widens equatorward at depth leading to a generally denser water column below 1000m depth. At mid-high latitudes (between 45°N and 90°N) the upper levels (0-500m) show a negative density anomaly of about 0.25 Kg/m^3. The northern North Atlantic waters hence become less
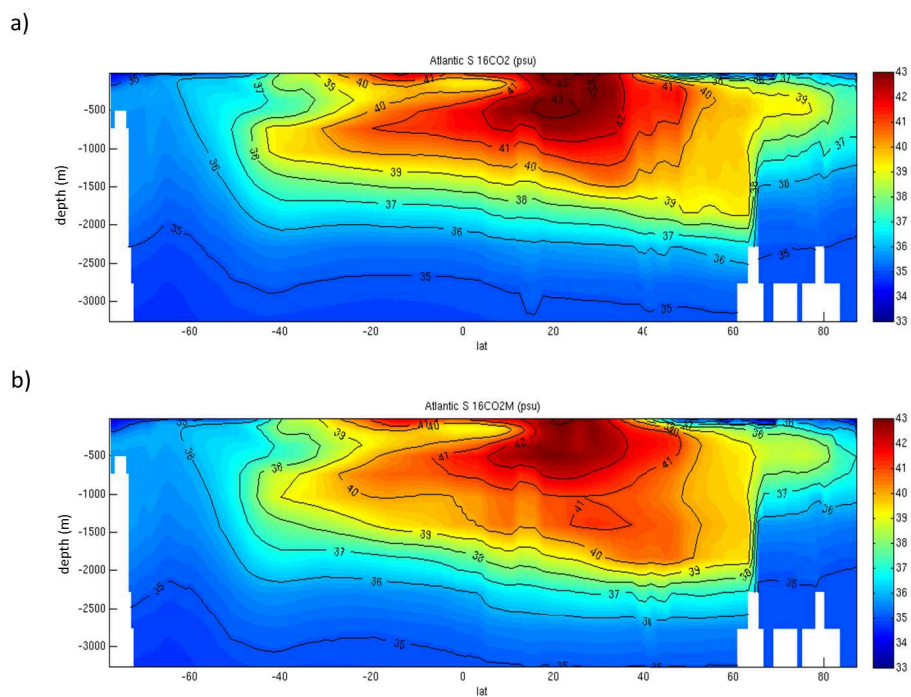
Figure 4.7: Vertical profile (0-3000m) of annual mean salinity (psu) computed for (a) 16xCO_2 and (b) 16xCO_2M experiments averaged in the Atlantic Ocean longitudes.
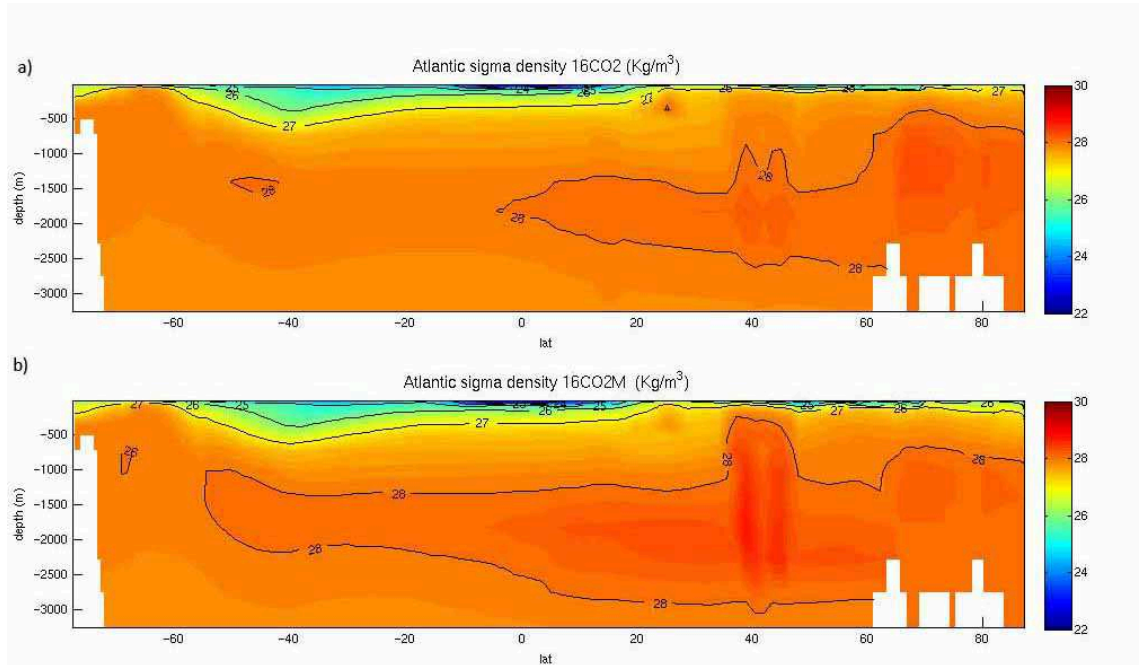
Figure 4.8: Vertical profile (0-3000m) of annual mean sigma density (Kg/m^3) averaged in the Atlantic Ocean longitudes for (a) $16CO_2$ and (b) $16CO_2$M experiments.

dense and lighter influencing the formation of the NADW at high latitudes. On the other hand, at low latitudes (between 40°S and 30°N) the upper layer (0-1000m) density does not show striking differences.

The water column density front in the $16CO_2$M experiment is generated by an enhanced input of denser waters through the Gibraltar Strait. The salinity increase in the Mediterranean Sea leads to a stronger zonal density gradient (1.3 Kg/m^3 in $16CO_2$ experiment and 3.5 Kg/m^3 in $16CO_2$M case) between the Alboran Sea and the Gulf of Cadiz (GoC), the part of the Atlantic Ocean close to Gibraltar Strait. In response to the increased density contrast between the two basins, the water transport from the Mediterranean Sea through the Gibraltar Strait increases (1.19 Sv in $16CO_2$ experiment and 3.12 Sv in $16CO_2$M case).

At the Gibraltar Strait the intense mixing in the GoC increases the trans-

port of the MOW by a factor of 3 by entraining the overlying North Atlantic Central Water (NACW), as suggested by several studies (Ambar and Howe, 1979; Ochoa and Bray, 1991; Baringer and Price, 1997). In the case of $16CO_2$ experiment the MOW transport in the GoC increases to 2.91 Sv while in the $16CO_2$M simulation to 8.31 Sv with respect to the transport through the Gibraltar Strait. This entrainment process in the GoC introduces a sink at the Atlantic ocean eastern boundary capable of inducing and influencing strong zonal flows such as the Azores Current (Jia, 1999).

The Azores Current (AC) is the southern branch of the Gulf Stream split southeast of the Grand Banks of Newfoundland. The AC heads southeastward across the Mid-Atlantic Ridge to the south of the Azores then flowing mainly eastward at a latitude of about 35°N to the GoC. The eastward flow is mostly in the latitudinal band between 35°N and 50°N in the upper few hundred meters but can deepen to 2000m. The water mass transformation associated with the Mediterranean overflow in the GoC may influence the AC intensity (Jia, 1999). Fig. 4.9 shows the path of the AC computed at 100m for $16CO_2$ and $16CO_2$M experiments mainly included between 15°N and 35°N. In the $16CO_2$M the sink of denser waters with respect to $16CO_2$ simulation in the GoC leads to an intensification of the AC, computed over the upper 1000m of water column, to 10.31 Sv versus the 8.86 Sv of the $16CO_2$ experiment. The increased transport leads in the $16CO_2$M simulation to the recirculation at mid-latitudes of the dense MOW reinforcing the density front.

The density changes through the water column in response to the salinity input at the Gibraltar Strait influence the Atlantic THC. The streamfunction of the meridional overturning circulation into the basin (fig. 4.10) shows in fact a different pattern of the oceanic circulation in the $16xCO_2$M experiment. The ATHC stops at 40°N, becomes weaker with its maximum value decreasing by 0.5 Sv (from 13.2 Sv in $16xCO_2$ to 12.7 Sv in $16xCO_2$M) and deepening to 3000m depth (fig. 4.10b). Northward of 40°N the ATHC strongly decreases with its maximum weakening of 4 Sv at the Gibraltar Strait latitude.
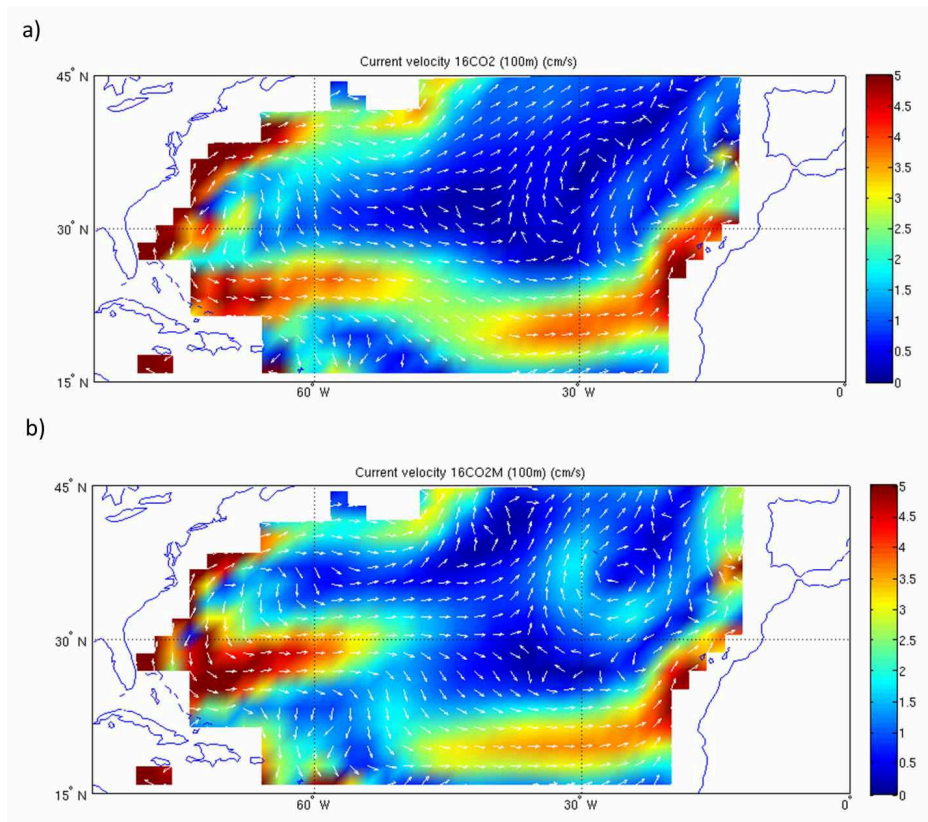
Figure 4.9: Annual mean ocean currents (arrows give direction and shaded the intensity (cm/s)) computed at 100m depth for (a) 16xCO_2 and (b) 16xCO_2M experiments.

The salinity input of 2psu provided by the MOW into the Atlantic basin acts hence creating a strong density front through the water column at the latitude of the Gibraltar Strait obstructing the northward flow of the Atlantic THC. The tropical warm waters reaching the front and the high density waters are constrained to sink at that latitude and they are not allowed to reach the high latitudes. On the other hand, in the North Atlantic the waters become lighter and the NADW stop to form. A further contribution to the ATHC stop at mid-latitudes in $16\mathrm{x}CO_2\mathrm{M}$ experiment may be given by the zonal intensification of the AC preventing the meridional northward flow.

Our findings show hence that a salinity input by the MOW may strongly influence under extreme CO_2 forcing the ATHC intensity and the North Atlantic hydrography.

4.6 Conclusions

The mechanisms involved in the response of the Atlantic THC to the radiative forcing have been investigated and specific attention has been posed to changes in meridional density gradients between high and low latitudes, in water column vertical diffusivity and in Southern Ocean wind stress as main factors influencing the ocean circulation intensity.

The density pattern, influenced by changes in temperature and salinity anomalies, shows a lighter water column when the CO_2 atmospheric concentration is enhanced. We found an anti-correlation between the strength of the Atlantic THC at 25°N and the meridional density gradient: the circulation weakens as the density gradient increases.This result is not sensitive to integrating the density difference over different ocean depths or to using the Equator or 30°S latitude as the southern endpoint. However the $16CO_2$ experiment behaves differently since even though the computed meridional density gradient is close to the CTRL one, the Atlantic THC strongly weakens. The distinctive behavior of the $16CO_2$ experiment with respect to the $4CO_2$ and $8CO_2$ simulations may suggest the reaching of a threshold beyond
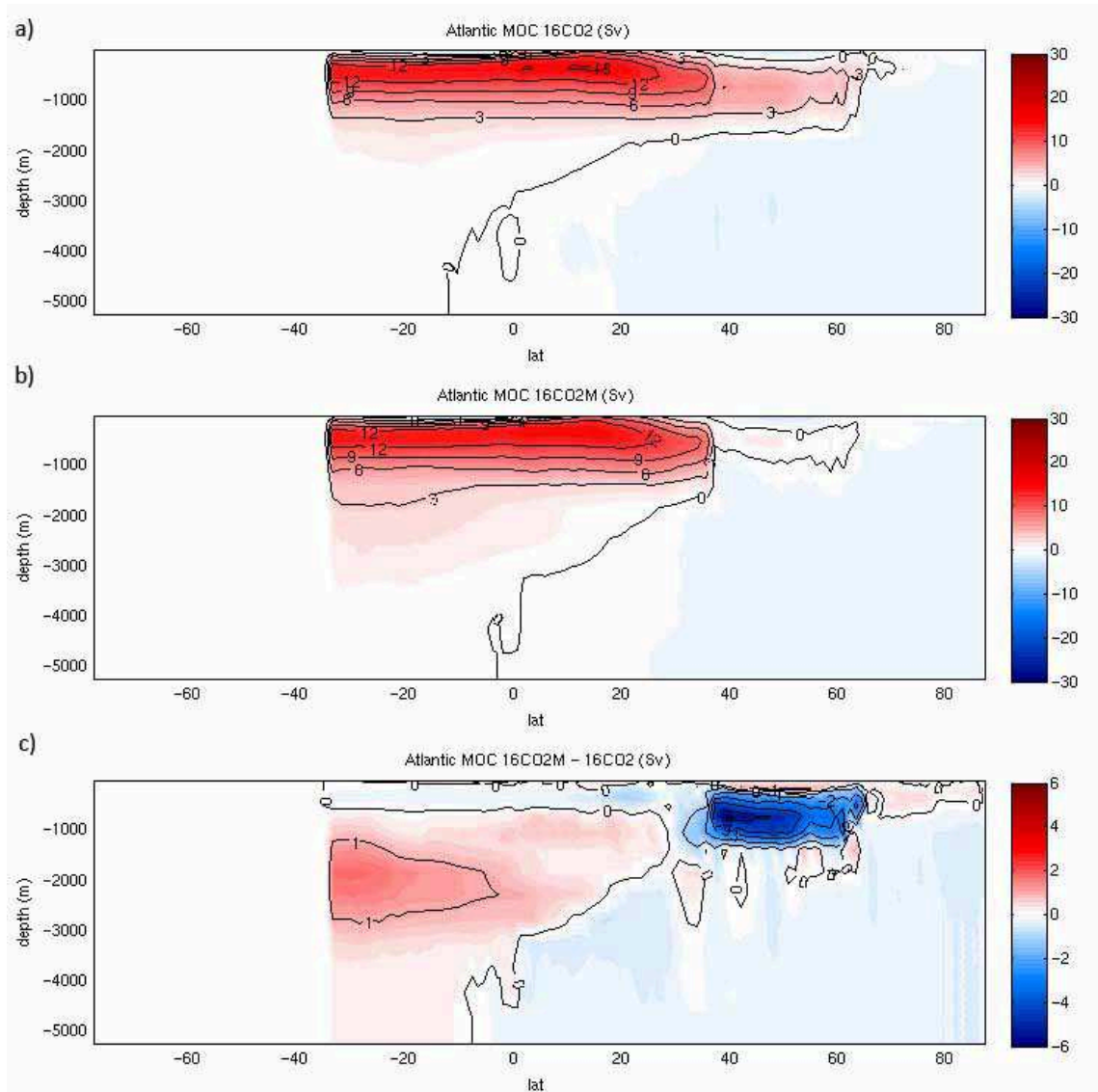
Figure 4.10: Atlantic annual mean thermohaline circulation (Sv) computed for (a) 16xCO_2, (b) 16xCO_2M experiments and differences (Sv) between (c) 16xCO_2M and 16xCO_2 experiments

which the climate system responds to the radiative forcing in a different way. An hysteresis of the system could exist, but to confirm this hypothesis several experiments with different CO_2 atmospheric forcing would be necessary.

The anti-correlation found in the $4CO_2$ and $8CO_2$ between the meridional density differences and the ATHC strength suggests the importance to take into account other mechanisms influencing the oceanic circulation. Bryan et al. (1987) indicated the vertical diffusivity processes in the ocean interior as controlling the strength of the ATHC (Bryan, 1987). In the present study, a close to linear relationship is found in all the CO_2 simulations between the circulation intensity and the North Atlantic vertical diffusion: when the forcing applied increases, the vertical mixing through the water column decreases at high latitudes, as response to vertical density stratification, and the Atlantic THC weakens. This finding is in agreement with Nillsson et al. (2001,2003) who showed a decreased vertical diffusion, linked to an increased stratification of the water column, as the cause of a weakened ocean circulation.

Another mechanism considered as a possible driver for the Atlantic THC is the wind stress over the Southern Ocean surface. Despite many studies stress the strong dependence of the ocean circulation intensity from the wind forcing at the Southern Hemisphere (Toggweiler and Samuels, 1995; Saenko and Weaver, 2004; Gnanadesikan, 2007; Hirabara et al, 2007), with an increasing wind forcing leading to an increasing overturning in the Atlantic Ocean, our set of experiments does not show any particular relation between the two variables. The intensity of the Atlantic THC seems indeed disconnected from the forcing acting over the Southern Ocean surface, except for the $16CO_2$ simulation where a reduction in the Atlantic THC is related to a weakening of the westerlies stress (in addition to changes in diffusivity). The reason may lie in the meridional density gradients changes since the theory according to which the Southern Ocean wind stress affects the ATHC intensity assumes that the meridional density differences between high and low latitudes are kept fixed (Gnanadesikan, 1999). Furthermore, in the $4CO_2$

and $8CO_2$ simulations an important role may be played by vertical diffusion being strong enough to sustain the maximum part of the overturning and leading to a less sensitive Atlantic THC to the Southern Ocean wind stress, as suggested by Sevellec and Fedorov (2011).

The analysis of the Atlantic THC mechanisms shows that, under an extreme radiative forcing, a good indicator of the Atlantic THC strength resides in the high latitudes vertical diffusivity: as the latter decreases as response to a global warming so does the former. Our results suggest that only after the ocean vertical diffusion has strongly decreased due to large vertical density stratification that it can not longer sustain the maximum overturning, other mechanisms may play a role to maintain the Atlantic THC. The energy supply by the Southern Ocean wind stress could represent a further circulation driving mechanism when the meridional density gradients between high and low latitudes do not suffer variations in response to a global warming: if the meridional density differences are held fixed, the Atlantic THC may weaken as response to a decreasing wind stress over the Southern Ocean, as shown for the most extreme case ($16CO_2$).

Another factor influencing the ATHC is represented by the water mass properties of the MOW. The input of very high density waters through the Gibraltar Strait, as shown in $16CO_2$M simulation, leads to an intensification at mid-latitudes of the Azores Current which, recirculating zonally the high density MOW, forms a density front close to 40°N involving the whole Atlantic water column. That front acts over the ATHC obstructing the northward flow and leading the warm and salty tropical waters to sink at mid-latitude. As a consequence, the high latitudes surface waters become lighter preventing the NADW formation.

Nevertheless, it is worth pointing out some shortcomings of this study. We used a coupled model with relatively low ocean resolution, which may overrepresent the importance of diffusive processes compared to those in the real ocean. Moreover, the freshwater input due to land-ice melting and river runoff changes, not considered in the present study, could affect our results

acting over the high latitudes water column stratification and hence over the ocean vertical diffusivity. A stronger Atlantic THC weakening should be expected in the CO_2 simulations if this process is taken into account. Furthermore, given the influence of the MOW property on the North Atlantic hydrography and its effect on ATHC, a better representation of the Mediterranean waters, without relaxation in temperature and salinity fields, should be considered into the model.

Chapter 5

A preliminary study of the energy balance in extreme climate regimes

5.1 Introduction

The energetics properties of the climate system have been analyzed by several authors (Carissimo et al, 1984; Kiehl and Trenberth, 1997; Trenberth and Caron, 2001; Trenberth et al, 2009; Lucarini and Rangone, 2011) and the atmospheric and oceanic energy budget components have been widely investigated in order to understand which of them mostly contribute to the climate system total energy (Lorenz, 1955; Munk and Wunsch, 1998; Wunsch and Ferrari, 2004).

Kinetic energy (KE), potential energy (PE) and internal energy (IE) are the main intrinsic forms of the energy of the climate system and they can be written as:

$$KE = \frac{1}{2}\rho(\mathrm{u}^2 + \mathrm{v}^2) \tag{5.1}$$

$$PE = \rho g z \tag{5.2}$$

$$IE = \rho c_v T \qquad (5.3)$$

where ρ is the fluid density, u and v are the velocity horizontal components, g the gravity acceleration (9.81 m/s^2), z the geometric height in the ocean or geopotential height in the atmosphere , c_v the specific heat at constant volume (717 J/KgK for atmosphere and 4187 J/KgK for the ocean), and T the temperature.

In the atmosphere an additional contribution to the total energy is given by the latent energy (LE), coming from the evaporation and condensation of water vapor

$$LE = \rho L q \qquad (5.4)$$

where L is the latent heat of evaporation (2501 J/g) and q the specific humidity. The total energy of the atmosphere is hence given by:

$$E = IE + PE + LE + KE \qquad (5.5)$$

The heat absorbed by the atmosphere leads to an increase of IE and PE which is partially (less than 1%) converted into KE to maintain the atmospheric and oceanic general circulations against friction (Peixoto and Oort, 1992). Only a part of the total potential energy (sum of IE and PE, as defined by Lorenz, 1955) is involved in the transformation process and is thus available to be converted into KE.

In the atmosphere, the smaller energy contribution is due to the KE (0.05%), while the largest forms of energy are the IE (70.4%), PE (27.1%) and LH (2.5%) (Peixoto and Oort, 1992). Nevertheless, KE represents a considerable part of the energy available for the atmospheric general circulation and plays an important function in the general circulation energetics. The destruction of the atmospheric KE can be induced by the work done by the atmospheric circulation against the frictional forces which acts converting KE in IE in an irreversible process. The KE zonal energy transport

in the atmosphere is delivered mainly by the jet stream in the upper tropesphere and a well-defined convergence of total kinetic energy is found at mid-latitudes (Peixoto and Oort, 1992). The most important mechanism of meridional energy transport in the atmosphere is the mean meridional cell circulation (Hadley cell) between 20°S and 20°N.

The available potential energy (APE) is defined, following the so-called "approximate" expression of Lorenz (1955), by

$$APE = \frac{1}{2}\rho c_p \left(\Gamma_d \frac{(T - \tilde{T})^2}{(\Gamma_d - \tilde{\Gamma})\tilde{T}} \right) \tag{5.6}$$

where

$$\Gamma = -\frac{\partial T}{\partial z} \tag{5.7}$$

is the vertical lapse rate of temperature, Γ_d=g/c_p is the dry-adiabatic lapse rate and c_p the atmospheric specific heat at constant pressure. The $\sim$ denotes an average over an entire isobaric surface.

From eq. 5.6, it follows that the APE may be approximated by a weighted average of the horizontal variance of temperature. Furthermore, KE is produced when cold air sinks and warm air rises at the same level. In order to have such a process, there must be different temperatures at the same level. If the stratification is stable, the temperature at a fixed elevation will rise in the sinking air and fall in the rising air and the process will thereby reduce the horizontal temperature contrast. Moreover, the less stable the stratification, the farther the cold air must sink and the warm air must rise in order to eliminate the temperature contrast. Thus more KE is attainable and so more APE is present when the horizontal temperature contrast is greater and when the stratification is less stable.

In the ocean, as in atmosphere, the maximum part of total energy comes from IE and PE (or total potential energy, as defined by Lorenz, 1955). KE is very small if compared with the total energy. However, the availability of energy can be described in terms of the potential and internal energy

changes with respect to a reference state. According to Reid et al. (1981), the gravitational potential energy in the oceans is the dominant term in the total available energy while the available internal energy can at most contribute 10% to 20% to the total. Furthermore, the contribution of the internal energy to the total available energy seems to be negative, contrary to what is observed in the atmosphere. This can be attributed to the different compressibility as a function of temperature in the oceans and atmosphere.

In agreement with Oort et al. (1989) the contribution of the available internal energy in the ocean can be neglected and the available (gravitational) potential energy is given by

$$APE = -\frac{1}{2}g\frac{(\rho - \tilde{\rho})^2}{\frac{\partial \tilde{\rho}_\theta}{\partial z}} \tag{5.8}$$

where ρ is the local density, $\tilde{\rho}$ is the reference density obtained by the horizontal average of the local density in the basin of interest and $\frac{\partial \tilde{\rho}_\theta}{\partial z}$ is the vertical gradient of the local potential density.

The APE represents the energy stored in the horizontal variations of the density field and it is the relevant form of potential energy in a stratified fluid (Lorenz, 1955). The highest values of APE in the world's ocean are observed in mid to high latitudes. At the Southern Ocean, in particular, the strong westerly winds blowing over the surface hold up the dense water around the Antarctic continent facilitating the storage of APE. In the event of a decline of wind stress over the Southern Ocean, the relaxation of the currents should give a slump of density fronts resulting in a large amount of mechanical energy released (Huang, 2005).

The ocean's mechanical energy is continuously dissipated through friction. To maintain a steady state circulation an energy source is required to overcome friction. In such state the pressure gradient forces must do work against friction in order to balance frictional energy dissipation. Any extra positive work by pressure gradient forces contribute to accelerate the fluid. As concluded by Sandstrom (1908,1916), the work by the pressure forces against frictional forces is produced only if heating (expansion) takes place

at larger pressure (i.e.depth) rather than cooling (compression). This implies that heat flowing into the system is converted into work.

The ocean is heated at the tropics and cooled at high latitudes at the surface with the heating and cooling sources roughly at the same depth, but heating and cooling are not the sole forcing. The ocean is forced at its surface by atmospheric winds which result in turbulent mixing capable of driving the flow (Munk and Wunsch, 1998; Huang, 1999). In addition, the wind forcing directly contributes to the large-scale kinetic energy of the ocean.

The turbulent kinetic energy induced by the winds is considered one of the main energy source needed to sustain THC. When internal waves generated by winds break, turbulent KE is supplied to the ocean. Since the ocean is stably stratified, a part of the dissipated turbulent KE is converted into available (gravitational) potential energy which is then converted into KE and used to compensate viscous dissipation (Urakawa and Hasumi , 2009).

The budget of globally integrated oceanic KE is thus given by (Toggweiler and Samuels, 1998):

$$\frac{dK}{dt} = B + W + D \tag{5.9}$$

where

$$B = \int -\mathbf{u_h} \cdot \nabla_\mathbf{h} P dV = \int \left(-\mathbf{u} \cdot \nabla P + w \frac{\partial P}{\partial z} \right) dV \tag{5.10}$$

is the rate at which KE is added (or removed, if negative) by the pressure-gradient work, with u_h the ocean horizontal velocities. B represents the sum of the work done by pressure gradients ($-\mathbf{u} \cdot \nabla P$) plus the conversion term between APE and KE ($w\frac{\partial P}{\partial z}$) (Toggweiler and Samuels, 1998; Gregory and Tailleux, 2010). When globally integrated, the work done by the pressure gradients vanishes and B represents the rate of conversion of APE to KE only.

The work done by the wind to change KE is defined as

$$W = \int \mathbf{u_h} \cdot \tau dA \tag{5.11}$$
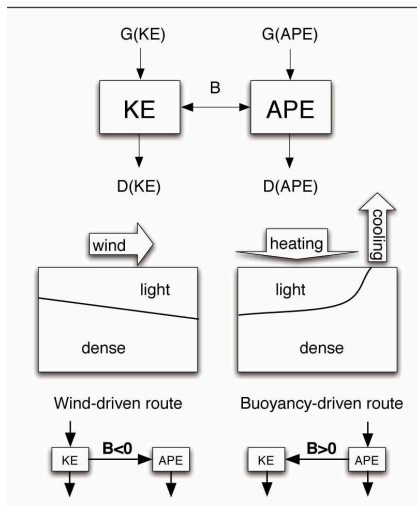
Figure 5.1: Schematic depiction of the wind- and buoyancy-driven routes for energy conversion. B is the conversion between kinetic energy (KE) and available potential energy (APE), G is generation, D is dissipation (from Gregory et al, 2010)

where τ is the wind stress vector while

$$D = D_h + D_v = \rho \int k_h \mathbf{u} \nabla_\mathbf{h}^2 \mathbf{u} dV + \rho \int k_v \mathbf{u} \frac{\partial^2 \mathbf{u}}{\partial z^2} dV \qquad (5.12)$$

represents the dissipation of KE (sum of the horizontal and vertical dissipation) by viscous forces with k_h and k_v the horizontal and vertical diffusivity coefficients, respectively.

Integrated over the global ocean, the work done by the pressure gradients force becomes zero hence $B < 0$ indicates that APE is produced and KE decreases mainly in the Southern Ocean, and generally in near-surface layers where the wind stress leads to the outcrop of the isopycnals (Gregory and Tailleux, 2010). Fig. 5.1 illustrates the paths of energy conversion as indicated by Toggweiler and Samuels (1998) and Hughes et al. (2009).

Worldwide the oceanic KE is generated by the pressure-gradient work mainly within the western boundary currents, including the Atlantic Ocean, and in deeper layers. On the other hand at almost all longitudes in the South-

ern Ocean APE is generated. The maximum KE production is accounted for by the regions where North Atlantic Deep Water is formed meaning that in the Atlantic the pressure-gradient work supply KE to the ATHC driving the circulation (Gregory and Tailleux, 2010).

The studies of the ocean energetics under CO_2-forced climate have shown a very good correlation between the Atlantic THC strength and the rate of KE generation by pressure-gradient work between 50°N-70°N in the Atlantic basin (Gregory and Tailleux, 2010). The analysis of the kinetic energy balance of the circulation, in experiments with CO_2 increasing at 1% per year, indicates in fact that the largest change is the weakening of the KE production by the pressure-gradient work in the North Atlantic, which correlates strongly in time with the declining strength of the Atlantic THC and is matched by a decrease in dissipation of KE (Gregory and Tailleux, 2010). Under increased CO_2, the changes in the rate at which KE is increased by the pressure-gradient work (Gregory and Tailleux, 2010) seem to contradict the pump/valve mechanism proposed by Samelson (2004) in which the southern winds control the strength of the Atlantic THC by pumping APE into the system, which is then released by high-latitude cooling, an idea supported by the model experiments of Urakawa and Hasumi (2009). However, Gregory et al. (2010) found that the sink of KE in the Southern Ocean increases as the climate warms, while the Atlantic THC strength decreases. Some other studies agree that changes in wind stress are not responsible for weakening the Atlantic THC in climate change simulations (Dixon et al, 1999; Gregory et al, 2005).

As response to global warming conditions, the atmospheric energy increases as well. At low latitudes the potential energy stored can be converted into kinetic energy by atmospheric vertical motions, as suggested by Lorenz (1955).

As climate warms, the planetary and atmospheric energy imbalance enhances providing more available potential energy in the atmosphere, since the upper troposphere in the tropics warms up more than that at higher lat-

itudes. The strong horizontal temperature gradient causes the mid-latitude jet streams to intensify and to shift towards the poles (Kushner et al, 2001; Williams, 2006; Lorenz et at, 2007).

The tropical atmosphere shows a stabilization (Sugi et al, 2002) and a weakening of the circulation due to an increase in the tropical precipitation lower than the rate of increase in the atmospheric moisture (Betts, 1998; Allen and Ingram, 2002; Held and Soden, 2006). The differential rate of response to surface warming of water vapor and precipitation implies a weakening of the boundary layer/troposphere mass exchange reflecting into a reduction of the Hadley circulation (Vecchi et al, 2006). The Hadley circulation shows as well a vertical displacement and a poleward expansion (Bengtsson et al, 1996; Gastineau et al, 2009; Schneider et al, 2010) due to the tropopause upward displacement (Santer et al, 2003).

The weakening of the ATHC associated to a diminished kinetic energy input into the ocean in warmer conditions suggests to investigate the energetic properties of the climate system in order to answer to the following scientific questions:

1. How do the energetics of the Earth's system respond to an extreme CO_2 radiative forcing?

2. Which is the relation between the sources and sinks of KE into the ocean and the Atlantic THC strength?

This chapter is organized as follows: section 5.2 focuses on the energetics budget of the troposphere, section 5.3 analyzes the relation between the generation and removal of KE into the ocean and the Atlantic THC changes in CO_2-forced simulations and section 5.4 gives some concluding remarks.

5.2   The atmospheric energy budget

Table 5.1 summarizes the value of the total atmospheric energy and its components in the CTRL and in the CO_2 experiments computed as in Eq.s 5.1 - 5.5 for the last 100 years of integration. In the atmosphere the

	CTRL	**4 × CO2**	**8 × CO2**	**16 × CO2**
Internal energy (10^{23} J)	7.42	7.61	7.74	7.99
Potential energy (10^{23} J)	2.33	2.39	2.44	2.52
Latent energy (10^{23} J)	0.37	0.54	0.70	1.09
Kinetic energy (10^{20} J)	2.63	3.20	3.70	4.85
Total atmopheric energy (10^{23} J)	10.12	10.54	10.89	11.61
APE (10^{20} J)	5.33	5.49	5.75	6.51

Table 5.1: Atmospheric total energy components and available potential energy (APE), computed as reported by the Eq.s 5.1- 5.5, integrated over the global domain for all simulations for the last 100 years of each simulation (J).

total energy (eq. 5.5) increases by about 4%, 8% and 15% in $4CO_2$, $8CO_2$ and $16CO_2$ experiments, respectively, from the CTRL experiment.

Fig. 5.2a shows the zonal and vertical mean profile of the atmospheric total energy. It consists of the sum of the different energy components (IE, PE, LE, KE) and in terms of intensity the largest (more than 70%) contribution comes from the IE (fig. 5.2c). Because of its large values, most of the increase of total energy in the CO_2 sensitivity experiments is given by the increase of the internal energy. Its increase is related with large tropospheric warming in response to the increased CO_2 forcing (fig. 5.3). In fact, maximum values of IE are found in the Tropics where the troposphere shows its maximum warming (fig. 5.3). As the low latitudes (equator) warm more than the high latitudes (North Pole), the meridional temperature gradient increases in response to the radiative forcing applied (4°C, 9°C, 1 9°C and 26°C as difference between Tropics and North Pole latitudes in CTRL, $4CO_2$, $8CO_2$ and $16CO_2$ experiments, respectively).

The PE (fig. 5.2d) increases as well, showing an increasing rate among the experiments similar to the IE (about 3%, 5% and 8% in $4CO_2$, $8CO_2$ and $16CO_2$ experiments, respectively) (tab. 5.1). The maximum increase
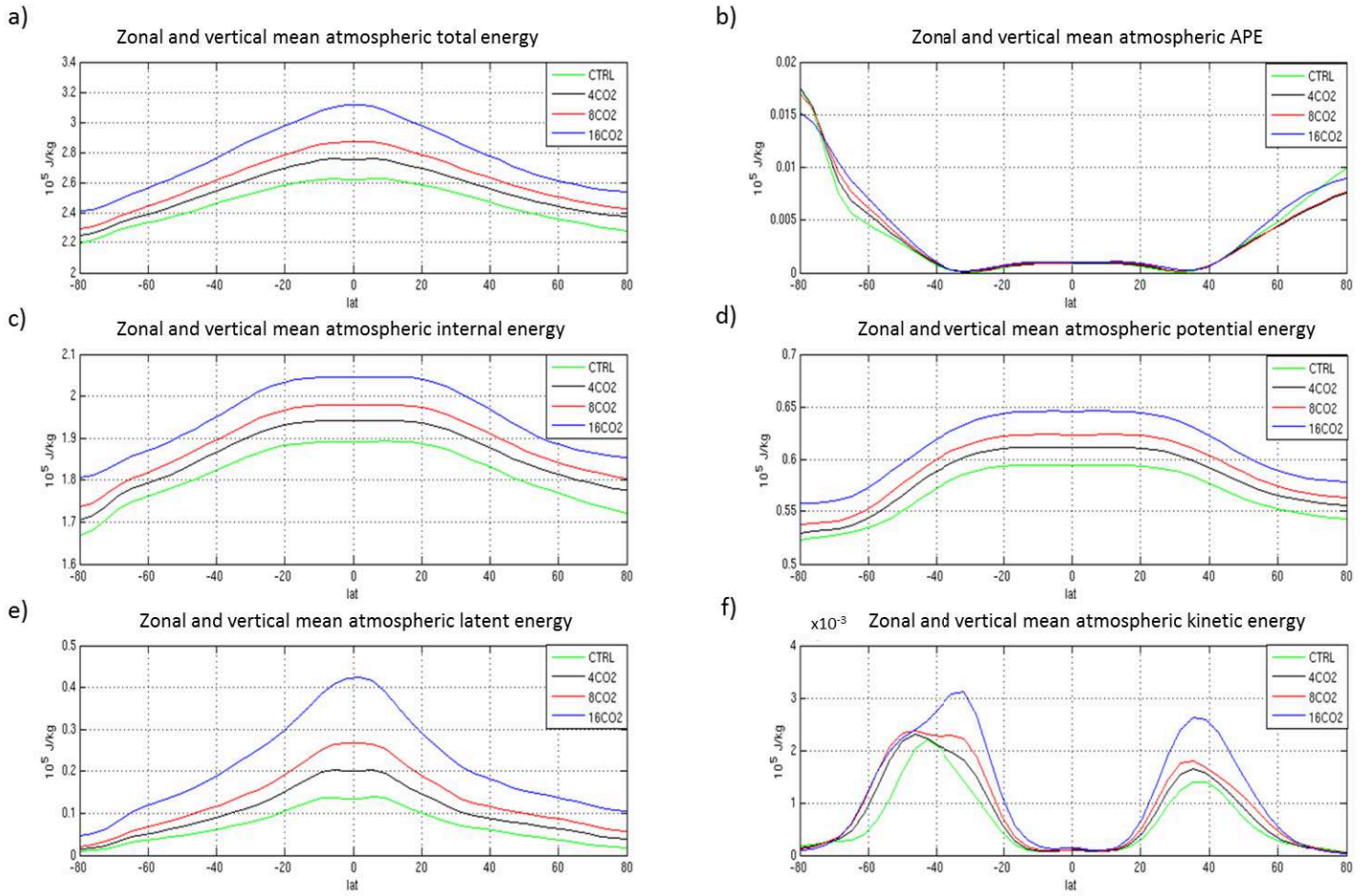
Figure 5.2: Zonal and vertical mean of atmospheric a) total energy, b) APE, c) IE, d) PE, e) LE, f) KE (10^5 J/Kg) computed as reported by the Eq.s 5.1-5.5 for annual-mean conditions for CTRL (green line), 4xCO_2 (black line), 8xCO_2 (red line) and 16xCO_2 (blue line).
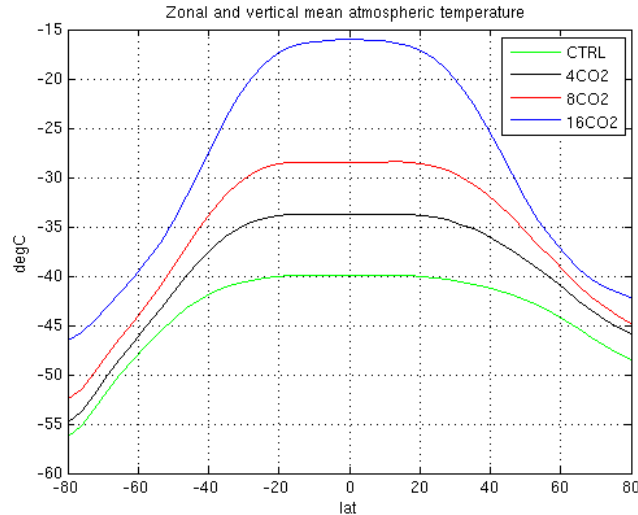
Figure 5.3: Zonal and vertical annual mean tropospheric temperature (°C) computed for CTRL (green line), 4xCO_2 (black line), 8xCO_2 (red line) and 16xCO_2 (blue line).

is at the Tropics following the changed pattern of geopotential height (not shown).

The different warming at low and high latitudes, in particular in the upper troposphere (fig. 3.16), provides more APE. Fig. 5.2b shows the meridional profile of mean atmospheric APE, computed as in eq. 5.6, with differences between the Northern and Southern Hemispheres. Poleward of 50° latitude the contribution of APE is greater in the SH than in the NH. This is because the temperatures are lower over the Antarctic continent than over the Arctic Ocean, leading to a larger meridional temperature gradient in the SH. The APE globally integrated shows an increase by 3%, 8% and 22% in $4CO_2$, CO_2 and $16CO_2$ experiments with respect to the CTRL case (tab. 5.1) possibly due to stronger horizontal temperature contrast in the upper troposphere.

The atmospheric energy component which is subjected to the greatest variation in response to the applied radiative forcing is the LE (fig. 5.2e). It increases by 46% and 89% in the $4CO_2$ and $8CO_2$ experiments and more than doubles in the $16CO_2$ case. The huge increase is linked with larger

water vapor available because of increased ocean-surface evaporation in the warmer tropical latitudes (fig. 3.9), increased amount of specific humidity in the lower troposphere associated with both larger evaporation and increased atmospheric temperature (fig. 3.20).

The lower-tropospheric water vapor, besides being important for the Earth's radiative balance, plays an active role in the dynamic of the global atmospheric circulation through the latent heat released when it condenses (Schneider et al, 2010). In this set of experiments, the increase in the tropical precipitation is much less than the rate of increase in the atmospheric moisture (Cherchi et al, 2008, 2011), in agreement with previous studies (Betts, 1998; Allen and Ingram, 2002; Held and Soden, 2006), leading to important consequences for the atmospheric circulation. In fact, the differential rate of response to surface warming of water vapor and precipitation implies a stabilization of the tropical atmosphere and the energy balance is achieved by a weakening of the atmospheric circulation (Sugi et al, 2002; Chou and Neelin, 2004; Vecchi et al, 2006; Vecchi and Soden, 2007).

Fig. 5.4 shows the meridional atmospheric stream-function for the CTRL experiment and the CO_2 simulations. The Hadley cell dominates the tropical atmosphere with rising motion near the equator, poleward flow in the upper troposphere, descending motions in the subtropics and equatorward flow near the surface. The stream-function corresponding to a clockwise circulation is positive, whereas the stream-function corresponding to a counterclockwise circulation is negative. As the climate warms, the Hadley circulation weakens with its 15°N maximum decreasing by 14%, 29% and 43% in $4CO_2$, $8CO_2$ and $16CO_2$ experiments with respect to the CTRL. It experiences a vertical displacement as well since the tropopause is displaced upward (fig. 3.17), coherently with several studies (Bengtsson et al, 1996; Santer et al, 2003; Gastineau et al, 2009; Schneider et al, 2010).

The upward displacement of the tropopause influences the location of the mid-latitude jet streams, as well. In fact, they intensify and expand upward and poleward (fig. 3.18), in agreement with previous studies (Kushner et
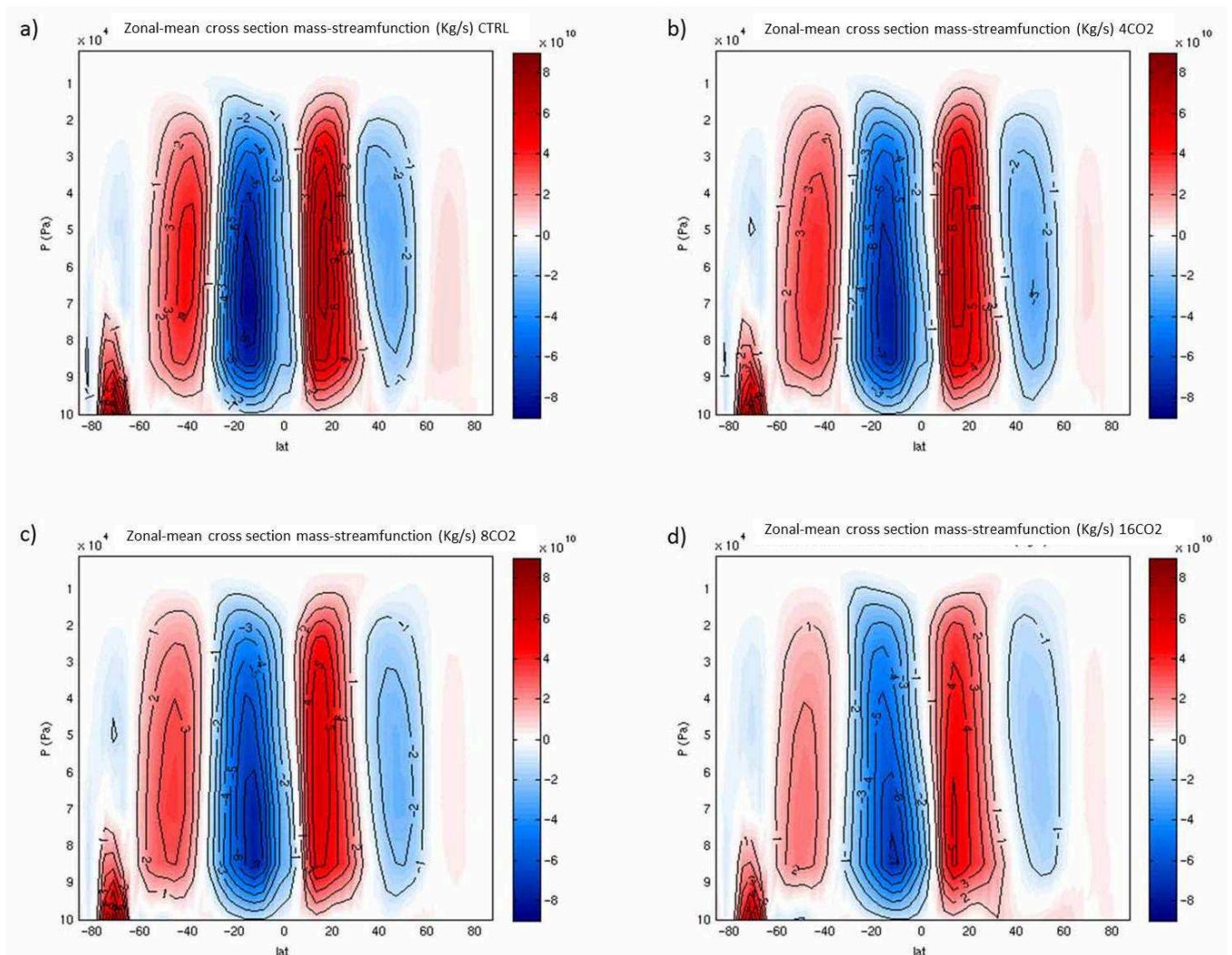
Figure 5.4: Zonal-mean cross sections of the mass stream-function (10^{10} Kg/s) for annual-mean conditions for (a) CTRL and (b) $4xCO_2$, (c) $8xCO_2$ and (d) $16xCO_2$ experiments.

al, 2001; Bengtsson et al, 2006; Williams, 2006; Lorenz et at, 2007). The increase in the KE component (fig. 5.2f) is of the order of $+22\%$, $+41\%$ and $+84\%$ in $4CO_2$, $8CO_2$ and $16CO_2$ experiments, with respect to the control simulation, and it seems to be strictly connected with the intensification of the upper tropospheric jet streams (fig. 5.5). In response to the CO_2 increase, the energy in correspondence of the jet-streams intensifies with a southern jet more energetic than the northern one. That difference may be related to the presence of stronger zonal winds in the Southern Hemisphere (fig. 3.18).

Fig. 5.6 shows the vertically integrated meridional transport of the total tropospheric energy approximately symmetric with respect to the equator. The changes in the atmospheric total energy transport in the CO_2 experiments compared with the control simulation (green line in fig. 5.6) are very small but little differences exist among the two hemispheres. The SH in fact shows greatest variations of the energy transport in response of the radiative forcing applied with its maximum close to 15°S increasing by 5%, 17% and 23% with respect to the CTRL case in $4CO_2$, $8CO_2$ and $16CO_2$ experiments, respectively. In the NH instead the maximum at 15°N increases by 2%, 5% and 9% in $4CO_2$, $8CO_2$ and $16CO_2$ experiments, respectively. The difference among the Hemispheres is associated mainly with an asymmetry in the response of the Hadley cell to the forcing applied. The Hadley cell, in fact, shows in all the experiments a southern cell stronger than the northern one and the rate of decrease of their maximum differs among the CO_2 experiments with the strength of the cell in the NH decreasing more (fig. 5.4). Further the increase in the subtropical sectors (both in the northern and southern hemisphere) may be related to the increased internal energy influenced by the increased tropospheric temperature. The internal energy is in fact the energy giving the greatest contribution to the total balance of the atmospheric energy and it is associated with the heat transport trough the troposphere.

Fig. 5.7 shows the atmospheric and oceanic global meridional heat transports and the sum of the two components for all the simulations. The forcing
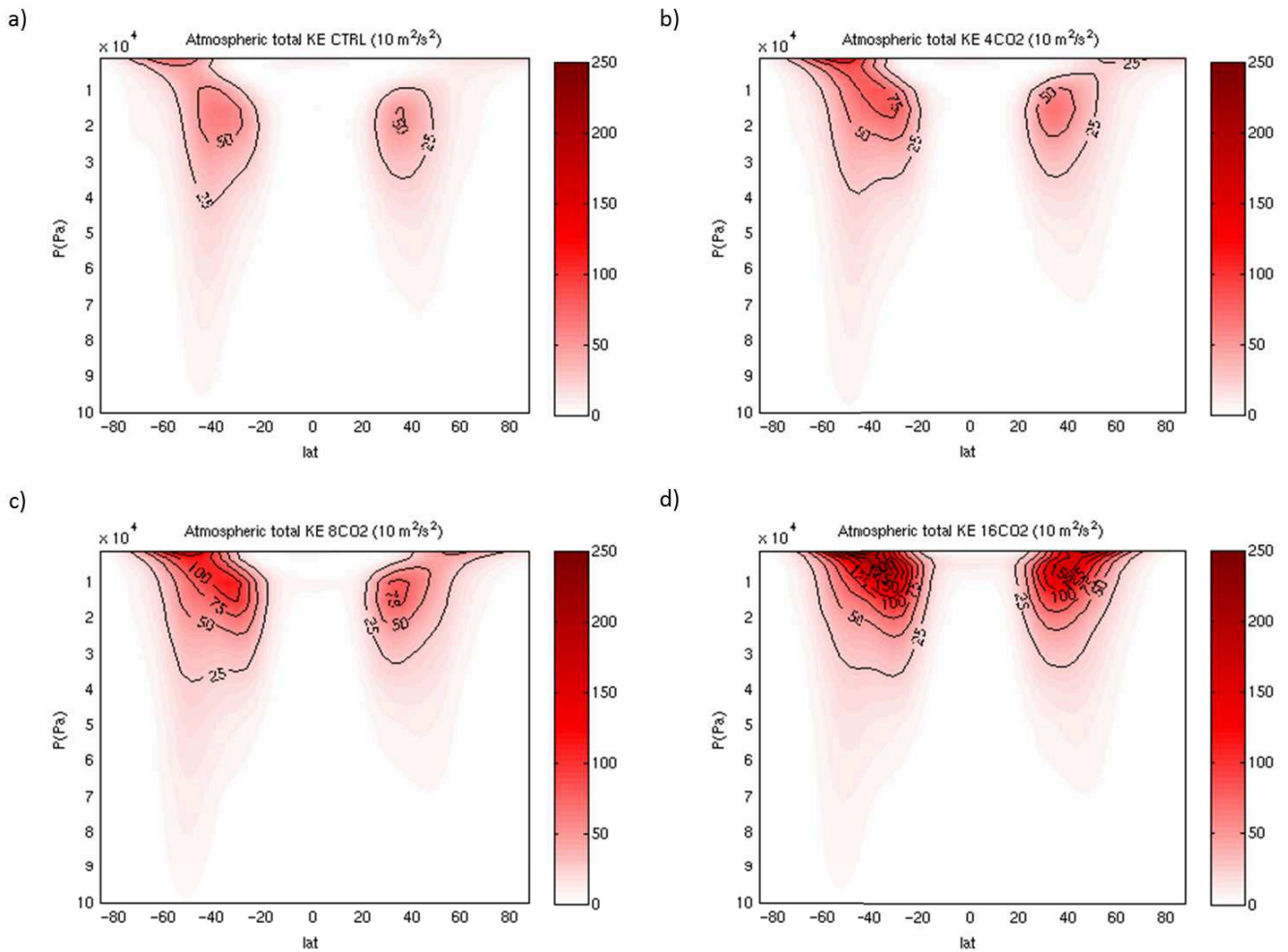
Figure 5.5: Zonal-mean cross section of the atmospheric kinetic energy (10 m^2/s^2) for annual-mean conditions for (a) CTRL, (b) 4xCO_2, (c) 8xCO_2 and (d) 16xCO_2 experiments.
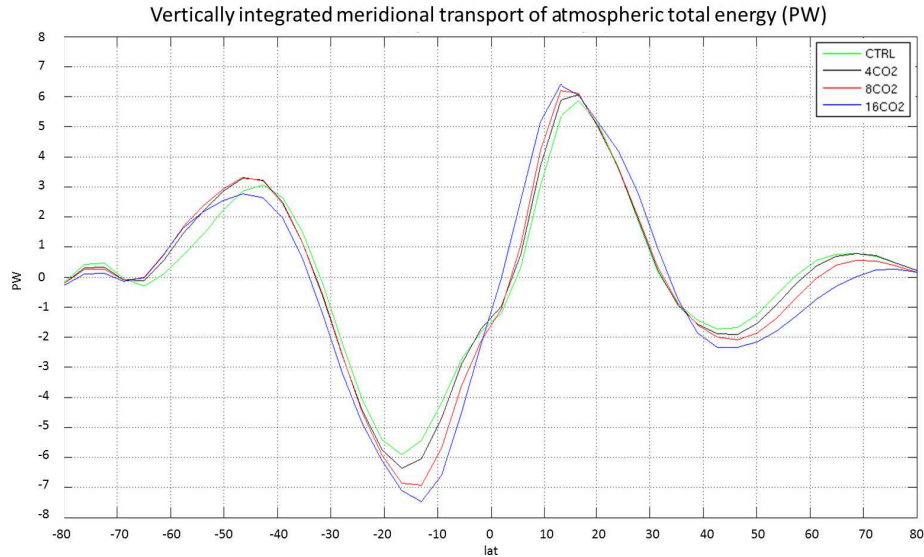
Figure 5.6: Annual mean atmospheric total energy transport (PW) computed for CTRL (green line), $4xCO_2$ (black line), $8xCO_2$ (red line) and $16xCO_2$ (blue line) experiments.

applied does not influence the total heat transport of the system since it remains almost constant among the experiments. Nevertheless, the individual components are subjected to changes. While the atmospheric heat transport increases in response to global warming, the ocean heat transport decreases. It seems that the two climate system components balance to maintain a globally balanced energy transport. In particular, in the northern hemisphere the atmospheric heat transport increases while the oceanic component decreases possibly because of one mainly due to the weakening of the ATHC (fig. 3.13). In the $16CO_2$ experiment a density front forms at $40°N$ (fig. 4.1d), and north of it the oceanic circulation is mainly wind driven and the atmosphere provides the transport of heat. In this extreme case the role of the atmosphere therefore becomes crucial to convey heat at high latitudes.
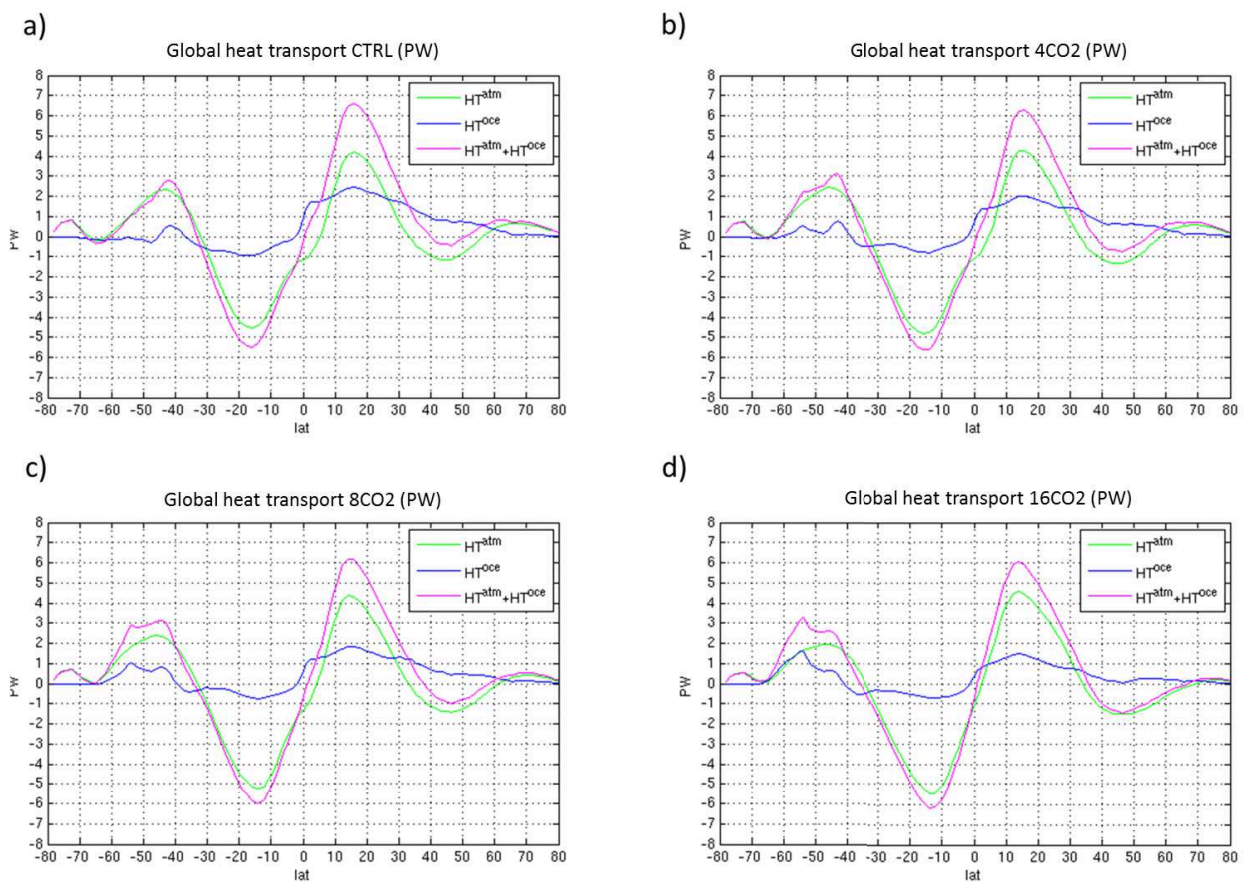
Figure 5.7: Annual mean global atmospheric (green line), oceanic (blue line) and total (violet line) heat transport (PW) computed for (a) CTRL, (b) 4xCO_2, (c) 8xCO_2 and (d)16xCO_2 experiments.

	CTRL	**4 × CO2**	**8 × CO2**	**16 × CO2**
Internal energy (10^{27}J)	1.47	1.49	1.49	1.50
Potential energy (10^{27}J)	0.04	0.04	0.04	0.04
Kinetic energy (10^{17}J)	3.99	3.70	3.34	2.89
Total oceanic energy (10^{27}J)	1.52	1.53	1.54	1.54
Global APE (10^{20}J)	4.21	5.67	5.08	2.86
Atlantic APE (10^{20}J)	0.49	0.64	0.56	0.21

Table 5.2: Oceanic energy components, computed as in eq.s 5.1, 5.2, 5.3, 5.5, 5.8, integrated over the global domain and available potential energy (APE) integrated over the Global and the Atlantic oceans for the last 100 years of all simulations (J)

5.3   The energetics of the ocean circulation

The weakening of the ocean heat transport among the CO_2 simulations suggests a less energetic ocean in response to the radiative forcing applied.

The table 5.2 summarizes the amounts of the oceanic energetic components computed, as reported in Eq.s 5.1, 5.2, 5.3, 5.5, 5.8, for the last 100 years of each experiment integrating over the global domain.

The oceanic total energy, sum of IE, PE, and KE remains almost constant under global warming conditions, as shown in fig. 5.8a by the meridional profile of the zonal and vertical mean total energy.

As for the atmosphere, the largest contribution to the total energy is given by the internal energy (tab. 5.2).

IE reflects the pattern of the oceanic waters temperature (fig. 3.12a,c,e,g) and density. The highest values are located at the Southern Ocean latitudes (40°S-60°S) in response to high density waters (fig. 5.8b).

The potential energy contributes for about 3% to the total energy and the global integrals evidence that it remains almost unchanged in response to the increased CO_2 forcing applied.

Figure 5.8: Zonal and vertical mean of atmospheric a) total energy, b) IE, c) KE, d) APE (10^5 J/m^3) computed as reported by the Eq.s 5.1, 5.3, 5.5 5.8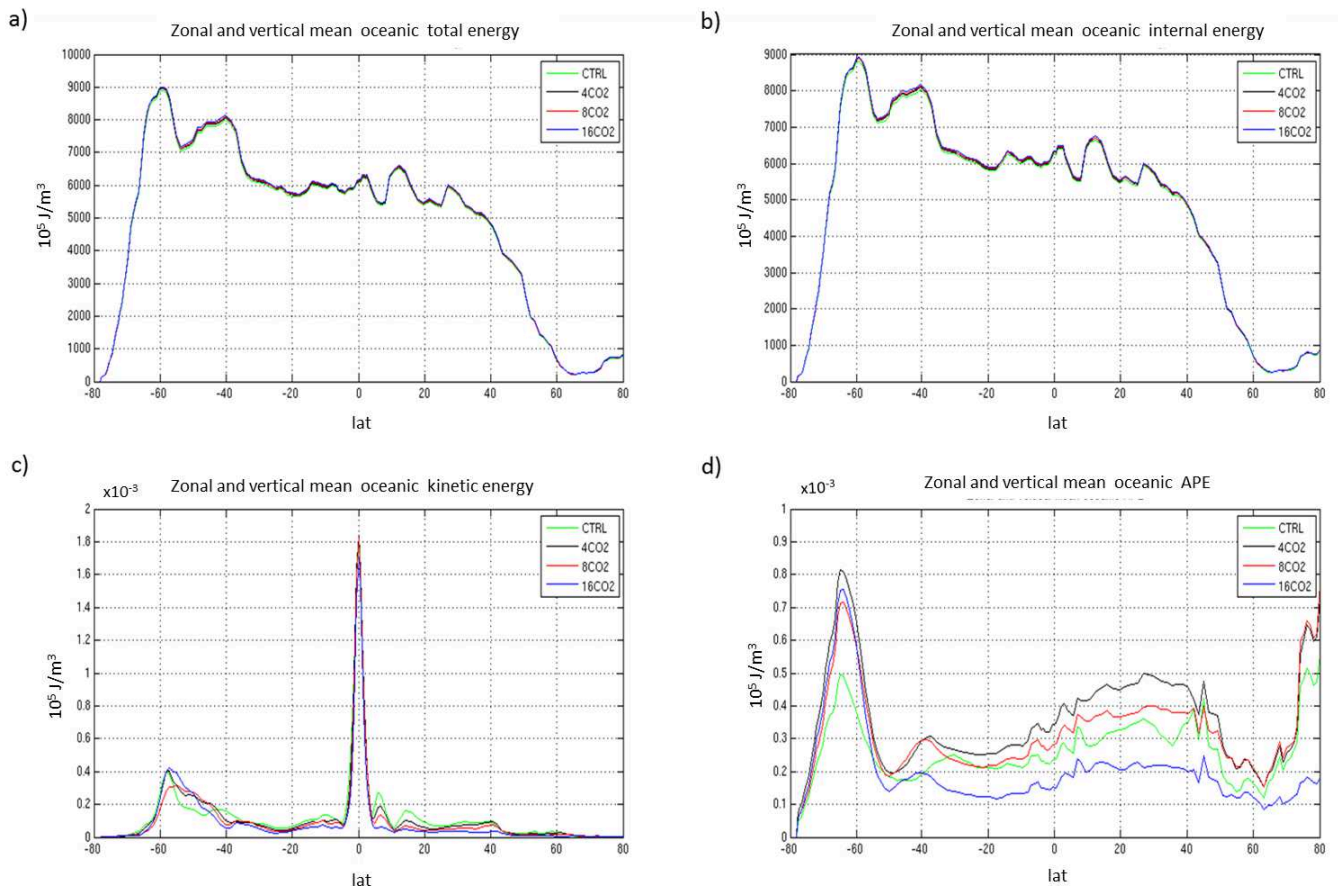 for annual-mean conditions for CTRL (green line), 4xCO_2 (black line), 8xCO_2 (red line) and 16xCO_2 (blue line).

Although IE and PE represent the maximum part of the total oceanic energy, most of such a huge energy is dynamically inert and only a very small fraction, the APE, is dynamically active and participates in the conversion into and from KE. As suggested by Oort et al. (1989), the contribution of IE to APE can be neglected and the availability of energy is mainly gravitational.

Table 5.2 shows the APE computed as in eq. 5.8 integrating over the global domain in each experiment. The global-mean density over each model depth level has been taken as the reference state. The APE shows a non linear behavior in response to the global warming. It globally increases by 35% and 21% in $4CO_2$ and $8CO_2$ experiments, respectively, with respect to the CTRL, while it decreases by 32% in $16CO_2$ simulation. The increase of APE in $4CO_2$ and $8CO_2$ experiments is due to an increased horizontal density-difference mainly at high latitudes and in particular in the Southern Ocean, as suggested by fig. 4.2 for the Atlantic Ocean sector. The Westerlies, blowing over those latitudes and outcropping the isopycnals, help to increase the APE. As shown in fig. 5.8d, the global APE in $16CO_2$ experiment decreases northward of 40°N in response to an increasing stratification and stabilization of the water column, as shown in fig. 4.2d for the Atlantic basin. The APE shows a maximum within high-latitudes (60°N-80°N)(fig. 5.8d) in correspondence of the location of convective sites in the North Atlantic (fig. 3.14). This finding is in accordance with the physical process happening in the ocean where the potential energy is released when dense water sinks into deep ocean.

The APE computed in the CTRL has a comparable value to previous APE estimates (Oort et al, 1989), i.e. $4.21*10^{20}$J versus $1.55*10^{20}$J. Furthermore, the APE computed for the Atlantic Ocean (tab. 5.2), using as the reference state the Atlantic horizontal mean density over each model depth level, in the CTRL experiment is closer to previous estimates (i.e. $0.49*10^{20}$J versus $0.52*10^{20}$J in Oort). The APE in the Atlantic Ocean, as in the global domain, does not show a linear response to the increased forcing. It increases by 31% and by 14% with respect to the CTRL case in the $4CO_2$ and $8CO_2$ experiments, respectively, while it decreases by 57% in $16CO_2$ case with

respect to the CTRL.

The APE represents a great source of energy available to be converted into KE. The total KE computed as in eq. 5.1 is indeed only a minute fraction of the total oceanic energy. In response to the forcing applied the KE decreases by 7%, 16% and 28% in $4CO_2$, $8CO_2$ and $16CO_2$ experiments with respect to the CTRL case (tab. 5.2). Fig. 5.8c shows the KE mean meridional profile with the maximum values in the equatorial regions and secondary maxima in the Southern Ocean region mainly due to the KE generation by the wind work on the ocean surface. The weakening of the wind stress in response to the global warming leads to a decreased supply of KE into the ocean (tab. 5.3).

An important contribution to the total KE is given by the amount of energy converted between APE and KE, identified by B when globally integrated as in eq. 5.10. Locally B takes into account the work done by pressure gradients as well, nevertheless, due to time deficiency, in our analyses we do not differentiate the two terms of eq. 5.10.

B computed for the Global and the Atlantic Ocean is reported in tab. 5.3. Globally $B<0$, meaning that KE is converted to APE. Fig. 5.9 shows $\int -\mathbf{u_h} \cdot \nabla_\mathbf{h} P dz$ computed for all the experiments. In the CTRL case the negative values are located mainly at the equator and at the Southern Ocean latitudes indicating a removal of KE by the pressure-gradient work partly balanced by the KE input by the wind.

Even if in response to CO_2 forcing the wind stress over the Southern Ocean weakens and less work has to be done against the wind stress, B becomes globally more negative, mainly due to the areas around the equatorial latitudes and to a decreased KE generation by pressure-gradient work along the western boundary currents. Over the Indian and the Pacific Ocean in fact B becomes more negative within the Tropics since the surface winds intensify and more work has to be done against the pressure- gradient force (not shown).

The areas where KE is generated by the pressure-gradient work are con-

	CTRL	**4 × CO2**	**8 × CO2**	**16 × CO2**
B (Glob. O.) (TW)	-0.050	-0.120	-0.240	-0.380
B (Atl. O.) (TW)	0.050	0.031	-0.001	-0.014
W (Glob. O.) (TW)	1.266	1.276	1.224	1.040
W (Atl. O.) (TW)	0.143	0.126	0.112	0.088
Dh (Glob. O.) (TW)	-0.423	-0.414	-0.402	-0.384
Dh (Atl. O.) (TW)	-0.037	-0.030	-0.027	-0.026
Dv (Glob. O.) (TW)	-0.898	-0.818	-0.796	-0.770
Dv (Atl. O.) (TW)	-0.030	-0.022	-0.020	-0.012
Q (Glob. O.) (TW)	0.105	0.077	0.214	0.495
Q (Atl. O.) (TW)	-0.126	-0.106	-0.064	-0.035

Table 5.3: Kinetic energy budget components integrated over the Global and the Atlantic Ocean computed for all the simulations (TW) for the last 100 years of all simulations (J). B is the KE change by the pressure-gradient work, W the KE change by the wind work, Dh and Dv the dissipation by horizontal and vertical (viscous) diffusion of momentum, respectively, Q the loss of the KE due to other processes influencing the KE budget not taken into account. Positive terms tend to increase KE.

fined along the Gulf Stream and the Kuroshio currents and in the area of NADW formation indicating that KE is supplied to the Atlantic THC, in accordance with Gregory et al. (2010).

When B is computed for the Atlantic Ocean, a positive pressure-gradient work is found in the CTRL case (tab. 5.3), with a value in agreement with Gregory et al. (2010). As the CO_2 forcing increases, B becomes less positive in the $4CO_2$ experiment and it reverses sign in the $8CO_2$ and $16CO_2$ experiments. Less KE is converted from APE by the pressure-gradient work and, in particular, in $8CO_2$ and $16CO_2$ experiments KE is converted to APE in the Atlantic Ocean.

Nevertheless, KE is mostly supplied to the ocean by the surface wind stress and its dissipation through the water column decreases as the KE input diminishes, as shown by values reported in tab. 5.3. The horizontal (Dh) and vertical (Dv) dissipations, defined as in eq. 5.12, have been calculated for the Global and the Atlantic Oceans and reported in tab. 5.3. In addition to the terms in eq. 5.10, a residual term Q has been computed for the geographical domains considered and it is reported in tab. 5.3. This term includes the source of errors due to the discretization of continue variables and to the approximation to single precision variables. In the residual term another uncertainty included is the time average of the energy budget terms done over monthly means rather over the model time step (96 minutes). Since our analyses consider a stable climate in all the simulations, the Q term has been computed in order to have the KE balance closed.

In response to the increased CO_2 forcing, W, computed as in Eq. 5.11 for the global domain, reflects the variations of the Southern Ocean wind stress (tab. 3.1) indicating the importance of that region for the global supply of KE by the winds. Fig. 5.10 shows the KE changes associated to the wind work over the ocean surface and computed as $\mathbf{u_h} \cdot \tau$ for all simulations. The largest KE input is near the equator and in the Southern Ocean latitudes (Atlantic and Indian sector) due to strong westerly winds. In the $4CO_2$ experiment there is an intensification of the global W in response to increased
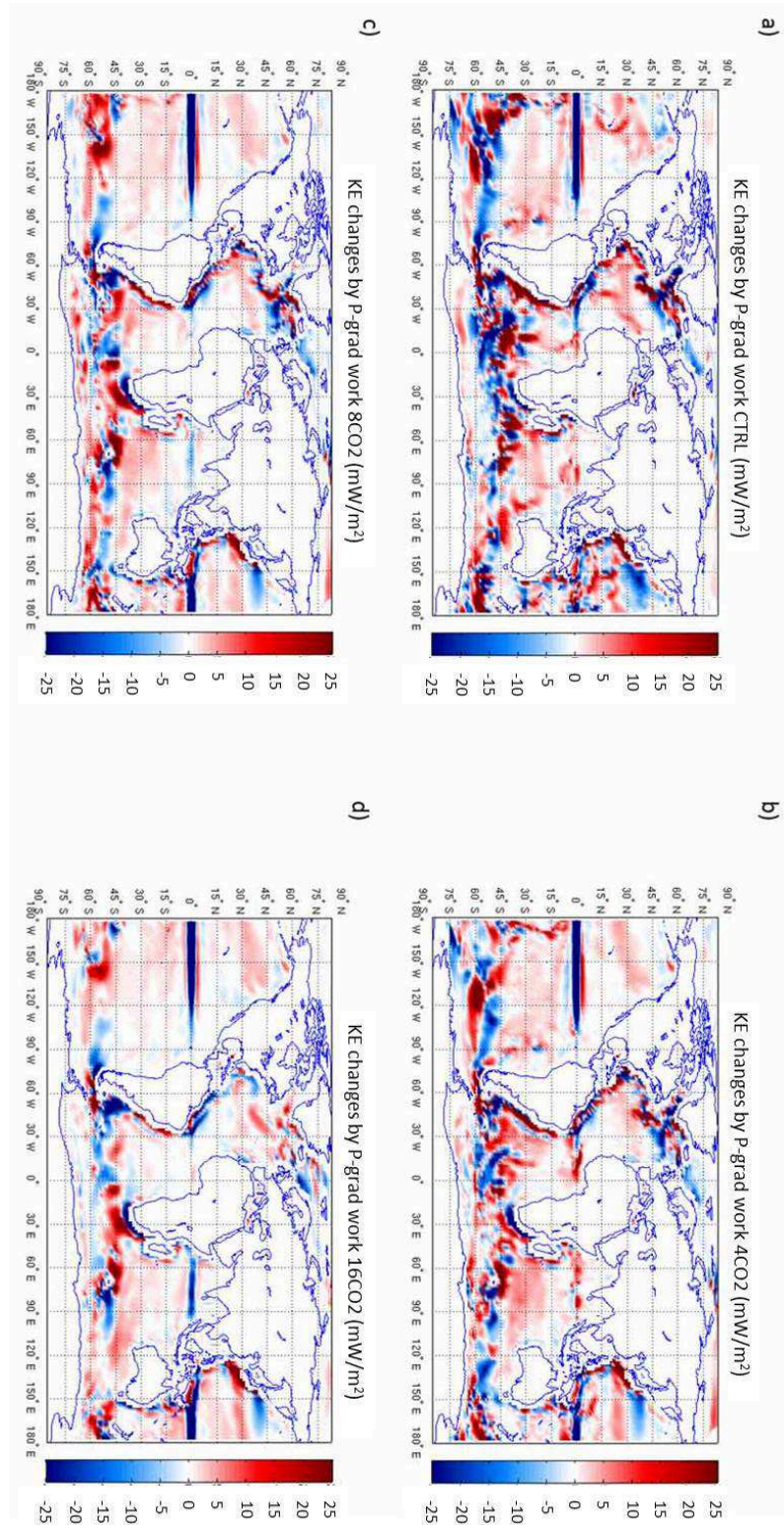
Figure 5.9: Annual mean kinetic energy changes into the ocean by pressure-gradient work (W/m²) integrated over the water-column ($\int -\mathbf{u_h} \cdot \nabla_\mathbf{h} P dz$) for (a) CTRL, (b) $4xCO_2$, (c) $8xCO_2$ and (d) $16xCO_2$ experiments .
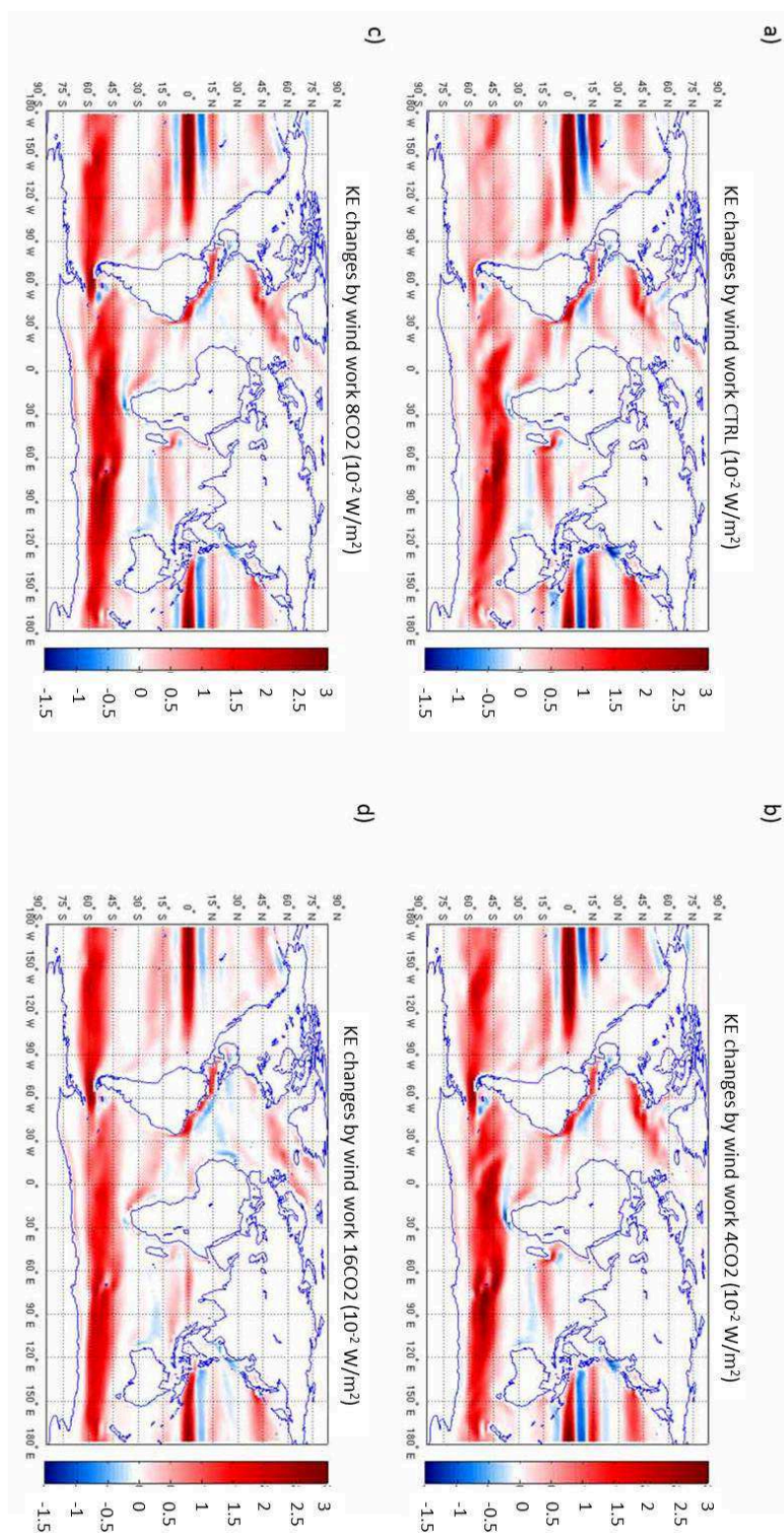
Figure 5.10: Annual mean kinetic energy changes into the ocean by the winds work ($\mathbf{u_h} \cdot \tau$) (10^{-2} W/m²) for (a) CTRL, (b) $4xCO_2$, (c) $8xCO_2$ and (d) $16xCO_2$ experiments .

westerly winds over the Southern Ocean (fig. 5.10b) , in the $8CO_2$ and $16CO_2$ experiments there is a little decrease in the input of KE associated with the global weakening of the wind stress over the ocean surface (tab. 5.3). The reduced input of KE is then reflected into reduction in its vertical dissipation (tab. 5.3).

A large W decrease is found among the simulations in the Atlantic Ocean (tab. 5.3). It decreases by 12%, 22% and 39% with respect to the CTRL in $4CO_2$, $8CO_2$ and $16CO_2$ experiments, respectively, indicating a smaller supply of KE to the ATHC circulation. Fig. 5.11 shows the KE change (W) associated to wind work in the North Atlantic where it is evident the maximum value of KE input along the Gulf Stream pathway. As the wind intensity decreases at mid-latitudes in response to the global warming, so does the KE input by the winds integrated over the Atlantic basin (fig. 5.11b,c,d).

Although W is the term giving the largest contribution to the KE balance, in the Atlantic basin it shows relative small reduction in response to the CO_2 forcing if compared to the changes occurring to B in the same basin. In fact, B computed in the Atlantic Ocean decreases by 38% with respect to the CTRL in the $4CO_2$ experiment and becomes negative in the $8CO_2$ and $16CO_2$ experiments.

Fig. 5.12 shows $\int -\mathbf{u_h} \cdot \nabla_{\mathbf{h}} P dV$ versus the ATHC maximum at 25°N computed for all simulations. B has been obtained integrating the eq. 5.10 in the Atlantic basin between 15°N-60°N, in order to consider the latitudes of maximum ATHC overturning in each simulation (fig. 3.13), and in the water column below the Ekman layer, to avoid the negative contribution in upper layers from work done against the sea-surface slope, associated with the northward flow of the ATHC, as already done by Gregory et al. (2010).

B, computed over this domain, shows a positive sign in all the experiments suggesting a KE conversion by pressure-gradient work. In response to the CO_2 forcing, B decreases by 29%, 57% and 90% in $4CO_2$, $8CO_2$ and $16CO_2$ experiments, respectively. The decreased B matches with the decreased ATHC showing a strong linear relation, as already found by Gregory
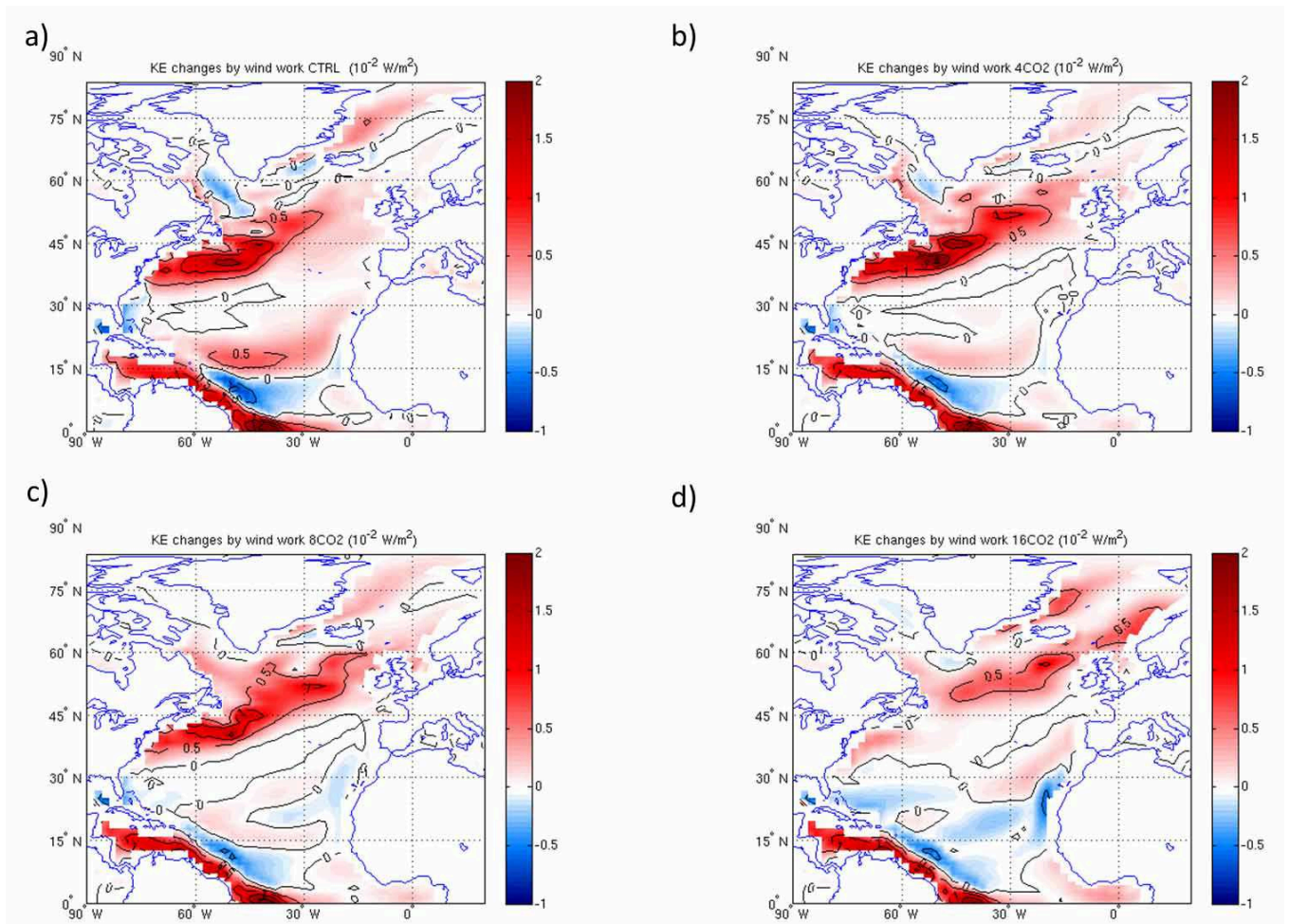
Figure 5.11: Annual mean kinetic energy changes into the North Atlantic Ocean by the winds work ($\mathbf{u_h} \cdot \tau$) (10^{-2} W/m^2) for (a) CTRL, (b) 4xCO_2, (c) 8xCO_2 and (d) 16xCO_2 experiments .
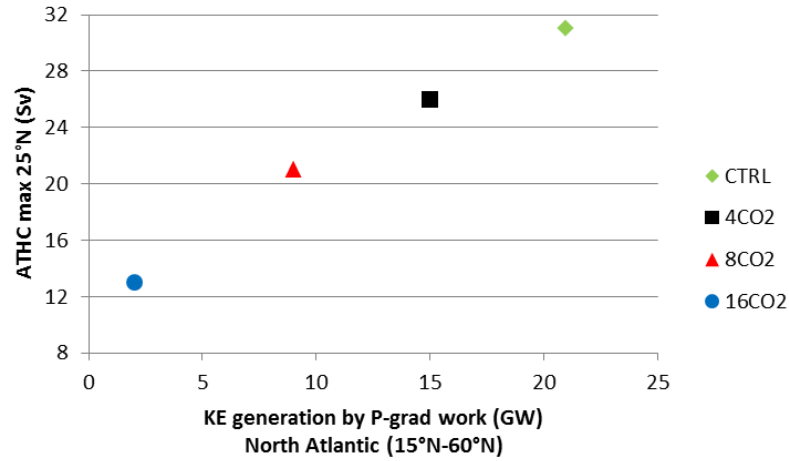
Figure 5.12: Max Atlantic THC intensity (Sv) at 25°N versus annual mean KE generation (GW) by the pressure-gradient work ($\int -\mathbf{u_h} \cdot \nabla_\mathbf{h} P dV$) integrated over the Atlantic latitudes between 15°N-60°N and below the Ekman layer and above the southward flow of the ATHC for CTRL (green diamond), 4xCO_2 (black square), 8xCO_2 (red triangle) and 16xCO_2 (blue circle) experiments .

et al. (2010) under CO_2-forced simulations. The positive sign of B indicates that the KE input by the pressure-gradient work drives the Atlantic circulation, as suggested by Gregory et al. (2010). The KE generated by the pressure-gradient work is then dissipated by the viscosity at all latitudes.

The result above indicates that when the KE input into the ocean by pressure-gradient work as well as the wind work decreases in response to the CO_2 forcing applied, so does the Atlantic THC in order to match the decreased mechanical energy provided into the ocean system. Under global warming conditions then the term which shows greatest variation is the one associated with the pressure-gradient work which provides less KE to the ocean circulation in the North Atlantic latitudes leading to ATHC weakening, in agreement with Gregory et al. (2010).

5.4 Conclusions

The Earth's climate system in response to warming conditions induced by large CO_2 atmospheric forcings shows an almost constant total energy budget.

The two components, atmosphere and ocean, respond to the radiative perturbation in a different way: while the atmospheric total energy increases in dependence on the intensity of the forcing applied (by 4%, 8% and 15% in $4CO_2$, $8CO_2$ and $16CO_2$ experiments, respectively), the ocean does not show striking variations in its total energy balance due to its great thermal capacity.

The radiative forcing applied influences the atmospheric budget leading to a more energetic troposphere where the greatest contribution to the total balance is given by the internal energy. The atmosphere in response to the global warming shows increasing temperature through all the air column with the maximum values at the tropics. At that latitudes in the upper troposphere the warming is greater than that at higher latitudes and the strong zonal temperature gradient leads to more available potential energy provided in the atmosphere. Part of that available potential energy may be converted in kinetic energy intensifying the mid-latitudes jet streams which further expand upward and shift poleward, in agreement with previous studies (Kushner et al, 2001; Williams, 2006; Lorenz et at, 2007).

The atmospheric energy component experiencing the greatest variations under global warming condition is the latent energy, in particular at low latitudes, mainly in response to the greater water vapor concentration due to an enhanced evaporation in the CO_2 simulations. However, the rate of increase of water vapor in the atmosphere is not associated with the same rate of increase in precipitation leading to a stabilization of the tropical atmosphere and a weakening of the Hadley circulation, as already found by Sugi et al. (2002). The weakening of the circulation is associated to a reduction and an upward expansion of the Hadley circulation although with an asymmetry among the cells in the two hemispheres which influences the

meridional transport of the total atmospheric energy.

Since the internal energy is the form of energy that more contributes to the total atmospheric budget and it depends on the temperature field, the energy transport is mainly associated with the atmospheric meridional heat transport. That transport globally increases among the CO_2 simulations in order to balance the decreased oceanic northward heat transport mainly due to the weakening of the ATHC.

The reduction of the oceanic circulation strength is related to a large decrease in kinetic energy input into the ocean. The kinetic energy is supplied to the ocean by the wind work at the surface, in particular by the Westerlies over the Southern Ocean, which decreases in response to the global warming. In the CO_2 simulations the KE time rate change that shows the greatest variations is the pressure-gradient work term, which contains the conversion between APE and KE. In the large CO_2 experiments the pressure work term becomes globally more negative indicating an increased of KE conversion to APE in the areas of strong surface winds.The APE, on the other hand, does not show a linear response to the forcing applied since it increases in $4CO_2$ and $8CO_2$ experiments and decreases in $16CO_2$ simulation in relation to changed meridional density differences in the water column. The latitudinal distribution of the APE shows that it is stored in the Southern Ocean latitudes in response to the large wind stress work. In the North Atlantic, KE is instead generated by conversion from APE which is in turn destroyed by the deep water formation processes.

In the Atlantic Ocean, as in the global domain, the energy term showing the greatest variations is the one associated with the pressure-gradient work, which is positive in the CTRL indicating a conversion from APE to kinetic energy. However, in the sensitivity experiments the conversion term decreases strongly in $4CO_2$ experiment and reverses the sign in the $8CO_2$ and $16CO_2$ simulations indicating a stabilization of the water column in response to the increasing forcing with less APE converted into kinetic energy. This is because less deep water is formed and APE is not converted as efficiently

to KE. A linear relationship then has been found between the maximum variations of the conversion term in the area between 15°N-60°N where it is always positive and the strength of the ATHC maximum. This suggests that the pressure-gradient work term in this region drives the circulation converting from APE: this input decreases among the CO_2 simulations when the Atlantic THC intensity decreases. A similar result has been found by Gregory et al. (2010) under CO_2-forced simulations.

The analysis of the Earth's system energetics under global warming conditions is an actual topic of research.

The present study gives a preliminary contribution to widen the present day knowledge on the energy cycle involved in the climate system and on the relationship between the Earth's system energetics and the atmospheric and oceanic large scale circulation.

Chapter 6

Conclusions

The present study examines the sensitivity of the climate system, with a focus on the North Atlantic Ocean and on the Atlantic THC, to strong, but nonetheless within the range of observed values in past climates, CO_2 atmospheric forcing as well as the consequences for the energetics of the Earth's climate system. The analysis is done using a set of long experiments (600 years) obtained with a state of the art coupled climate model at low resolution. In particular we analyze a control experiment (CTRL) and a set of sensitivity experiments with increased atmospheric carbon dioxide concentration. In the CTRL the carbon dioxide concentration is 353 ppmV, corresponding to the present's day mean value. It has been multiplied by a factor of 4, 8 and 16 to build $4CO_2$, $8CO_2$ and $16CO_2$ experiments, respectively.

Increased atmospheric CO_2 concentration leads to a warmer global climate with a warmer and more saline Atlantic Ocean. However, the Labrador Sea shows a distinctive behavior since it is subjected to a freshening caused by changes in surface heat and freshwater fluxes.

The sea-ice Arctic cap completely melts under global warming conditions in the two more extreme experiments while stabilizes at 1% of its initial volume in the $4CO_2$ experiment. This melting induces a freshwater input in the North Atlantic of 0.01 Sv, 0.02 Sv and 0.06 Sv in $4CO_2$, $8CO_2$ and $16CO_2$ simulations, respectively, which is far enough from the freshwater

111

forcing of the traditional hosing-experiments (Stouffer et al, 2006), except for the $16CO_2$ case which has an almost comparable value. Furthermore, the model does not simulate the freshwater input of the land-ice melting and the river runoff contribution which could be an important source of freshwater at high latitudes.

Differently from the hosing experiments, the set of simulations used in this thesis permits to investigate changes in the ATHC due to density field variations associated with heat fluxes changes. The imposition of an increased radiative forcing, as the enhanced atmospheric CO_2 concentration, leads in fact to changes in the ocean properties through changes in the density because of warmer temperature and of the freshwater input in the North Atlantic latitudes,as a consequence of the sea-ice melting. The advantage of the present study is hence the possibility to evaluate the overall impact of strong CO_2 forcing over the climate system considering the atmosphere-ocean interaction using a global coupled general circulation model.

One of the most important effects obtained in the climate system in response to the application of CO_2 radiative forcing is the increase of the tropospheric temperature. The global warming conditions cause a tropopause height increase and a wind pattern variation, as suggested by several studies (Kushner et al, 2001; Raisanen , 2003; Williams, 2006; Lorenz et at, 2007). In the upper troposphere, the jet-streams intensify and shift poleward while at the atmosphere-ocean surface the westerlies become weaker and more zonal at mid-latitudes leading the Gulf Stream to vanish in the most extreme case.

In response to the CO_2 forcing, the Atlantic THC weakens and becomes shallow, in agreement with previous studies (Dixon et al, 1999; Wood et al, 1999; Mikolajewicz and Voss, 2000; Thorpe et al, 2001; Schmittner et al, 2005; Gregory et al, 2005; Weaver et al, 2007). It never shows a collapse not even in the most extreme case since the freshwater input at high latitudes is probably far from the "Stommel bifurcation point", the threshold beyond which no NADW formation can be sustained (Rahmstorf, 2000; Rahmstorf

et al , 2005). The ATHC shows in fact a monostable regime influenced by the continuous salt-advection through the southern boundary of the Atlantic basin, as suggested by Hawkins (2011). Nevertheless, to analyze the ATHC hysteresis behavior a larger number of experiments with increasing CO_2 levels would be necessary.

In the most extreme case, the ATHC shows also a spatial reorganization, with the collapse of the convective sites in the Labrador Sea, because of a stratification of the water column and inhibition of NADW formation, but the creation of new convective sites southeast of Greenland. In the $16CO_2$ experiment the maximum overturning shifts at mid-latitudes. The heat transport is affected as well by the weakening of the ATHC and the stabilization of the water column with a decreased northward heat transport.

The mechanisms involved in the response of the Atlantic THC to the radiative forcing have been investigated and specific attention has been posed to changes in meridional density gradients between high and low latitudes, in water column vertical diffusivity and in Southern Ocean wind stress as main factors influencing the ocean circulation intensity.

We found an anti-correlation between the strength of the Atlantic THC maximum value at 25°N and the meridional density gradient computed between high and low latitudes: the circulation weakens as the density gradient increases. However, the simulation subjected to the largest radiative forcing ($16CO_2$) behaves differently since, even though the computed meridional density gradient is close to the CTRL one, the Atlantic THC strongly weakens. The $16CO_2$ experiment differences with respect to the $4CO_2$ and $8CO_2$ simulations and the reason may lie in a freshwater input amount at high latitudes comparable with the one used in the hosing experiments (i.e. close to a threshold beyond which the system may show an hysteresis regime).

The anti-correlation found in the $4CO_2$ and $8CO_2$ between the meridional density differences and the ATHC strength suggests the importance of the vertical diffusivity processes in the ocean interior controlling the strength of the ATHC (Bryan, 1987). A relationship close to linear is found in all the

CO_2 simulations between the circulation intensity and the North Atlantic vertical diffusion: when the forcing applied increases, the vertical mixing through the water column decreases at high latitudes, as response to vertical density stratification, and the Atlantic THC weakens. This finding is in agreement with Nillsson et al. (2001;2003) who showed a decreased vertical diffusion, linked to an increased stratification of the water column, causing a weakened ocean circulation.

Despite many studies stress the strong dependence of the ocean circulation intensity from the wind forcing at the Southern Hemisphere (Toggweiler and Samuels, 1995; Saenko and Weaver, 2004; Gnanadesikan, 2007; Hirabara et al, 2007), with an increasing wind forcing leading to an increasing overturning in the Atlantic Ocean, our set of experiments does not show any particular relation between the two variables. The intensity of the Atlantic THC seems indeed disconnected from the forcing acting over the Southern Ocean surface, except for the $16CO_2$ simulation where a reduction in the Atlantic THC is related to a weakening of the westerlies stress (in addition to changes in diffusivity).

Another factor influencing the ATHC is represented by the water mass properties of the Mediterranean Outflow Waters (MOW). Previous studies suggest that the MOW is a source of warm and saline water at depth, but it has also a strong dynamic impact on the upper-layer circulation in the subtropical eastern North Atlantic (Jia, 1999). The input of very high density waters through the Gibraltar Strait, as shown in the $16CO_2$M simulation, which is identical to the $16CO_2$ experiment apart from an extra salinification of the Mediterranean waters, leads to an intensification at mid-latitudes of the Azores Current which, recirculating zonally the high density MOW, forms a density front through the Atlantic water column close to 40°N (not only at the surface as in the $16CO_2$ experiment described). That front acts over the ATHC obstructing the northward flow and leading the warm and salty tropical waters to sink at mid-latitude. As a consequence, the high latitudes surface waters become lighter preventing the NADW formation.

The weakening of the Atlantic THC under increasing CO_2 atmospheric concentration and the related decreased northward heat transport are associated with a large decrease of oceanic kinetic energy, even though the total oceanic energy slightly increases in the sensitivity experiments.

The global kinetic energy budget performed indicates that the largest energy input is supplied mainly by the wind work, in particular the westerly winds over the Southern Ocean, which slightly decreases in response to the global warming. In the CO_2 simulations the term of the KE budget that shows the greatest variations is the pressure-gradient work term, which contains the conversion between APE and KE. In the large CO_2 experiments the pressure gradient work term becomes globally more negative indicating an increased conversion of KE to APE in the areas of strong surface winds.

The APE, on the other hand, does not show a linear response to the forcing applied since it increases in $4CO_2$ and $8CO_2$ experiments and decreases in $16CO_2$ simulation in relation to changed meridional density differences in the water column. The latitudinal distribution of the maximum values shows the APE mainly stored at the Southern Ocean latitudes, due to the great wind stress which leads to strong meridional density differences through the outcrop of the isopycnals, and in the North Atlantic, associated with the areas of deep convection.

In the Atlantic Ocean, as in the global domain, the energy term showing the greatest variations is the one associated with the pressure-gradient work, which is positive in the CTRL case indicating a conversion from APE to KE. However, in the sensitivity experiments the conversion term decreases strongly in $4CO_2$ experiment and reverses the sign in the $8CO_2$ and $16CO_2$ simulations indicating a stabilization of the water column in response to the increasing forcing with less APE converted into KE.

In the sensitivity experiments, the maximum variations of this term have been found in the regions of ATHC maximum overturning. A linear relationship then has been found between the maximum variations of the conversion term in the North Atlantic and the strength of the ATHC maximum sug-

gesting that the pressure-gradient work drives the circulation through the input of KE: as this input decreases among the CO_2 simulations so does the Atlantic THC intensity. A similar result has been reported by Gregory et al. (2010) under CO_2-forced simulations.

Differently from the global ocean, the atmosphere becomes significantly more energetic. The greatest contribution to the total atmospheric energy balance is given by the internal energy, with the maximum values at the tropics in correspondence of the maximum warming. Since the upper troposphere in the tropics warms up more than that at higher latitudes, more available potential energy is provided in the atmosphere. The strong horizontal temperature gradient in the atmosphere causes an increase of kinetic energy and the mid-latitudes jet streams to intensify, to expand upward and to shift poleward (Kushner et al, 2001; Williams, 2006; Lorenz et at, 2007).

However, the atmospheric energy component which is subjected to the greatest variation is the latent energy at low latitudes mainly in response to the greater water vapor concentration in the CO_2 simulations. The increased latent heating in the atmosphere, in response to greenhouse warming, is associated with an increase of the global averaged precipitation at the tropics and at high-latitudes. Nevertheless, the increase in the tropical precipitation is much less than the rate of increase in the atmospheric moisture, in agreement with several studies (Betts, 1998; Held and Soden, 2006; Cherchi et al, 2011), leading to a stabilization of the tropical atmosphere and a weakening of the atmospheric circulation (Sugi et al, 2002). The differential rate of response to surface warming of water vapor and precipitation implies in fact a weakening of the boundary layer/troposphere mass exchange (Held and Soden, 2006) which reflects into a reduction and an upward expansion of the Hadley circulation (Vecchi et al, 2006) which shows an asymmetry among the cells in the two hemispheres influencing the meridional transport of the total atmospheric energy.

That energy transport is mainly associated with the meridional heat transport since the energy component giving the most contribution to the

total atmospheric energy is the internal energy. Under global warming conditions the heat transport by the atmosphere increases, mainly at high latitudes, in order to balance the decreased oceanic northward heat transport, due to the weakening of the ATHC, and to maintain almost constant the Earth's system total energy budget even under extreme regimes.

The understanding of the physical mechanisms driving the Atlantic THC is an hot topic in the scientific community and the main results are still controversial. A lot of interest is posed over the response of the ATHC to a CO_2 forcing since this oceanic circulation transports a huge amount of heat to the North Atlantic latitudes. Here we found that even under an extreme radiative forcing, as the 16 times the present's day atmospheric CO_2 concentration, the ATHC never collapses but it subject to a spatial reorganization due to the shift of the North Atlantic convective sites. Nevertheless, this finding may be affected by a salinity bias due to the model configuration used which computes the hydrological cycle not considering the runoff contribution, hence leading to more saline and dense waters that can easily sink at high latitudes reinforcing the ATHC strength. Further, a better representation of the Mediterranean waters, without any relaxation in temperature and salinity, would be necessary in order to have a better evaluation of the MOW impact over the ATHC.

According to the IPCC scenarios (IPCC, 2007), the global warming due to increased GHGs in the atmosphere will increase in the future and the actual ATHC could be subjected to reorganization because of heat and freshwater flux changes in a warmer world. This study advances the knowledge of the mechanisms influencing the Atlantic THC under extreme CO_2 radiative forcing and the energetics of the Earth system under global warming conditions.

Acknowledgments

I wish to dearly thank Simona Masina for supervising me, to help me through challenging times to achieve compelling scientific results and for encouraging me to improve my research methods.

I thank Annalisa Cherchi for the time she dedicated to discuss together the issues I've had to face during this research and for the moral support in moments of discouragement.

I am infinitely grateful to Marcelo Barreiro for giving me the opportu-

nity to spend few months at the University of Montevideo, for his valuable scientific contribution and for keeping me motivated.

I would like to sincerely thank Nadia Pinardi and Alessio Bellucci who carefully read a preliminary draft of the thesis and provided useful comments for its improvement.

My gratitude goes also to Pierluigi Di Pietro for technical support in managing and analyzing data.

These four years of PhD would have been definitely much harder without the strong support of my family, my parents and my sisters Cristina, Claudia and Francesca, who have always believed in me and encouraged me to pull out the determination to pursue the goal.

I consider myself very lucky because despite being far from home, I found some good friends in Ferrara with whom I shared laughs, tears and lots of drinking. Thank you so much to the occupants of the "people's house": Vito, Claudia, Daniela, Pierpaolo and Francesco, Toso, Silvia, Simone, Chiara and Alberto, Francesco, Matteo, Maria Chiara, Monir, Losc, Max and Domenico.

The sale of the house and the move will put an end to an era, but not to the deep affection that binds me to you.

New/old city means new/old friends. A special thanks goes to Francesco who supported me for the last 10 years and who seems ready to do so for at least another 10, and to Marcello and Domenico who have already welcome me as one of them probably because they have gotten themselves into.

A great thank to Iolanda, Federica, Lucia, Nadia, Mariangela, Nella and Anto, friends who have broken down the physical distances in every time of need with precious and fundamental advices.

Thanks to my old colleague and friend, as well as my spirit guide,Giuseppe. In the past three years by your side I have grown so much not only scientifically but humanly as well.

Thanks also to my current deskmate Miriam, dear trusted friend rather than a fearful colleague.

I thank Flo as well, a great scientific and moral supporter, always present and ready to devote her precious time just to make me feel better.

Then I can only thank my colleagues but also friends of long talks and confidences, of afternoon breaks in front of the junk food machine, of lunch breaks at "mensino" with the special potatoes and of coffee breaks to the "ladrone". Thanks a lot then Stefano, Damiano, Paolo, Ida, Leone, Jenny, Fabri, Tete, Sara, Toto, Michela, Andrea, Ilaria, Claudine, Matteo, Giacomo and Irene.

Finally, a last and greatest thank you goes to Savio who was always close to me in the difficult and important times of the PhD and whose support was critical to the achievement of this important goal.

Bibliography

Allen MR and Ingram WJ (2002) Constraints on future changes in climate and the hydrologic cycle. Nature 419:224-232

Ambar I and Howe MR (1979) Observations of the Mediterranean outflow. II. The deep circulation in the vicinity of the Gulf of Cadiz. Deep-Sea Res, 26A: 555-568

Alley R and Clark P (1999) The deglaciation of the Northern Hemisphere: A global perspective. Annu Rev Earth Planet Sci 27: 149-182.

Artale V, Calmanti S, Sutera A (2003) Thermohaline circulation sensitivity to intermediate level anomalies. Tellus 54A: 159-174

Artale V, Calmanti S, Malanotte-Rizzoli P, Pisacane G, Rupolo V, Tsimplis M (2006) The Atlantic and the Mediterranean Sea as connected systems. In: Lionello P, Malanotte-Rizzoli P, Boscolo R (eds), Mediterranean climate variability. Elsevier, Amsterdam, Teh Netherlands, pp.283-323

Baringer MO and Price JF (1997) Mixing and spreading of the Mediterranean outflow. J Phys Oceanogr 27: 1654 -1677

Barreiro M, Fedorov A, Pacanowski R, Philander SG (2008) Abrupt climate changes: How freshening of the northern atlantic affects the thermohaline and wind-driven oceanic circulations. Ann Rev Earth Planet Sci 36:33-58

Beckmann A and Dorscher(1997) A method for improved representation of

dense water spreading over topography in geopotential-coordinate models. J Phys Oceanogr 27:581-591

Bengtsson L, Botzet M, Esch M (1996) Will greenhouse gas-induced warming over the next 50 years lead to higher frequency and greater intensity of hurricanes? Tellus 48: 57-73

Bengtsson L, Hodges KI, Roeckner E (2006) Storm tracks and climate change. J Clim 19: 3518-3543

Betts AK (1998) Climate-convection feedbacks: some further issues. Clim Change 39: 35-38

Blanke B, Delecluse P (1993) Low frequency variability of the tropical Atlantic ocean simulated by a General Circulation Model with mixed-layer physics. J Phys Oceanogr 23:1363-1388

Bower AS, Cann B, Rossby T, Zenk W, Gould J, Speer K, Richardson PL, Prater MD, Zhang HM (2002) Directly measured mid-depth circulation in the northeastern North Atlantic. Nature 41: 603-607.

Bryan F (1987) Parameter sensitivity of primitive equation ocean general circulation models. J Phys Oceanogr 17: 970-985.

Cai W (1994) Circulation driven by observed surface thermohaline fields in a coarse resolution ocean general circulation model. J Geoph Res 99: 163-181.

Cai W, Syktus J, Gordon HB, O' Farrell S (1996) Response of a Global Coupled Ocean-Atmosphere-Sea Ice climate model to an imposed North Atlantic high-latitude freshening. J Clim 10: 929-948.

Cai W, Whetton PH, Karoly DJ (2003) The response of the Antarctic Oscillation to increasing and stabilized atmospheric CO_2. J Clim 16: 1525-1538.

Candela J (2001) Mediterranean water and global circulation. Ocean circulation and climate. Academic Press, New York, pp.419-429

Carissimo BC, Oort AH, Vonder Haar TH (1984) Estimating the meridional energy transports in the atmosphere and ocean. J Phy Oce 15: 82-91

Cherchi A, Masina S, Navarra A (2008) Impact of extreme CO_2 levels on tropical climate: a CGCM study. Climate Dyn 31:743-758

Cherchi A, Alessandri A, Masina S, Navarra A (2011)Effects of increased CO_2 levels on monsoons. Climate Dyn 37:83-101

Chou C and Neelin JD(2004) Mechanisms of global warming impacts on regional tropical precipitation. J Clim 17: 2688-2701.

Clark PU, Pisias NG, Stocker TF, Weaver AJ (2002) The role of the thermohaline circulation in abrupt climate change. Nature 415: 863-869

Clarke GKC, Leverington DW, Teller JT, Dyke AS (2003) Superlakes, megafloods, and abrupt climate change. Science 301: 922-923

Cubash U and Coauthors(2001) Projections of future climate change. Climate Change 2001: The scientific basis. Houghton JT et al., Eds., Cambridge University Press: 525-582

Curry R, Dickson B, Yashayaev I(2003) A change in the freshwater balance of the Atlantic Ocean over the past four decades. Nature 426: 826-829

Da Silva A, Young AC,Levitus S (1994) Atlas of Surface Marine Data 1994, vol 1: algorithms and procedures. NOAA Atlas NESDIS 6, U.S. Department of Commerce, Washington, D.C.

De Boer AM, Gnanadesikan A, Edwards N and Watson AJ (2010) Meridional density gradients do not control the Atlantic Overturning Circulation. J Phys Oceanogr 40:368-380

Dixon KW, Delworth T, Spelman M, Stouffer RJ (1999) The influence of transient surface fluxes on North Atlantic overturning in a coupled GCM climate change experiment. Geophys. Res. Lett. 26:2749-2752

Fichefet T and Morales Maqueda MA (1997) Sensitivity of a global sea ice model to the treatment of ice thermodynamics and dynamics. J Geophys Res 102:12, 609- 12,646

Ganachaud A and Wunsch C (2000) Improved estimates of global ocean circulation, heat transport and mixing from hydrographic data. Nature 408: 453-457.

Ganopolski, A, Rahmstorf S, Petoukhov V, Claussen M (1998) Simulation of modern and glacial climates with a coupled global model of intermediate complexity. Nature 391: 351-356.

Gargett A E and Holloway G (1984) Dissipation and diffusion by internal wave breaking. J Mar Res 42: 15-27.

Gastineau G, Li L, Le Treut H (2009) The Hadley and Walker circulation changes in global warming conditions described by idealized atmospheric simulations. J Clim 22: 3993-4013

Gerdes R, Koberle C, Beckmann A, Hermann P, Willebrand J(1999) Mechanisms for spreading of Mediterranean water in coarse-resolution numerical models. J Phys Ocean 29: 1682-1700

Gill AE and Bryan K(1971). Effects of geometry on the circulation of a three-dimensional southern-hemisphere ocean model. Deep Sea Res18: 685-721.

Gnanadesikan A (1999) A simple predictive model for the structure of the oceanic pycnocline. Science 283:2077-2079

Gnanadesikan A, Dixon KW, Griffies SM, Balaji V, Barreiro M, Beesley JA, Cooke WF, Delworth TL, Gerdes R, Harrison MJ, Held IM, Hurlin WJ, Lee H, Liang Z, Nong G, Pacanowski RC, Rosati A, Samuels BL, Spelman MJ, Stouffer RJ, Winton M, Wittenberg AT, Dunne J (2006) GFDL‚Äôs CM2 global coupled climate models. part II: the baseline ocean simulation. J Clim 19:675-697

Gnanadesikan A, De Boer AM and Mignone BK (2007) A simple theory of the pycnocline and overturning revisited. Geophysical monograph 173: 19-32

Greatbatch RJ, Fanning AF, Goulding AD, Levitus S (1991) A diagnosis of interpentadal circulation changes in the North Atlantic. J Geoph Res 96: 9-23

Gregory JM and Coauthors (2005) A model intercomparison of changes in the Atlantic thermohaline circulation in response to increasing atmospheric CO_2 concentration. Geophys. Res. Lett. 32:L12703, doi: 10.1029/2005GL023209

Gregory JM and Tailleux R (2010) Kinetic energy analysis of the response of the Atlantic meridional overturning circulation to CO_2-forced climate change . Clim Dyn doi: 10.1007/s00382-010-0847-6

Gualdi S,Navarra A,Guilyardi E,Delecluse P (2003) Assessment of the tropical Indo-Pacific climate in the SINTEX CGCM. Ann Geophys 46:1-26

Gualdi S,Scoccimarro E, Navarra A (2008) Changes in the tropical cyclone activity due to global warming: results from a high-resolution coupled general circulation model. J Clim 21: 5204-5228

Guilyardi E and Madec G (1997) Performance of the OPA/ARPEGE-T21 global ocean-atmosphere coupled model. Clim Dyn 13:149-165

Guilyardi E,Delecluse P, Gualdi S,Navarra A (2003) Mechanisms for ENSO phase change in a coupled GCM. J Clim 16:1141-1158

Hawkins E, Smith RS, Allison LC, Gregory JM, Woolings TJ, Pohlmann H, De Cuevas B(2011) Bistability of the Atlantic overturning circulation in a global climate model and links to ocean freshwater transport. Geophys Res Lett 38:L10605, doi:10.1029/2011GL047208

Heinrich H (1988) Origin and consequences of cyclic ice rafting in the north-east Atlantic Ocean during the past 130.000 years. Quat. Res., 29: 143-152.

Held IM, Hou AY(1980) Nonlinear axially symmetric circulations in a nearly inviscid atmosphere. J Atmos Sci 37: 515-533

Held IM and Soden BJ (2006) Robust responses of the hydrological cycle to global warming. J Clim 19: 5686-5699

Hemming S (2004) Heinrich events: Massive late Pleistocenecdetritus layers of the North Atlantic and their global climate imprint. Rev Geophys 42, RG1005, doi:10.1029/2003RG000128.

Hide R (1969) Dynamics of the atmosphere of the major planets with an appendix on the viscous boundary layer at the rigid bounding surface of an electrically-conducting rotating fluid in the presence of a magnetic field. J Atmos Sci 26: 841-853

Hirabara M, Ishizaki H and Ishikawa I (2007) Effects of the wind stress over the southern ocean on the meridional overturning. J. Phys. Oceanogr. 37: 2114-2132

Hofmann M and Rahmstorf S(2009) On the stability of the Atlantic meridional overturning circulation. PNAS 106: 20584-20589

Huang RX (1999) Mixing and energetics of the oceanic thermohaline circulation, J Phys Oceanogr 29: 727-746. (Corrigendum, J Phys Oceanogr 32, 1593, 2002)

Huang RX (2005) Available potential energy in the world's ocean. J Mar Res 63: 141-158

Hughes TMC and Weaver J (1994) Multiple equilibria of an asymmetric 2-Basin Ocean Model. J. Phys. Oceanogr. 24:619-637

Hughes GO, Hogg AM, Griffiths RW (2009) Available potential energy and irreversible mixing in the meridional overturning circulation. J Phys Oceanogr 39:3130-3146, DOI 10.1175/2009JPO4162.1

Intergovernmental Panel on Climate Change (2007), Climate change 2007: The physical science basis, summary for policymakers, IPCC Secr., Geneva, Switzerland.

Jia Y(1999) Formation of an Azores Current due to Mediterranean Overflow in a modeling study of the North Atlantic. J Phys Oceanogr 30: 2342-2358

Jungclaus JH, Keenlyside N, Botzet M, Haak H, Luo J, Latif M, Marotzke J, Mikolajewicz U, Roeckner E (2006b) Ocean circulation and tropical variability in the coupled model ECHAM5/MPI-OM. J Clim 19:3952-3972

Kattemberg A and Coauthors (1996) Climate models-Projections of future climate. Climate Change 1995: The Science of Climate Change, J. T. Houghton et al., Eds., Cambridge University Press, 285-358.

Keigwin L, Curry W, Lehman S, Johnsen S(1994) The role of the deep ocean in North Atlantic climate change between 70 and 130 kyr ago. Nature 371: 323-326.

Kiehl JT and Trenberth KE (1997) Earth's annual global mean energy budget. Bulletin of the American Meteorological Society 78:197-208

Klinger B and Marotzke J (1999) Behavior of double-hemisphere thermohaline flows in a single basin. J. Phys. Oceanogr. 29: 382-399

Kuhlbrodt T, Griesel A, Montoya M, Levermann A, Hofmann M and Rahmstorf S (2007) On the driving processes of the Atlantic meridional overturning circulation. Rev Geophys 45:RG2001. doi:10.1029/2004RG000166

Kushner PJ, Held IM, Delworth TL (2001) Southern Hemisphere atmospheric circulation response to global warming. J Clim 14: 2238-2249

Latif M, Roeckner E, Mikolajewicz U, Voss R (2000) Tropical stabilization of the thermohaline circulation in a greenhouse warming simulation. J Clim 13: 1809-1813.

Levitus S, Boyer T, Conkright M, O'Brein T, Antonov J, Stephens C, Stathoplos L, Johnson D, Gelfeld R(1998) WORLD OCEAN DATABASE 1998: Vol 1: Introduction, vol. NOAA Atlas NESDIS 18, 346 pp., US Gov Printing Office, Washington DC

Lorenz EN (1955) Available potential energy and the maintenance of the general circulation. Tellus 7: 157-167

Lorenz EN (1967) The nature and theory of the general circulation of the atmosphere. WMO Publication, 218, World Meteorological Organization, Geneva, Switzerland, 161 pp.

Lorenz DJ, DeWeaver ET (2007) Tropopause height and zonal wind response to global warming in the IPCC scenario integrations. J Geophys Res 112, D10119, doi:10.1029/2006JD008087.

Lu V, Vecchi GA, Reichler T (2007) Expansion of the Hadley cell under global warming. Geo Res Lett 34, L06805, doi:10.1029/2006GL028443

Lucarini V and Rangone F (2011) Energetics of climate models: net energy balance and meridional enthalpy transport. Rev Geophys 49, RG1001, doi:10.1029/2009RG00323

Luis JF (1979) A parametric model of vertical eddy fluxes in the atmosphere. Boundary Layer Meteorology 17:187-202

Luo J-J ,Masson S, Becera S, Delecluse P, Gualdi S, Navarra A, Yamagata T (2003) South Pacific origin of the decadal ENSO-like variation as simulated by a coupled GCM. Geophys Res Lett 30 (24), 2250

Luo JJ, Masson S, Roeckner E, Madec g, Yamagata T (2004) Reducing climatology bias in an ocean-atmosphere CGCM with improved coupling physics. J Clim 18: 2344-2360.

Madec G and Imbard I (1996) A global ocean mesh to overcome the North Pole singularity. Climate Dyn 12:381-388

Madec G,Delecluse P,Imbard I, Levy C (1998) OPA version 8.1 Ocean general circulation model reference manual, Note du Pôle de modélisation, Inst Pierre-Simon Laplace (IPSL), France, No. 11, 91pp.

Manabe S,Stouffer RJ(1994) Multiple-century response of a coupled ocean-atmosphere model to an increase of atmospheric carbon dioxide. J Clim 7:5-23

Manabe S,Stouffer RJ(1999) The role of the thermohaline circulation in climate. Tellus 51: 91-109.

Mariotti A, Struglia MV, Zeng N, Lau KM (2002) The hydrological cycle in the Mediterranean region and implications for the water budget of the Mediterranean Sea. J Clim 15: 1674-1690.

Marzeion B and Drange H (2006) Diapycnal mixing in a conceptual model of the Atlantic meridional overturning circulation. Deep-Sea Res II 53:226-238

Marzeion B, Levermann A, Mignot J (2010), Sensitivity of North Atlantic subpolar gyre and overturning to stratification-dependent mixing: response to global warming, Clim Dyn 34:661-668

Marzeion B, Levermann A, Mignot J (2007), The role of stratification-dependent mixing for the stability of the Atlantic overturning in a global climate model, J. Phys. Oceanogr 37:2672-2681

McCartney M, Mauritzen S(2001), On the origin of the warm inflow in the Nordic Sea. Progr in Oceanogr 51: 125-214

Meehl GA et al (2007) Global climate projections. In: Solomon S, Qin D, Manning M, Chen Z, Marquis M, Averyt KB, Tignor M, Miller HL (eds) Climate Change 2007: The Physical Science Basis. Contribution of Working Group I to the Fourth Assessment Report of the Intergovernmental Panel on Climate Change, Cambridge University Press, Chap. 10, pp 747-846

Mikolajewicz U and Voss R (2000) The role of the individual air-sea flux component in CO_2-induced changes of the ocean's circulation and climate. Clim Dyn 16:627-642

Morcrette JJ (1984) Sur la paramétrisation du rayonnement dans le modéĺes de la circulation geńeŕale atmospheŕique. Theśe de Doctorat d,ÄôEtat, Universitedé Sciences et Techniques de Lille 630

Morcrette JJ, Fouquart Y (1985) On systematic errors in parameterized calculations of longwave radiation transfer. Q J R Meteorol Soc 111:691-708

Munk W and Wunsch C (1998) Abyssal recipes II: energetics of tidal and wind mixing. Deep-Sea Res I 45:1977-2010

Murray RJ (1996) Explicit generation of orthogonal grids for ocean models. J Comput Phys 126: 251-273

Nilsson J, and Walin G (2001) Freshwater forcing as a booster of thermohaline circulation. Tellus 53A:628-640

Nilsson J, Brostrom G, and Walin G (2003) The thermohaline circulation and vertical mixing: Does weaker density stratification give stronger overturning? J Phys Oceanogr 33:2781-2795

Nordeng TE (1996) Extended versions of the convective parameterization scheme a ECMWF and their impact on the mean and transient activity of the model in the tropics. Technical Memorandum 206, ECMWF, Reading, UK

Ochoa J and Bray NA(1991) Water mass exchange in the Gulf of Cadiz. Deep-Sea Res 38: 5465-5503

O'Hare G, Johnson A, Pope R (2005) Current shifts in abrupt climate change: the stability of the North Atlantic conveyor and its influence on future climate. Geography 90: 250-266

Oort AH, Ascher SC, Levitus S, Peixoto JP (1989) New estimates of the available potential energy in the world ocean. J Geophys Res 94: 3187-3200

Peixoto JP and Oort AH (1992) Physics of climate. Springer-Verlag New York, Inc

Rahmstorf S (1996) On the freshwater forcing and transport of the Atlantic thermohaline circulation. Clim Dyn 12:799-811

Rahmstorf S (1998) Influence of the Mediterranean outflow on climate. Eos Trans AGU 79: 281-282

Rahmstorf S (2000) The thermohaline ocean circulation - a system with dangerous thresholds? Clim Change 46: 247-256

Rahmstorf S (2002) Ocean circulation and climate during the past 120.000 years. Nature 419:207-214

Rahmstorf S et al.(2005) Thermohaline circulation hysteresis: a model inter-comparison. Geophys Res Lett 32: L23605, doi:10.1029/2005GL023655

Raisanen J (2003) CO2-induced changes in atmospheric angular momentum in CMIP2 experiments. J Clim 16: 132-143.

Reid JL(1979) On the contribution of the Mediterranean sea outflow to the Norwegian-Greenland sea. Deep-Sea Res 26: 1199-1223.

Reid RO, Elliott BA, Olson DB (1981) Available potential energy: a clarification. J Phys Oceanogr 11: 15-29.

Rockel B, Raschke E, Weyres B (1991) A parameterization of broad-band radiative transfer properties of water, ice and mixed clouds. Beitr Physik Atmos 64:1-12

Roeckner E (1995) Parameterization of cloud radiative properties in the ECHAM4 model. In: Proc of the WCRP Workshop on "Cloud Microphysics Parameterizations in Global Atmospheric Circulation Models", May 23-25, Ananaskis, Alberta, Canada, WCRP-Report No.90: 105-116, WMO/TD-No.713

Roeckner E,Arpe K, Bengtsson L,Christoph M, Claussen M,Dumenil L, Esch M, Giorgetta M,Schelse U,Schulzweida U (1996) The Atmospheric general circulation Model ECHAM4:model description and simulation of present-day climate. Max Planck Institut fur Meteorologie, Report no.218, Hamburg, 86 pp

Rooth C (1982) Hydrology and ocean circulation. Progress in Oceanography 11:131-149

Sabine CL, Feely RA, Gruber N, Key RM, Lee K, Bullister JL, Wanninkhof R, Wong CS, Wallace DWR, Tilbrook B, Millero FJ, Peng TH, Kozyr A, Ono T, Rios AF (2004) The oceanic sink for anthropogenic CO_2. Science 305: 367-371

Saenko OA and Weaver AJ (2004) What drives heat transport in the Atlantic: Sensitivity to mechanical energy supply and buoyancy forcing in the Southern Ocean, Geophys Res Lett 31: L20305. doi:10.1029/2004GL020671.

Sandstrom JW (1908) Dynamische Versuche mit Meerwasser, Ann Hydrogr Mar Meteorol 36: 6-23.

Sandstrom JW (1916) Meteorologische Studien im Schwedischen Hochgebirge, Goteborgs K. Vetensk. Vitterhetssamhallets Handkl, 27, 48 pp.

Santer BD and Coauthors (2003) Behavior of tropopause height and atmospheric temperature in models, reanalyses, and observations: decadal changes. J Geophys Res 108, 4002, doi:10.1029/2002JD002258.

Sarmiento JL and Le Quere C (1996) Oceanic carbon dioxide uptake in a model of century-scale global warming. Science 274: 1346-1350

Sarnthein MK, Winn SJ, Jung A, Duplessy JC, Labeyrie L, Erlenkeuser H, Ganssen G (1994) Changes in east Atlantic deepwater circulation over the last 30.000 years: Eight time slice reconstructions. Paleoceanogr 9:209-267.

Schaeffer M, Selten FM, Opsteegh JD, Goosse H (2002) Intrinsic limits to predictability of abrupt regional climate change in IPCC SRES scenarios. Geo Res Lett 29 (16), 1767, doi:10.1029/2002GL015254.

Schmittner A, Latif M and Schneider B (2005) Model projections of the North Atlantic thermohaline circulation for the 21st century assessed by observations. Geoph Res Letters 32: L23710. doi:10.1029/2005GL024368

Schneider T (2006) The general circulation of the atmosphere. Annu Rev Earth Planet Sci 34: 655-688

Schneider T, O'Gorman PA, Levine XJ (2010) Water vapor and the dynamics of climate changes. Rev Geophys 48, RG3001, doi:10.1029/2009RG000302

Scott J, Marotzke J and Stone P (1999) Interhemispheric thermohaline circulation in a coupled box model. J. Phys. Oceanogr. 29: 351-365

Sevellec F and Fedorov A V (2011) Stability of the Atlantic meridional overturning circulation and stratification in a zonally averaged ocean model: effects of freshwater, Southern ocean wind and diapycnal diffusion. Deep-Sea Res doi:10.1016/j.dsr2.2010.10.070.

Severinghaus JP et al. (2003) A method for precise measurement of argon 40/36 and krypton/argon ratios in trapped air in polar ice with applica-

tions to past firn thickness and abrupt climate change in Greenland and at Siple Dome, Antarctica. Geochim Cosmochim Acta 67: 325-343.

Sparrow M, Boebel O, Zervakis V, Cantos-Figuerola WZA, Gould WJ(2002) Two circulation regimes of the Mediterranean outflow revealed by lagrangian measurements. J Phys Oceanogr 32: 1322-1330.

Stocker TF and Schmittner A (1997) Influence of CO_2 emission rates on the stability of the thermohaline circulation. Nature 388:862-865

Stommel H (1961) Thermohaline convection with two stable regimes of flow. Tellus 13:224-230

Stouffer RJ, Yin J, Gregory JM, Dixon KW, Spelman MJ, et al. (2006) Investigating the causes of the response of the thermohaline circulation to past and future climate changes. J Clim 19:698-722

Sugi M, Noda A, Sato N (2002) Influence of the global warming on tropical cyclone climatology: An experiment with the JMA global model.J Met Soc Jap 80:249-272

Sundquist (1978) A parameterization scheme for non-convective condensation including prediction of cloud water content. Quart J Roy Meteor Soc 104:677-690

Thorpe RB, Gregory JM, Johns TC, Wood RA and Mitchell JFB (2001) Mechanisms determining the Atlantic thermohaline circulation response to greenhouse gas forcing in a non-flux-adjusted coupled climate model. J Clim 14:3102-3116

Tiedtke M (1989) A comprehensive mass flux scheme for cumulus parameterization in large-scale models. Mon Wea Rev 117:1779-1800

Timmermann R, Goosse H, Madec G, Fichefet T, Etheb C , Duliére V (2005) On the representation of high latitude processes in the ORCA-LIM global coupled sea ice-ocean model. Ocean Modell 8:175-201

Toggweiler JR and Samuels B (1995) Effect of Drake passage on the global thermohaline circulation. Deep-Sea Res Part I 42: 477-500

Toggweiler JR and Samuels B (1998) On the ocean's large-scale circulation near the limit of no vertical mixing. J Phy Oce 28: 1832-1852

Toggweiler JR (2009) Shifting Westerlies. Science 323: 1434-1435

Trenberth KE and Caron JM (2001) Estimates of meridional atmosphere and ocean heat transports. J Clim 14: 3433-3443

Trenberth KE, Fasullo JT, Kiehl J (2009) Earth's global energy budget. Bulletin American Meteorological Society 90: 311-323

Urakawa LS, Hasumi H (2009) The energetics of global thermohaline circulation and its wind enhancement. J Phys Oceanogr 39: 1715-1728, DOI 10.1175/2009JPO4073.10

Valcke S, Terray L, Piacentini A (2000) The Oasis coupler user guide version 2.4. Tech Rep TR/CMGC/00-10, CERFACS

Vecchi GA, Soden BJ, Wittenberg AT, Held IM, Leetmaa A, Harrison MJ (2006) Weakening of tropical Pacific atmospheric circulation due to anthropogenic forcing. Nature 441: 73-76.

Vecchi GA and Soden BJ (2007) Global warming and the weakening of the tropical circulation. J Clim 20: 4316-4340.

Zachos JC, Dickens GR, Zeebe RE (2008) An early Cenozoic perspective on greenhouse warming and carbon-cycle dynamics. Nature 451: 279-283

Zhang R, Kang SM, Held IM (2010) Sensitivity of climate change induced by the weakening of the Atlantic Meridional Overturning circulation to cloud feedback.J Clim 23: 378-389

Zickfeld K, Levermann A, Granger Morgan M, Kuhlbrodt T, Rahmstorf S, Keith D (2007) Expert judgements on the response of the Atlantic meridional overturning circulation to climate change. Clim Change 82: 235-265

Wang C, Dong S and Munoz E (2010) Seawater density variations in the North Atlantic and the Atlantic meridional overturning circulation. Clim Dyn 34:953-968

Weaver AJ, Bitz CM, Fanning AF, Holland MM(1999) Thermohaline circulation: high latitude phenomena and the difference between the Pacific and Atlantic. Ann Rev Earth Planet Sci 27: 231-285

Weaver AJ, Eby M, Kienast M, Saenko OA (2007) Response of the Atlantic meridional overturning circulation to increasing atmospheric $CO2$: sensitivity to mean climate state. Geoph Res Letters 34: L05708. doi:10.1029/2006GL028756

Welander P (1986) Thermohaline effects in the ocean circulation and related simple models. Large-scale transport processes in the oceans and atmosphere. J. Willebrand and D. L. T. Anderson,Eds., D. Reidel, 16xxxx3-200. 16:2875-2889

Williams GP (2006) Circulation sensitivity to tropopause height. J Atmos Sci 63: 1954-1961

Williamson DL and Rasch PR (1994) Water vapor transport in the NCAR CCM2. Tellus 46A:34-51

Wood R, Keen AAB, Mitchell JFB, Gregory JM, (1999) Changing spatial structure of the thermohaline circulation in response to atmospheric $CO2$ forcing in a climate model. Nature 399: 572-575.

Wu W, Danabasoglu G, Large WG(2007) On the effects of parameterized Mediterranean overflow on North Atlantic ocean circulation and climate. Ocean Modelling 19: 31-52

Wu Y, Ting M, Seager R, Huang HP, Cane MA (2010) Changes in storm tracks and energy transports in a warmer climate simulated by the GFDL CM2.1 model. Clim Dyn doi:10.1007/s00382-010-0776-4

Wunsch C (2002) What is the Thermohaline Circulation?. Science 298:1179-1181

Wunsch C and Ferrari R (2004) Vertical mixing, energy, and the general circulation of the oceans. Annu Rev Fluid Mech 36: 281-314

Yin JH (2005) A consistent poleward shift of the storm tracks in simulations of 21 st century climate. Geo Res Lett 32, L18701, doi:10.1029/2005GL023684